EINDHOVEN UNIVERSITY OF TECHNOLOGY

Department of the Built Environment
Unit Structural Engineering and Design
RESED Research Group

Splitting of Laminated Bamboo Lumber Connections Loaded Perpendicular to the Grain

Master's Thesis

MSc Architecture, Building and Planning
Track Structural Engineering and Design

Jonas M. A. Chenderasa

Supervisors:
Emanuela Bosco
(Chair, Associate Professor, PhD, MSc)
Arjan P.H.W. Habraken
(Guiding Supervisor, Assistant Professor, MSc)
Roy Crielaard
(External: Arup, Senior Structural Engineer, MSc)

Eindhoven, May 2026

EINDHOVEN UNIVERSITY OF TECHNOLOGY

Department of the Built Environment
Unit Structural Engineering and Design
RESED Research Group

Splitting of Laminated Bamboo Lumber Connections Loaded Perpendicular to the Grain

Master's Thesis

MSc Architecture, Building and Planning
Track Structural Engineering and Design

Jonas M. A. Chenderasa

Supervisors:
Emanuela Bosco
(Chair, Associate Professor, PhD, MSc)
Arjan P.H.W. Habraken
(Guiding Supervisor, Assistant Professor, MSc)
Roy Crielaard
(External: Arup, Senior Structural Engineer, MSc)

Eindhoven, May 2026

Abstract

Engineered bamboo offers a fast-growing bio-based structural alternative to softwood, but Eurocode 5 (EC5) does not cover laminated bamboo lumber (LBL), so projects in Europe currently require special project approvals that make LBL implementation difficult and limit its carbon storage potential. Bamboo can be harvested for structural use after only 4-5 years, sequestering CO2 on each cycle. One specific gap in EC5 is the splitting check for dowel-type connections loaded perpendicular to the grain. These checks are needed to design structural connections and dowels are one of the most common fastener type. Closing that gap means calibrating the existing splitting equations against LBL test data so the code can be applied without a special approval each time.

Specifically, this thesis tests whether EC5 Gen 1 eq. 8.4 and EC5 Gen 2 eq. 11.54 are applicable to LBL dowel connections, and if so calibrates their parameters. Three lines of evidence are used: small-scale fracture tests (SENB for Mode I and ENF for Mode II), full-scale splitting tests on two beam geometries (flatwise and edgewise), and a finite-element simulation in LS-DYNA with prescribed cohesive crack paths. A literature review of LBL mechanical and fracture properties underpin the experimental and numerical results.

EC5 Gen 1 section 8.1.4 can be applied to LBL without modification based on the conducted tests. The full-scale splitting tests return a $C_{LBL,k} \approx 14.4$ N/mm$^{1.5}$, within 3% of the softwood value $C_k = 14$. The results calculated from SENB values returns $C_{LBL,k} \approx 17.9$. Both results are inside a 14-19 N/mm$^{1.5}$ range comparable to softwood timber.

EC5 Gen 2 eq. 11.54 needs a new material factor k_{mat} for LBL. This thesis proposes $k_{\text{mat},LBL} = 0.7$ (exact result is 0.779, rounded down conservatively), which is between sawn timber (0.6) and panels / LVL-P (0.8). The calibration only adjusts the material factor k_{mat} and leaves the density factor k_G untouched.

These results show that LBL is not more resistant to splitting compared to softwood timber, despite its higher density and the G_{IC} values found in the literature would suggest so. Both calibrations are not definitive results yet as they were done at only a $n = 4$ per-section sample size and single α value (edge distance to height ratio).

Other takeaways from this research are that the section build-up is important both for the experimental fracture results, as well as in turn the calibrated parameters. The flatwise section build-up returns $\approx 46\%$ higher splitting capacity than edgewise across both EC5 generations and across the SENB and ENF small-scale tests. This means the flatwise orientation should be the default for dowel connections loaded perpendicular to the grain. Furthermore, test have shown that splitting failure is Mode I dominated, with intra-lamella fibre delamination and no glue-line separation observed in any test.

Contents

List of Figures

List of Tables

Nomenclature

Symbol	Description	Units
α	Edge-distance to beam-height ratio, h_e/h	-
h	Beam height	mm
h_e	Loaded-edge distance (dowel to loaded edge)	mm
b	Beam thickness	mm
F_{max}	Peak load in fracture or splitting test	N
$F_{90,Rk}$	Characteristic splitting capacity, load perpendicular to grain	N
G_{IC}	Critical Mode I strain energy release rate	J/m^2
G_{IIC}	Critical Mode II strain energy release rate	J/m^2
K_{IC}	Critical Mode I stress intensity factor	$\text{MPa}\sqrt{\text{m}}$
K_{IIC}	Critical Mode II stress intensity factor	$\text{MPa}\sqrt{\text{m}}$
$\sqrt{GG_c}$	Fracture parameter in EC5 Gen 1 Eq. 8.4	$\text{N/mm}^{1.5}$
k_{mat}	Material parameter in EC5 Gen 2 Eq. 11.54	-
$C_{LBL,k}$	Characteristic LBL splitting parameter	$\text{N/mm}^{1.5}$
ρ	Density	kg/m^3
MC	Moisture content	%

List of Abbreviations

Abbreviation	Meaning
CBBM	Compliance-Based Beam Method
CCM	Compliance Calibration Method
CoV	Coefficient of Variation
CZM	Cohesive-Zone Model
EC5	Eurocode 5
EC5 Gen 1	Eurocode 5, first generation (EN 1995-1-1:2004)
EC5 Gen 2	Eurocode 5, second generation (FprEN 1995-1-1:2025)
ENF	End-Notched Flexure (Mode II test)
EW	Edgewise (section build-up, TL-aligned)
FEM	Finite Element Method
FW	Flatwise (section build-up, RL-aligned)
GLVL-P	Glued Laminated Veneer Lumber, parallel-grain
LBL	Laminated Bamboo Lumber
LEFM	Linear Elastic Fracture Mechanics
LVL-C	Laminated Veneer Lumber, cross-grain
LVL-P	Laminated Veneer Lumber, parallel-grain
MC	Moisture Content
RH	Relative Humidity
RL	Radial-Longitudinal crack system
SBT	Simple Beam Theory
SD	Standard Deviation
SENB	Single-Edge Notched Beam (Mode I test)
TBT	Timoshenko Beam Theory
TL	Tangential-Longitudinal crack system
TT	Tensile Test Parallel and Perpendicular to Grain

Section build-up orientation. Flatwise (FW) and edgewise (EW) refer to the orientation of the lamellae in the LBL cross-section. Flatwise has lamella seams running parallel to the top edge and is associated with the RL crack system under perpendicular-to-grain loading. Edgewise has lamella seams perpendicular to the top edge and is associated with the TL crack system. The two build-ups are shown in Figure 2.1.

Chapter 1

Introduction

1.1 Bamboo as a Sustainable Structural Building Material

Bamboo is a structurally efficient, fast-growing grass that has been used as a building material for centuries [1], but only recently as a modern engineered one. Its round hollow cross-section is naturally efficient, and its along the grain strength is exceptionally high (approx. $f_k = 50$ MPa) [28]. It is harvested for structural use after 4-5 years, an order of magnitude faster than softwood [17, 21], potentially storing CO2 on each cycle. The reputation as the poor man's timber has held it back more than its mechanics have.

Full-culm bamboo, although beautiful, has some limitations. The round hollow section does not work well with rectangular architecture. The low weight-to-volume ratio makes shipping in culm-form inefficient. Bamboo is also less durable than timber and must be treated to last [1, 17, 21]. Stiffness (approx. 9.7 GPa), though species-dependent, is generally slightly lower than softwood timber [2].

This is where engineered bamboo comes in. Engineering the raw material removes most of the geometric and dimensional drawbacks. To mention a few, there is laminated bamboo lumber (LBL), the direct analogue of glulam, scrimber, a densified variant, and other products such as cross-laminated bamboo, oriented strand bamboo, and ply-bamboo [30]. The result is a standardised, dimensioned building product that integrates with conventional construction. Of the thousands of bamboo species, only moso bamboo (*Phyllostachys edulis*) has industrial-scale economics behind it, driven by a mature processing industry in China.

1.2 Problem Description

Engineered bamboo cannot be used at scale in projects in Europe until it is aligned with Eurocode 5. Some material properties are missing and code applicability is unproven, which leaves designers and engineers without a defensible route to use the material. Harries & Trujillo [14] map the broader opportunities and limitations of designing engineered bamboo with wood standards. This thesis looks at one specific issue from that bigger picture.

One of the research gaps that needs to be filled is connection design, alongside fire safety and others. As with timber, the weak link in LBL is its behaviour perpendicular to the grain. Fibres are strong when loaded along their length but the inter-fibre bonding that resists transverse and splitting loads is much weaker [27]. For connection design especially this matters, so perpendicular-to-grain properties are governing. The flatwise and edgewise build-ups of the LBL section, together with the dowel loading mode studied here, are introduced in Figure 2.1.

1.3 Relevance of the Work

In order to design structures with LBL in Europe, Eurocode 5 alignment is needed including detailed connection design. Currently, getting special project approvals significantly impacts the project cost and duration. This study targets that issue directly: it tests perpendicular-to-grain properties against the splitting equations in Eurocode 5 and evaluates whether the code can be applied and, if so, calibrated for LBL. A concrete softwood-vs-LBL splitting-capacity comparison for one representative geometry is worked through in §4.3.1. Aligning LBL with the Eurocode, so that connections and in turn structures can be designed with it, could unlock its carbon sequestration potential, leveraging its quick harvesting cycles of 4-5 years. This work aims to contribute to that aim.

Earlier work has measured fracture properties and splitting behaviour of LBL in isolation, but has not carried those results back into the code. Contributing to that loop, from a small-scale fracture parameter to code-level splitting capacity, is what this thesis aims to do. The output is regulatory alignment, design guidance, and a sharper picture of how LBL splits.

1.4 Research Goals

The primary goal is to test whether Eurocode 5 Gen 1 equation 8.4, the characteristic splitting capacity for connections loaded perpendicular to the grain, is applicable to laminated bamboo lumber with dowel-type joints, and to calibrate the equation if it is. The secondary goal is the same exercise for the corresponding Gen 2 equation, 11.54.

Equation 8.4 sits in EC5 Gen 1 Section 8.1.4(3), Connection Forces at an Angle to the Grain [5]. It is calibrated for European softwood with fracture parameter $C = \sqrt{GG_c/0.6}$ and reads:

$$F_{90,Rk} = C_k \cdot b \cdot \sqrt{\frac{h_e}{1 - h_e/h}} \qquad \text{(EC5 Gen 1 Eq. 8.4)}$$

Its Gen 2 counterpart is equation 11.54 in Section 11.6, Brittle Failure of Connections Loaded Perpendicular to Grain [6]. EC5 Gen 2 works with a material factor k_{mat} and a density-driven term k_G:

$$F_{sp,Rd} = \frac{k_{\text{mod}}}{\gamma_M} \cdot k_{\text{mat}} \cdot k_G \cdot b_{ef} \cdot k_{\text{con},0} \cdot k_{\text{con},90} \cdot \sqrt{\frac{h_e}{1 - h_e/h}} \qquad \text{(EC5 Gen 2 Eq. 11.54)}$$

EC5 Gen 2 is in its late revision stage and will replace EC5 Gen 1 in the near future, so calibrating both versions covers both current and future practices.

The connection scope is dowel-type joints. Dowels are among the most common timber connection types and are the natural choice for a first calibration of the splitting equations against LBL.

1.5 Research Questions

The research goal translates into the following main research question (RQ):

> **Main Research Question:** How can the splitting capacity of Laminated Bamboo Lumber with dowel-type connections loaded perpendicular to the grain be established under the Eurocode 5 framework?

Twelve secondary research questions have been developed to supplement the main research question. They follow the workflow of the report: literature, experiments and simulation, regulatory calibration, and design.

- **RQ-1:** What are the mechanical properties of laminated bamboo lumber found in the literature?
- **RQ-2:** What values for the fracture properties of laminated bamboo lumber can be found in the literature?
- **RQ-3:** What is the Eurocode framework for Gen 1 and Gen 2 for splitting of connections loaded perpendicular to the grain, and the underlying mechanical theory?
- **RQ-4:** What are the experimental Mode I fracture characteristics of laminated bamboo lumber?
- **RQ-5:** What are the experimental Mode II fracture characteristics of laminated bamboo lumber?
- **RQ-6:** What is the fracture behaviour of laminated bamboo lumber for connections loaded perpendicular to the grain?
- **RQ-7:** Can the experimental results be numerically reproduced?
- **RQ-8:** How do experimental results compare to literature values?
- **RQ-9:** How do fracture properties derived from small-scale testing translate to full-scale splitting capacity?
- **RQ-10:** Is equation 8.4 from Eurocode 5 Gen 1 applicable to laminated bamboo lumber with dowel-type connections loaded perpendicular to the grain? If so, how can it be calibrated with an appropriate fracture parameter $C = \sqrt{GG_c/0.6}$ suitable for laminated bamboo lumber?
- **RQ-11:** Is equation 11.54 (including sub-equations) from Eurocode 5 Gen 2 applicable to laminated bamboo lumber with dowel-type connections loaded perpendicular to the grain? If so, how can it be calibrated with an appropriate material parameter k_{mat} suitable for laminated bamboo lumber?
- **RQ-12:** What practical learning can be taken from this research for perpendicular-to-grain connection design with Laminated Bamboo Lumber?

Each sub-research question is answered in the chapter shown in the flow chart below.

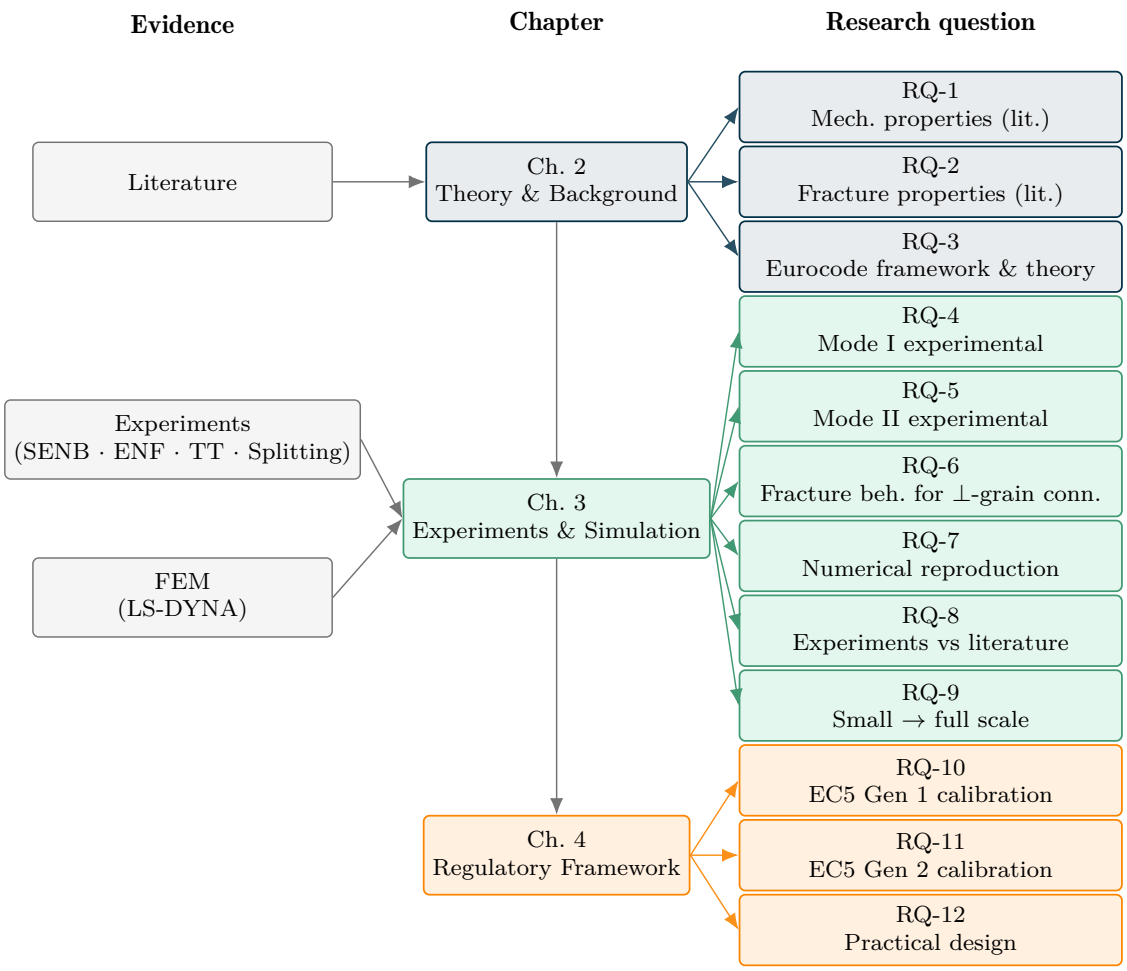

Figure 1.1: Research mapping. The twelve sub-research questions (right) are grouped by the chapter that answers them (centre) and the evidence streams that feed each chapter (left).

1.6 Methodology

To answer the research questions, three methodology directions were used: (i) an experimental study covering small-scale fracture specimens (SENB and ENF) and full-scale splitting beams; (ii) a finite-element (FEM) simulation with LS-DYNA to reproduce the experiments; and (iii) a literature study of LBL mechanical and fracture properties, serving as a baseline of comparison and numerical input. Detailed theory can be found in Chapter 2. The test setups can be found in section 3.1.

1.7 Structure of The Report

The report has four parts: theory & background, experiments & simulations, regulatory & design implications, and conclusions & recommendations.

Theory & background sets up mechanical and fracture properties of LBL found in the literature, introduction to connections loaded perpendicular to grain, and fracture mechanics. It addresses RQ-1, RQ-2, and RQ-3.

Experiments & simulations covers setup, methodology, and results & analysis for the SENB, ENF, tensile, and splitting tests (the latter on the two LBL build-ups and dowel loading mode of Figure 2.1), plus the LS-DYNA finite element work, and closes with a discussion of the combined findings. It addresses RQ-4 through RQ-9.

Regulatory & design implications answers the applicability and calibration question for EC5 Gen 1 equation 8.4 and EC5 Gen 2 equation 11.54. This chapter also gives practical design suggestions. It addresses RQ-10, RQ-11, and RQ-12.

Conclusions & recommendations summarises the findings for LBL dowel connections loaded perpendicular to the grain and restates each research question with its explicit answer.

1.8 Scope Limitations

This research has the following scope. The material is laminated bamboo made from moso bamboo, results do not extend to other species or to other engineered bamboo products. The connection type is dowels, not bolts, nails, or plates. The load orientation is perpendicular to the grain only. Within the design checks for such connections, only splitting capacity is covered. Embedment strength and load-carrying capacity are out of scope, as they require their own set of tests. The $C_{LBL,k}$ and $k_{mat,LBL}$ proposed in this thesis apply to the splitting branch only. An LBL-specific embedment calibration is future work.

The general EC5 design-conversion factors k_{mod} (load-duration and moisture modifier) and γ_M (partial safety factor) apply throughout EC5 are not splitting-specific. Their LBL-specific calibration requires separate testing programmes and is outside the scope of this thesis. Until those values are available, designers need to fall back on the timber values.

The experimental setup adds further limitations. Snap-back behaviour was not captured experimentally nor numerically, but this is only relevant for post-peak. Mechanical properties were measured only to a limited extent and were otherwise taken from the literature.

Specimens were not climate-conditioned to the 20,°C / 65% RH [16] prescribed by NT BUILD 422 §5.2 [44] and the timber literature. The lab averaged 35% RH across the tests, giving a measured mean moisture content of 4.55% (§3.2.1). The closest reference in the literature, Al-Rukaibawi *et al.* [2], tested the same MOSO N-finity product to ISO 23478-2022 [15] and reported $\approx$ 7% MC at 65% RH. The 8-10% MC window typical of timber testing and the manufacturer's equilibrium MC of 10% at 20,°C / 65% RH (Appendix C) was not reached. Although the nominal MC-level was not met, the dry state that was tested represents a more real-world indoor service environment. It also results in a more brittle response than a 65%-RH-conditioned dataset would. Because it is unfavourable to the material, the chapter 4 calibration therefore represent a conservative lower-bound value.

The shear modulus G that enters the EC5 Gen 1 splitting parameter $C = \sqrt{GG_c/0.6}$ (eq. 8.4) was not measured. The literature values used in the SENB route (§4.1) are themselves derived rather than directly measured. Only G_{IC} and G_{IIC} were tested, via SENB and ENF.

Splitting tests were run at a single edge-distance to beam-height ratio ($\alpha = 0.32$) and at a low sample size, which limits the statistical weight of the calibration and prevents resolving an α-dependence.

Chapter 2

Theory and Background

This chapter covers three topics: engineered laminated bamboo lumber, connections loaded perpendicular to the grain, and fracture mechanics. Together they set the material, structural, and analytical context for the experiments and the EC5 calibrations. This chapter addresses RQ-1 (literature mechanical properties), RQ-2 (literature fracture properties), and RQ-3 (the Eurocode splitting framework and its theoretical basis).

2.1 Engineered Laminated Bamboo

Laminated bamboo lumber (LBL), also called glued laminated bamboo, is an engineered-bamboo product [30]. The dominant commercial form is made from moso bamboo (*Phyllostachys edulis*) grown and processed in China [2, 17]. Moso is the only bamboo species with a large-scale industry around it. Other species such as *Dendrocalamus asper* in South-East Asia, *Guadua angustifolia* in South America, are used regionally in pole form [1]. Europe on the other hand, has no native bamboo species, limited cultivation, and relies on imports [14]. Engineered LBL is preferred over full bamboo poles for European construction because it has harmonised sizing and material properties, thus fitting better with the rectangular geometries of modern timber construction [30].

The next two sub-sections review the mechanical and fracture properties of LBL from the literature.

2.1.1 Mechanical Properties - Literature Review

The mechanical characterisation of bamboo as a structural material goes back to the work of Janssen [17], a former Eindhoven University of Technology professor, whose book was the first systematic study of bamboo as structural material.

Bamboo is orthotropic and bimodular. As a natural fibre composite the material has three independent principal directions: longitudinal L along the fibres, radial R through the wall of the culm, and tangential T perpendicular to the wall of the culm. The elastic modulus is significantly higher along the grain (L direction) than perpendicular to the grain (R and T directions) [2]. It is also bimodular, so the modulus and strength in tension and compression along the fibres are not equal.

The properties also vary by species, by position in the culm, and by processing. Mechanical and physical properties differ between species. Within a single culm, properties vary along the height of the culm and through the wall thickness. The outer wall has a higher fibre density than the inner wall, giving a density gradient that will be found also in the engineered product even after strip-cutting and lamination [8]. Age at harvest also matters: a four-year-old culm is a typical target for structural use [2, 17, 21].

Engineered laminated bamboo reduces but does not eliminate all the natural variability that comes with bamboo. Strip-cutting, planing, and edge-glueing of the culm into rectangular strips

averages the radial-position variation and removes the curvature. However, the resulting LBL board retains a flatwise or edgewise asymmetry inherited from the orientation of the strips. Flatwise and edgewise represent the strip orientation in the section of LBL. They yield different elastic moduli, strengths, and shear-modulus values that the literature reports separately [2]. Processing routes such as bleached, caramelised, or preservative-treated also further shifts the strength and stiffness relative to the untreated reference [34, 35]. The build-up and the two section orientations are illustrated in Figure 2.1, together with the perpendicular-to-grain dowel loading studied throughout the thesis.

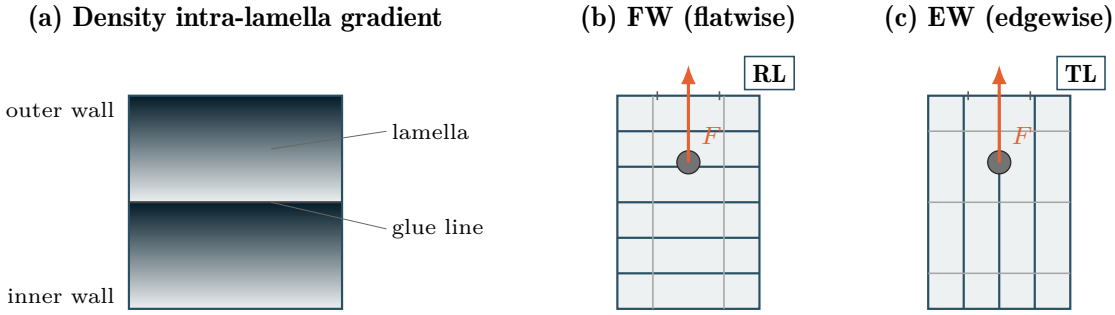

Figure 2.1: LBL build-up (a). Flatwise (b, RL splitting plane) and edgewise (c, TL splitting plane) sections under perpendicular-to-grain dowel loading at edge-distance h_e.

The mechanical-property dataset adopted in this thesis is anchored on *MOSO N-finity*, the commercial LBL product used for the experimental specimens [28]. The MOSO N-finity indoor-beam datasheet gives the manufacturer-reported reference values for density, moisture content, modulus of elasticity, and bending strength and is reproduced for completeness in Appendix C. As a structural-properties baseline, the most directly comparable peer-reviewed study is Al-Rukaibawi *et al.* [2], who tested the same N-finity product to ISO 23478-2022 and reported orthotropic compression elastic moduli and compressive strengths in all three directions. Their work formed the backbone of literature values used in the study. The reported compression values are listed in Table 2.1 below also. Because Al-Rukaibawi *et al.* only covers compression, the literature review of this thesis extends their dataset with tensile and bending values from the broader LBL literature [7, 24, 38, 39].

Moisture content and relative humidity also affect the properties of LBL, analogous to timber. Dryer LBL is more brittle.

Compared to softwood, LBL has substantially higher tensile and compressive strength along the grain and a comparable stiffness [2, 39]. The across-fibre tensile and shear strength is comparatively lower than its longitudinal capacity. The orthotropy ratio $\frac{E_L}{E_T}$ suggests that splitting failure is the limiting factor for connection design.

Table 2.1: LBL Mechanical Properties from the Literature

Property	Symbol	Tensor	n (pubs)	n (samples)	Mean	SD	CoV (%)	Char. 5%ile	Units
Elastic modulus (longitudinal)	E_L	E_11	7	155	9552.90	718.87	7.5	8370.37	MPa
Elastic modulus (longitudinal), bending	E_L_B	E_11_B	4	90	9762.11	666.83	6.8	8665.18	MPa
Elastic modulus (longitudinal), compression	E_L_C	E_11_C	1	5	8750.00	1550.00	17.7	6200.25	MPa
Elastic modulus (longitudinal), tension	E_L_T	E_11_T	2	60	9306.00	727.66	7.8	8108.99	MPa
Elastic modulus (radial)	E_R	E_33	2	45	1362.89	147.29	10.8	1120.60	MPa
Elastic modulus (radial), compression	E_R_C	E_33_C	1	5	1110.00	210.00	18.9	764.55	MPa
Elastic modulus (radial), tension	E_R_T	E_33_T	1	40	1394.50	139.45	10.0	1165.10	MPa
Elastic modulus (tangential)	E_T	E_22	2	45	1387.33	189.54	13.7	1075.54	MPa
Elastic modulus (tangential), compression	E_T_C	E_22_C	1	5	2190.00	110.00	5.0	2009.05	MPa
Elastic modulus (tangential), tension	E_T_T	E_22_T	1	40	1287.00	199.49	15.5	958.85	MPa
Shear modulus (LR)	G_LR	G_13	1	5	1380.00	—	—	—	MPa
Shear modulus (LT)	G_LT	G_12	1	5	1970.00	—	—	—	MPa
Shear modulus (TR)	G_TR	G_23	1	5	510.00	—	—	—	MPa
Strength (longitudinal)	f_L	f_11	8	176	71.87	6.86	9.5	60.59	MPa
Strength (longitudinal), bending (MOR)	f_L_B	f_11_B	4	90	74.61	5.78	7.7	65.11	MPa
Strength (longitudinal), compression	f_L_C	f_11_C	1	16	68.60	1.09	1.6	66.81	MPa
Strength (longitudinal), tension	f_L_T	f_11_T	3	70	69.09	9.56	13.8	53.35	MPa
Strength (radial)	f_R	f_33	2	56	6.80	1.90	28.0	3.66	MPa
Strength (radial), compression	f_R_C	f_33_C	1	16	13.16	4.43	33.7	5.87	MPa
Strength (radial), tension	f_R_T	f_33_T	1	40	4.25	0.89	21.0	2.78	MPa
Strength (tangential)	f_T	f_22	3	66	6.22	0.75	12.1	4.99	MPa
Strength (tangential), compression	f_T_C	f_22_C	1	16	15.41	0.50	3.2	14.59	MPa
Strength (tangential), tension	f_T_T	f_22_T	2	50	3.28	0.83	25.3	1.92	MPa
Shear strength	f_v	f_12	3	70	11.57	1.02	8.8	9.89	MPa
Poisson ratio (LR)	v_LR	v_13	1	5	0.32	0.07	21.9	0.20	-
Poisson ratio (LT)	v_LT	v_12	1	5	0.23	0.07	30.4	0.11	-
Poisson ratio (TR)	v_TR	v_23	1	5	0.53	0.25	47.2	0.12	-

2.1.2 Fracture Properties - Literature Review

Introduction to fracture mechanics including crack systems can be found in section 2.3, and the three classical fracture modes are illustrated in Figure 2.3. Published values for the Mode-I fracture energies for full-culm moso bamboo and LBL sit around 508 J/m^2 in the RL system and around 338 J/m^2 in the TL system. Mode-II values are sparser: roughly 967 J/m^2 in the TL system, with no values recorded for the RL system. Most data are on the moso culm rather than on engineered LBL, and most cover Mode I rather than Mode II - both of which are gaps the experimental study aims to close. The compiled values are shown in Table 2.2 below [8, 10, 12, 25, 26, 37, 41, 42, 45].

Table 2.2: LBL Fracture Properties from the Literature

Property	Symbol	Tensor	n (pubs)	n (samples)	Mean	SD	CoV (%)	Char. 5%ile	Units
Mode I critical fracture energy release rate	G_IC	G_IC	8	65	397.89	49.80	12.5	315.97	J/m^2
Mode I critical fracture energy release rate (RL crack)	G_IC_RL	G_IC_RL	4	23	507.88	65.00	12.8	400.95	J/m^2
Mode I critical fracture energy release rate (TL crack)	G_IC_TL	G_IC_TL	4	42	337.65	46.47	13.8	261.21	J/m^2
Mode II critical fracture energy release rate	G_IIC	G_IIC	2	86	966.59	135.91	14.1	743.02	J/m^2
Mode II critical fracture energy release rate (TL crack)	G_IIC_TL	G_IIC_TL	2	86	966.59	135.91	14.1	743.02	J/m^2
Mode I critical stress intensity factor	K_IC	K_IC	1	9	0.61	0.04	7.3	0.53	MPa.m$^{0.5}$
Mode I critical stress intensity factor (TL crack)	K_IC_TL	K_IC_TL	1	9	0.61	0.04	7.3	0.53	MPa.m$^{0.5}$
Mode II critical stress intensity factor	K_IIC	K_IIC	1	9	1.19	0.10	8.3	1.03	MPa.m$^{0.5}$
Mode II critical stress intensity factor (TL crack)	K_IIC_TL	K_IIC_TL	1	9	1.19	0.10	8.3	1.03	MPa.m$^{0.5}$

Splitting and Mode-I-dominant cracking is the typical failure in bamboo and LBL. Bamboo and LBL are strongly orthotropic with a much weaker inter-fibre bonding than intra-fibre strength, so a crack grows along the fibres once initiated [10]. In other words, the fibres separate rather than break. In a culm this shows up as longitudinal splitting of the wall under hoop tension.

One thing to be considered, moisture content, alongside treatment [35], shifts the mechanical properties of LBL. Chen Qi *et al.* [9] reported a $dG_{IC}/d\mathrm{RH}$ of about +7.6 J/m^2 per percentage-point of relative humidity. This forms the base of RH correction in this study.

2.2 Connections Loaded Perpendicular to The Grain

2.2.1 Splitting Capacity

When a dowel-type connection loads a beam perpendicular to the grain near the loaded edge, the beam is prone to a brittle splitting failure rather than the ductile embedment failure. A crack initiates at the dowel hole and propagates along the grain, dividing the beam into two sub-beams (Figure 2.2).

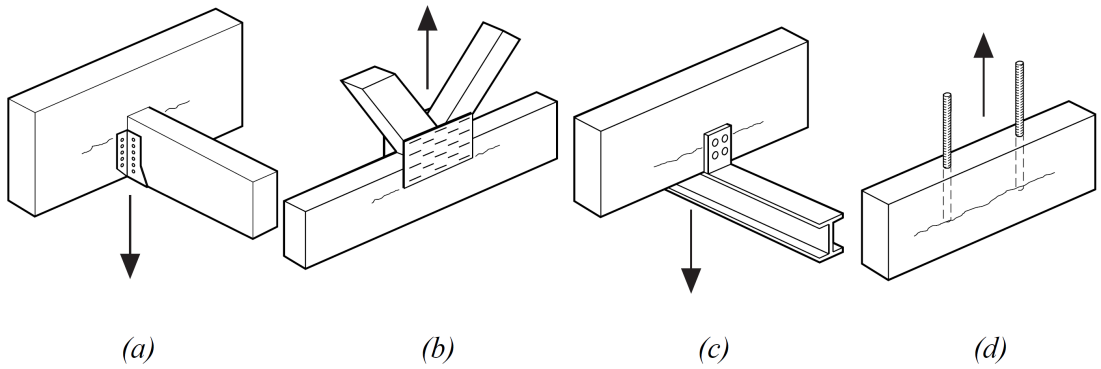

Figure 2.2: Examples of connection loaded perpendicular to the grain. Reproduced from [4], adapted from [11].

Design approaches for this failure mode fall into two families [18]: strength- based criteria (earlier strength-based design rules, see Ehlbeck *et al.* [11]), and fracture-mechanics approaches [3, 22, 32]. The latter of the two are adjusted by a $\sqrt{h}$ size effect from energy release. The fracture-mechanics route originates with van der Put's 1990 CIB-W18 derivation [32], later refined together with Leijten (also a former professor at TU/e), into the closed-form expression [33] that EC5 clause 8.1.4 eq. 8.4 ultimately adopted in preference to the strength-based rule. The framework was subsequently stress- tested experimentally and numerically by Schoenmakers [36], whose PhD at TU/e supplied a large dataset for nailed and dowelled splitting tests in spruce, and motivated the effective- width corrections that reappear in the EC5 Gen 2 *b_ef* clause. Malkowska *et al.* [27] adapted this fracture-mechanics model to full-culm bamboo, and Wang *et al.* [43] reported bolted steel-LBL connections loaded perpendicular to the grain. It remains to be validated if the same approach applies to dowelled LBL.

Van der Put and Leijten derived [33] the following. Their derivation equates the energy released as the split extends, computed from the compliance of the two sub-beams under combined shear and bending, to the fracture toughness G_c, which yields the given open form:

$$\frac{V_f}{b\sqrt{h}} = \sqrt{G \cdot G_c} \cdot \sqrt{\frac{\alpha}{0.6(1-\alpha)}} \tag{2.1}$$

Here V_f ($= F_{\max}/2$) is the reaction shear force on one side of the split, b and h are the beam thickness and depth, $\alpha = h_e/h$ is the loaded-edge ratio, and $G \cdot G_c$ couples the in-plane shear modulus to the Mode-I fracture toughness; rearranged for the EC5 design capacity:

$$F_{90} = b \cdot \sqrt{G \cdot G_c/0.6} \cdot \sqrt{\frac{h_e}{1-h_e/h}}. \tag{EC5 Eq. 8.4}$$

The coefficient $C_{\text{mean}} = \sqrt{GG_c/0.6}$ is a single material parameter. For timber its characteristic value $C_k = \frac{2}{3} \cdot C_{\text{mean}} \approx 14$ underpins the EC5 design rule, yielding $F_{90,Rk} = 14 \cdot b \cdot \sqrt{\frac{h_e}{1-h_e/h}}$. For LBL the value of C_{LBL} is an open question and one of the primary deliverables of this thesis.

Van der Put's and Leijten's [33] derivation assumes the splitting failure is Mode-I dominated.

2.2.2 Embedment vs Splitting Failure

A dowel-type connection loaded perpendicular to the grain can fail in two ways, sketched in Figure **??**: splitting or embedment. Splitting failure is brittle. The dowel hole acts as an imperfection where a crack starts growing, the crack runs along the grain, and the connection breaks before any yield plateau is reached. Embedment failure is ductile. The timber crushes under the dowel and the steel fastener bends, with the failure load determined by the smaller of the embedment strength $f_{h,90,k}$ and the dowel yield moment $M_{y,Rk}$.

Figure **??** Which mode governs depends on geometry and slenderness. Short loaded-edge distances and stocky dowels favour splitting, longer edge distances and slender dowels favour embedment. Both feed into the design resistance for the connection. EC5 takes the connection capacity as the smaller of the two branches, with the ductile branch given by the European Yield Model of Johansen [19] and the brittle branch by the splitting clause 8.1.4 eq. 8.4 in Gen 1 and clause 11.6 eq. 11.54 in Gen 2. Designers must consider that the two limit states are not strictly sequential. Schoenmakers [36] showed that local crushing under a slender dowel can trigger early splitting below the splitting resistance cap, an effect Gen 2 absorbs through the effective-width reduction b_{ef} (eq. 11.57) inside the splitting term rather than by penalising embedment.

The two failure modes are not interchangeable. Each requires its own tests (full-scale beam splitting tests with a dowel near the loaded edge, vs. small-specimen perpendicular-to-grain embedment tests per EN 383), its own code equation (EC5 splitting clause vs. Johansen EYM), and its own material-specific parameters (C_k or $k_{mat}{\cdot}k_G$ for splitting; $f_{h,90,k}$ and dowel yield moment $M_{y,Rk}$ for embedment). The present thesis calibrates only the splitting branch (§1.8); embedment characterisation of LBL is listed in §5.3 as a separate open research task.

2.2.3 EC5 Gen 2 Splitting Resistance Changes

The next-generation Eurocode 5 [6] drops the fracture-mechanics-based $\sqrt{GG_c}$ constant of Gen 1 eq. 8.4 in favour of a material factor and a density correlation. Clause 11.6, brittle failure of connections loaded perpendicular to grain, gives the design splitting resistance as:

$$F_{sp,Rd} = \frac{k_{\text{mod}}}{\gamma_M} \cdot k_{\text{mat}} \cdot k_G \cdot b_{ef} \cdot k_{\text{con},0} \cdot k_{\text{con},90} \cdot \sqrt{\frac{h_e}{1 - h_e/h}} \tag{11.54}$$

where k_{mod} and γ_M are the standard load-duration and partial-factor modifiers, b_{ef} is the effective member width (eq. 11.57), and $k_{\text{con},0}$ and $k_{\text{con},90}$ are geometric multi-fastener factors (eqs. 11.58 and 11.59) that collapse to 1 for a single-dowel single-row connection. The material parameter is:

$$k_{\text{mat}} = \begin{cases} 0.6 & \text{sawn timber,} \\ 0.8 & \text{plywood} \\ 1.0 & \text{LVL-P and GLVL-P wide face} \end{cases} \tag{11.55}$$

And the density-driven fracture parameter is given by:

$$k_G = 0.05 \cdot \rho_k + 2 \tag{11.56}$$

Comparing eq. 11.54 with the eq. 8.4 from Gen 1 shows that the two agree on the geometric square-root term but differ structurally in the coefficient. Gen 1 uses a single fracture- mechanics-derived constant $C = \sqrt{GG_c/0.6}$ with characteristic value $C_k = 14$ for timber. Gen 2 splits the equivalent role between a material factor k_{mat} and a density correlation k_G. The substantive change between the two generations is the load convention, not the resistance coefficient (which agrees within 10% for sawn softwood at $\rho_k = 380$ kg/m^3: Gen 1 uses 14, Gen 2 gives $k_{\text{mat}} \cdot k_G = 0.6 \cdot 21 = 12.6$). Gen 1 checks the per-side shear $V_{\max} = \max\{V_1, V_2\}$ against $F_{90,Rk}$, whereas Gen 2 checks the total connection load $F_{t,90,Ed}$ against $F_{sp,Rk}$.

2.3 Fracture Mechanics

Fracture mechanics is the study of how cracks initiate and grow in solids.

2.3.1 Fracture Modes

A crack can grow in three ways, defined by the relative motion of the two crack faces [31] (Figure 2.3). *Mode I* is the opening mode, in which the two faces separate normal to the crack plane under a tensile stress. *Mode II* is the in-plane shear mode, in which the faces slide over each other perpendicular to the crack front. *Mode III* is the out-of-plane shear mode, in which the faces slide parallel to the crack front in a tearing motion. Each mode has its own energy release rate G_i and stress-intensity factor K_i, with corresponding critical G_{iC} and K_{iC}.

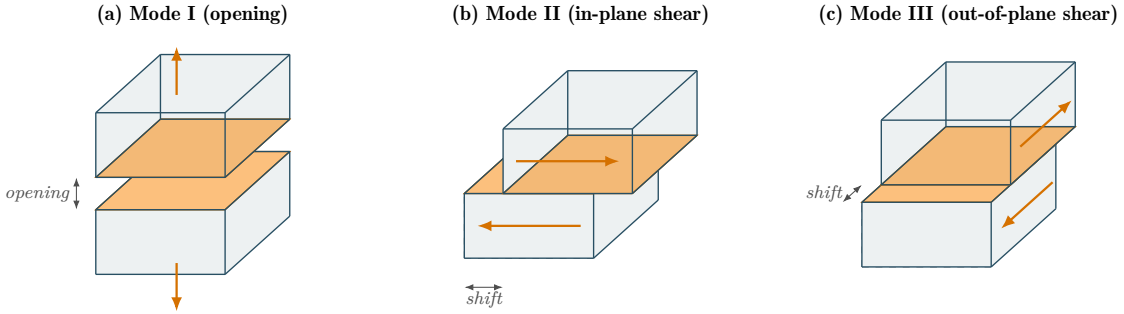

Figure 2.3: The three fracture modes - (a) Mode I (opening), (b) Mode II (in-plane shear) and (c) Mode III (out-of-plane shear).

2.3.2 Crack Systems (TL / RL)

Wood is anisotropic about three principal axes [20, 31]: longitudinal L (along the fibres), radial R, and tangential T. A crack system is labelled by two letters: the normal to the crack plane, then the direction of propagation (Figure 2.4). The along-grain systems of structural interest are RL and TL: both have the splitting direction parallel to the fibre direction (loading is perpendicular). Softwoods consistently show TL below RL in fracture energy [20]. Whether the same asymmetry holds for LBL, which has no annual-ring structure, is one of the open questions addressed in Chapter 4.

LBL follows the same logic and naming system as wood. The edgewise and flatwise section build-ups can be related to the crack system. Edgewise corresponds to TL and flatwise corresponds to RL, when loaded perpendicular to the grain.

(a) Radial-Longitudinal (RL) **(b) Transversal-Longitudinal (TL)**

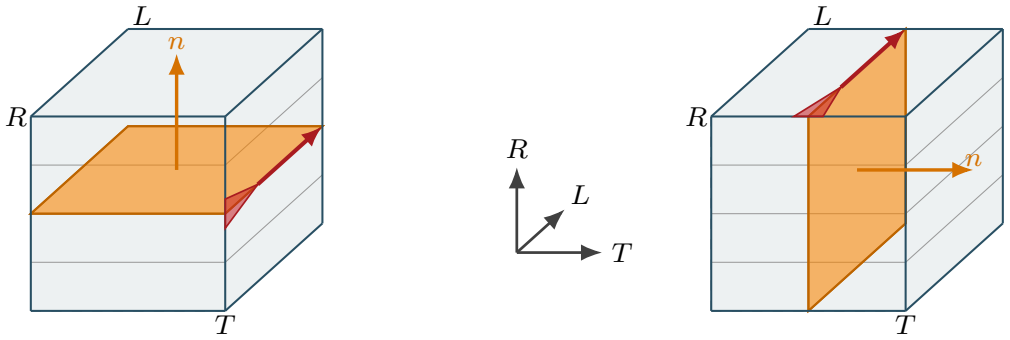

Figure 2.4: Crack-system labelling for RL and TL on the L-R-T axes (lamellae stacked along R). The first letter is the crack-plane normal (amber arrow), the second is the growth direction (red arrow along L). Both systems propagate along the fibres and differ only in the crack-plane orientation.

2.3.3 G and K Values

Fracture in a cracked solid is described by two related criteria [31]. The energy criterion says that a crack advances once the strain-energy release rate G (the elastic energy released per unit of new crack surface) reaches a critical value G_C. The stress-strength criterion says the same in terms of the stress-intensity factor $K = \lim_{r\to 0} \sigma_{ij}\sqrt{2\pi r}$, which fixes the mathematical stress singularity at the crack tip, and a corresponding critical value K_C. The two are not numerically interchangeable from the same test. K_C is linear-elastic by construction, set by the peak stress and the initial notch geometry, whereas G can be read either at peak (crack initiation) or as the total work of fracture under the full load-displacement curve. G_C, unlike K_C, captures the post-peak softening that is characteristic of quasi-brittle materials such as wood and LBL [20]. At the peak-load for an isotropic linear-elastic material, the two criteria are linked by Irwin's relation $G_i = K_i^2/E'$, with $E' = E$ in plane stress and $E/(1-\nu^2)$ in plane strain.

LBL is strongly orthotropic, so the isotropic E' understates G_{IC}. The thesis uses the Sih-Paris-Irwin compliance-tensor form [40], in which G_{IC} depends on E_L, E_T, ν_{LT}, and G_{LT}, and reports the isotropic form alongside it for comparability with the bamboo literature (methods I-2a and I-2b in §2.3.4).

2.3.4 Methods for Fracture-Energy Calculation

This thesis calculates fracture-energy criteria with different methods: *I-n* for Mode-I, *II-n* for Mode-II, and *D-n* for derived quantities (K_{IC}, K_{IIC}). The full version is in Appendix~B.

Mode-I (SENB):

- *I-1, work-of-fracture* (NT BUILD 422 [44]): the total work done, obtained by integrating the full load-displacement curve, normalised by the fracture area to give the total G_f.
- *I-2a, isotropic LEFM*: $G_{IC} = K_{IC}^2/E'$ with E' a single across-fibre modulus (E_T for TL, E_R for RL). Kept for comparability with the bamboo literature.
- *I-2b, orthotropic LEFM* [40]: G_{IC} depends on E_L and the crack-system elastic constants (E_T, ν_{LT}, G_{LT} for TL; E_R, ν_{LR}, G_{LR} for RL). Carried forward into the K_{IC} derivation of §4.

Mode-II (ENF):

- *II-1, simple beam theory* (SBT): closed-form peak-load G_{IIC}, modulus-dependent on E_L. Initiation cross-check.

- *II-2, Timoshenko beam theory* (TBT): SBT with shear correction, modulus-dependent on E_L and the in-plane shear modulus G_{13} (G_{LT} for TL, G_{LR} for RL). Initiation cross-check.
- *II-3, compliance-based beam method* (CBBM, [29]): an effective bending modulus calculated from the initial compliance and tracks an equivalent crack length over the full curve. Primary method.
- *II-4, compliance calibration method* (CCM): measures the compliance of multiple specimens cut to different initial crack lengths, fits the compliance-versus-crack-length trend, and reads G_{IIC} from its slope.

Derived quantities.

- *D-1, K_{IC} isotropic*: from I-2a via $K = \sqrt{GE'}$.
- *D-2, K_{IC} orthotropic*: Sih inverse from I-2b.
- *D-3, K_{IIC} orthotropic*: Mode-II Sih inverse from the CBBM G_{IIC} of II-3.

2.4 Discussion - Theory and Background

This section discusses the literature and regulatory background presented in this chapter, and answers the chapter's three research questions.

The literature consolidates into a coherent enough picture. LBL is orthotropic and bimodular, with along-grain properties dominating across-grain ones, and Mode I fracture energies in the RL crack system consistently above those in TL. The EC5 splitting section, in both its current Gen 1 form (eq. 8.4) and its imminent Gen 2 form (eq. 11.54), reduces all of this to a small handful of material parameters, none of which has been calibrated for LBL. That gap is what chapter 4 fills.

The mechanical baseline for the experimental work is the MOSO N-finity dataset reported by Al-Rukaibawi *et al.* [2], who tested the same product to ISO 23478-2022 and gave compressive moduli and strengths in all three orthotropic directions. Older anchor sources (Sharma *et al.* [38, 39] and Reynolds and co-workers [34, 35]) supply the tensile, and bending, that Al-Rukaibawi does not cover. Together these give fuction as inputs for G_{IC} and G_{IIC} calculations, as well as for the FEM setup.

The fracture baseline is sparser. Mode I literature sits around 508 J/m^2 in RL and 338 J/m^2 in TL, with most data from full-culm moso bamboo rather than engineered LBL. Mode II is at roughly 967 J/m^2 in TL and not reported at all in RL. Chen Qi *et al.* [9] also fit a humidity sensitivity of +7.6 J/m^2 per percentage-point of RH that the experimental work uses to correct the dry-conditioned specimens. The SENB and ENF results are compaired against these literature values in chapter 3.

Summary of findings: - LBL is orthotropic and bimodular, with a consistent RL > TL ranking in literature fracture energies. - LBL has high strength in grain direction (f_k = 60 MPa, see Figure 2.1). - Mode I literature: $\approx$ 508 J/m^2 in RL, 338 J/m^2 in TL, mostly on full-culm moso bamboo. - Mode II literature: $\approx$ 967 J/m^2 in TL only, with no values reported for RL. - Mode I fracture energy carries a RH sensitivity of +7.6 J/m^2 per percentage-point according to Chen-Qi. - EC5 Gen 1 eq. 8.4 uses one calibrated constant, $C_k = 14$ for timber. Gen 2 eq. 11.54 splits the role into a categorical k_{mat} and a density correlation $k_G(\rho_k)$. - Splitting and embedment are separate failure modes, and this thesis calibrates only the splitting branch. - Splitting is decribed by fracture mechanics.

RQ-1 - What are the mechanical properties of laminated bamboo lumber found in the literature? - LBL is orthotropic and bimodular, with longitudinal moduli and strengths an order of magnitude above the across-grain values [2]. - Tensile and compressive responses along the fibres differ, so a single Young's modulus cannot represent both. - Property values vary by species, by position in the culm, and by processing [34, 35]. - The MOSO N-finity dataset of Al-Rukaibawi *et al.* [2] is the peer-reviewed anchor for the product tested here, with compressive properties in all three orthotropic directions reported to ISO 23478-2022. - Tensile, bending, and shear values come

from the wider LBL literature [7, 24, 38, 39]. - Flatwise and edgewise build-ups carry different elastic and strength values per orientation [38].

RQ-2 - What values for the fracture properties of laminated bamboo lumber can be found in the literature? - Mode I: $\approx$ 508 J/m^2 in RL and $\approx$ 338 J/m^2 in TL [8, 10, 26, 37, 42, 45]. - Mode II: $\approx$ 967 J/m^2 in TL, no published values in RL [12, 41]. - Most data is on full-culm moso bamboo and engineered LBL, and most covers Mode I rather than Mode II. Both gaps are filled by the SENB and ENF tests of chapter 3. - Chen Qi *et al.* [9] reported a humidity sensitivity of +7.6 J/m^2 per percentage-point RH for G_{IC}. The dry-conditioned chapter 3 specimens (§3.2.1) are corrected against this slope.

RQ-3 - What is the Eurocode framework for Gen 1 and Gen 2 for splitting of connections loaded perpendicular to the grain, and the underlying mechanical theory? - Gen 1 clause 8.1.4, eq. 8.4: $F_{90,Rk} = C_k \cdot b \cdot w \cdot \sqrt{h_e/(1 - h_e/h)}$ with $C_k = 14$ for softwood timber. - The constant absorbs van der Put's fracture-mechanics derivation $C = \sqrt{GG_c/0.6}$, coupling the in-plane shear modulus G to the Mode-I critical energy release rate G_c [32, 33]. - Gen 2 clause 11.6 [6] replaces the lumped C with the product $k_{\text{mat}} \cdot k_G(\rho_k)$, where k_{mat} is categorical (0.6 sawn timber, 0.8 plywood, 1.0 LVL-P) and $k_G = 0.05\rho_k + 2$ is a density correlation. - The two generations agree on the geometric square-root term. - The substantive change between them is the load convention: Gen 1 checks per-side shear, Gen 2 checks total connection load. - Splitting and embedment remain separate failure modes with separate test routes (splitting beam vs EN 383 cube) and material parameters [18, 36]. - Splitting is decribed by fracture mechanics.

Chapter 3

Experiments and Simulation

In this chapter, the experiment and simulation that had been conducted are presented. This includes the single-edged notched beam (SENB), end-notched flexure (ENF), splitting capacity, tensile test (TT), moisture content (MC), density tests and finite element method (FEM) analysis. This chapter addresses RQ-4 to RQ-9, covering the Mode I and Mode II experimental fracture characteristics, fracture behaviour of connections loaded perpendicular to the grain, numerical reproduction by FEM, comparison with literature, and the small-to-full-scale translation.

3.1 Methodology and Setup

This section discusses the methodology and setup for all the tests. Figure 3.1 summarises why each test is run and how its result is used downstream. The Purpose column also tags the crack system (or load direction) tested and the research question(s) the row answers, so the figure doubles as the chapter test matrix (RQ-4 through RQ-9 collectively).

The end-to-end process for the SENB and ENF tests is shown in Figure 3.2, covering the thirteen steps from research question through to interpretation.

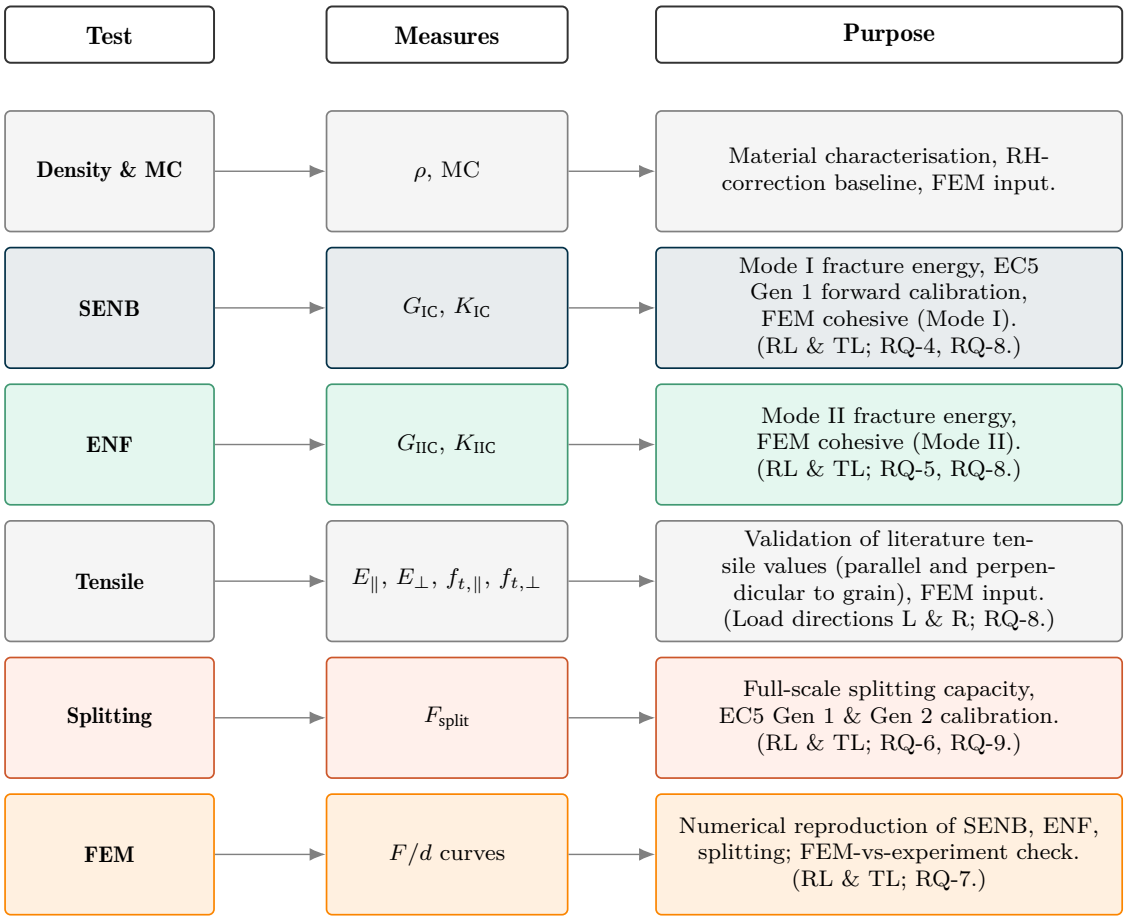

Figure 3.1: Chapter 3 test matrix: each test and FEM simulation, what it measures, and how the result is used. The Purpose cell tags the crack system or load direction and the research question(s) covered (RQ-4 through RQ-9).

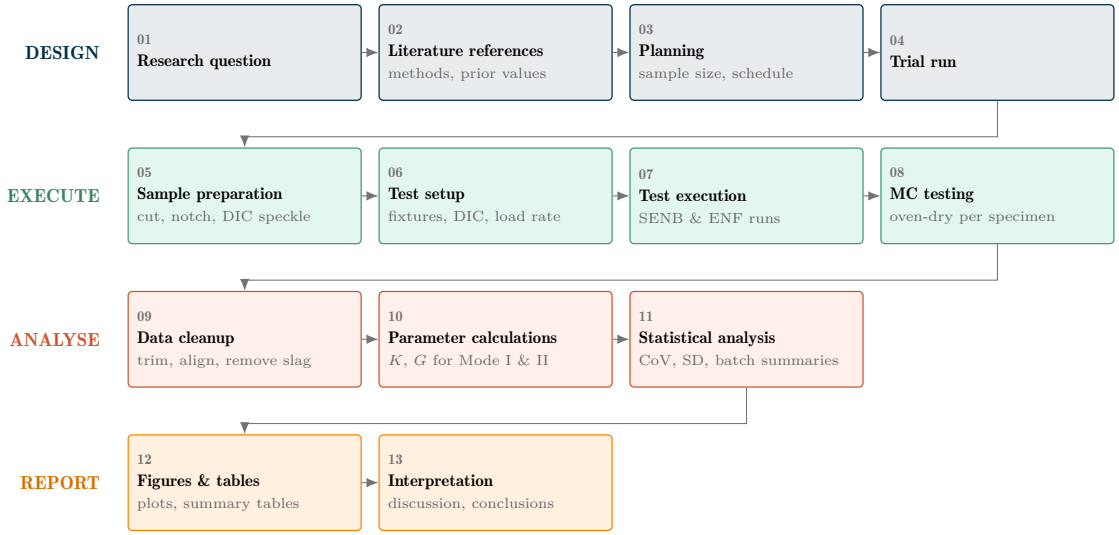

Figure 3.2: End-to-end SENB (Mode I) and ENF (Mode II) experimental process, organised into four phases - design, execute, analyse, report.

3.1.1 Density and Moisture Content Characterisation

Density was determined from 10 precisely cut cubes, each measured and weighed individually. Moisture content was measured with the oven-dry method on 61 samples taken from the SENB and ENF specimens. The samples were dried at 103,°C for 48 hours, until the weight had stabilised. Moisture content is reported on the **dry-mass basis** (oven-dry mass in the denominator):

$$\text{MC } (\%) = \frac{m_{\text{wet}} - m_{\text{dry}}}{m_{\text{dry}}} \times 100\% \tag{3.1}$$

3.1.2 Single-edged Notched Beam (SENB) Test - Mode I

Single-edged notched beam test is a three-point bending test with a notch in the centre of the beam. Depending on what crack system is tested, the beam can be built up from three elements with a central cube rotated to study the crack system of interest. The three-element specimen-preparation step is shown in Figure A.1. These tests are designed to study the mode I fracture behaviour. For timber, these types of tests are described by the standard NT BUILD 422, a Scandinavian standard published in 1993. The experiments are conducted following this standard. The specimen geometry is shown in Figure 3.3.

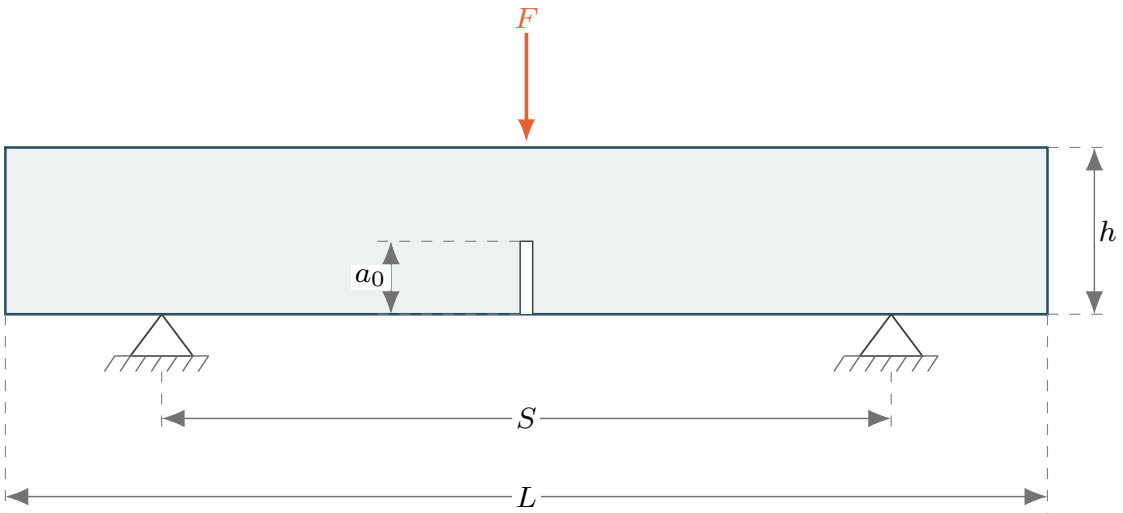

Figure 3.3: Free body diagram of the SENB three-point bending test, with span L, beam height h, central notch depth a_0 and applied load F.

Specimens were produced of two thicknesses in combination with the tested crack system. Both radial-longitudinal (RL) and tangential-longitudinal (TL) crack systems were studied. All variants can be seen in Table 3.1. What is measured is the applied force as well as the mid-span deflection. From this, the work done is represented by the integral of (area under) the F/d curve. The work done is normalised by the fracture area to derive the critical energy release rate.

This experiment was performed on an Instron 5985 machine with a 5 kN load cell and displacement controlled with a rate of 0.3 mm/min. Samples were cut from six beams of 83 x 86 mm with an average length of 1 m. Tests were carried out with a target test duration of 5 minutes, all tests were not shorter than 3 minutes, and not longer than 7 minutes.

Specimens were not climate-conditioned to the 20,°C / 65% RH prescribed by NT BUILD 422 §5.2 [44] and ISO 554[16]. Relative humidity was logged throughout the tests and averaged 35%. The results represent more real-world condtions, but are less comparable against the literature. The post-hoc RH correction is handled in section 3.2.1. Digital Image Correlation (DIC) was used as a backup mean to track the beam displacement.

Table 3.1: SENB test setup specimen geometry per crack system and depth code

Group	n	b [mm]	h [mm]	L [mm]	S [mm]	a_0 [mm]	h_c [mm]
RL / 2	23	17.7 ± 0.2	38.7 ± 0.3	273 ± 0	234 ± 0	22.5 ± 0.5	16.2 ± 0.2
RL / 4	8	39.1 ± 0.4	38.6 ± 0.3	273 ± 0	234 ± 0	22.5 ± 0.2	16.2 ± 0.3
TL / 2	23	17.7 ± 0.3	38.5 ± 0.8	273 ± 0	234 ± 0	22.4 ± 0.9	16.2 ± 0.3
TL / 4	8	38.9 ± 0.3	38.7 ± 0.3	273 ± 0	234 ± 0	22.6 ± 0.3	16.2 ± 0.2
RL (all)	**31**	23.2 ± 9.5	38.7 ± 0.3	273 ± 0	234 ± 0	22.5 ± 0.4	16.2 ± 0.2
TL (all)	**31**	23.1 ± 9.4	38.6 ± 0.7	273 ± 0	234 ± 0	22.4 ± 0.8	16.2 ± 0.2

3.1.3 End-Notched Flexure (ENF) Test - Mode II and Mixed Mode

The end-notched flexure test is also a three-point bending test, but rather than having the notch at the bottom, it has a notch on the side (end). It is designed to derive mode II fracture behaviour. Often the ENF test results show mixed-mode behaviour, from which the mode II can be derived. There is no standard for the application of the ENF test on timber. The setup for this study follows established research practice for timber [20]. Both radial-longitudinal (RL) and tangential-longitudinal (TL) crack systems were studied. The mid-plane pre-crack notch is cut on a milling machine (Figure A.21), and the specimen geometry is shown in Figure 3.4.

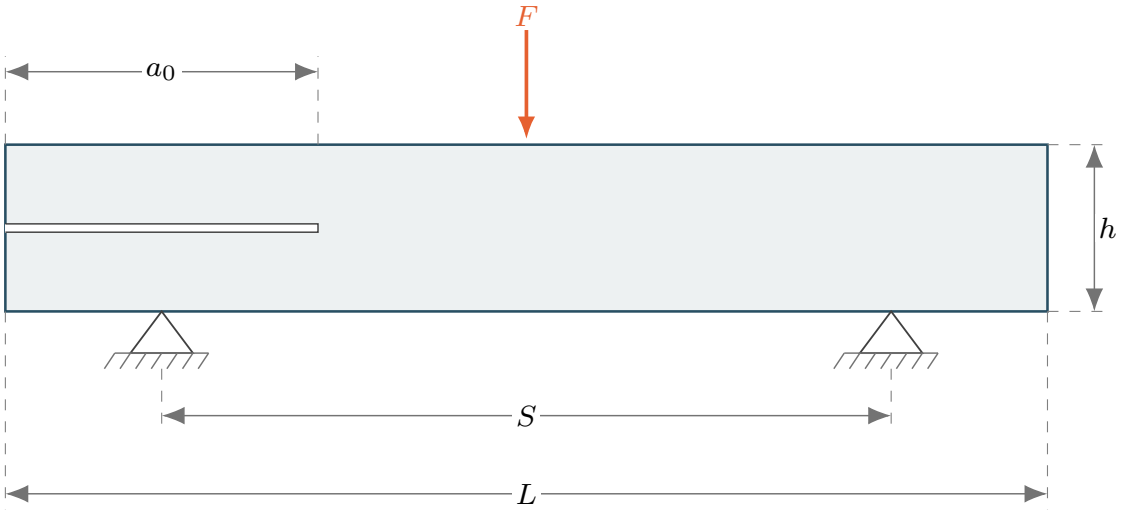

Figure 3.4: Free body diagram of the ENF (end-notched flexure) three-point bending test, with span L, beam height h, midplane pre-crack of length a_0 and applied load F.

Similarly to the SENB test, two thicknesses were tested. Sample variants are presented in Table 3.2.

This experiment was performed on an Instron 5985 machine with a 250 kN load cell and displacement controlled at a rate of 3 mm/min. Samples were cut from six beams of 83 x 86 mm with an average length of 1 m. Tests were carried out with a target test duration of 5 minutes, all tests are not shorter than 3 minutes, and not longer than 7 minutes. There is no ENF standard for timber (or LBL). ENF samples were also not climate conditioned leading to more brittle results. Relative humidity was logged throughout the tests and averaged 35%, matching the SENB tests (§3.1.2). Digital Image Correlation (DIC) was used as a backup mean to track the beam displacement.

Table 3.2: ENF test setup specimen geometry per crack system and load-point configuration

Group	n	b [mm]	h [mm]	L [mm]	S [mm]	a_0 [mm]	Load pt. [mm]
RL / A	5	26.3 ± 11.5	39.3 ± 0.2	273 ± 0	234 ± 0	57.5 ± 0.1	117.0 ± 0.0
RL / B	8	23.3 ± 10.0	39.3 ± 0.3	273 ± 0	234 ± 0	57.5 ± 0.1	97.5 ± 0.0
RL / C	10	24.4 ± 10.4	39.5 ± 0.1	273 ± 0	234 ± 0	57.4 ± 0.2	78.0 ± 0.0
RL / D	2	39.3 ± 0.1	38.9 ± 0.9	273 ± 0	234 ± 0	77.2 ± 0.0	117.0 ± 0.0
TL / A	5	26.7 ± 11.8	39.2 ± 0.4	273 ± 0	234 ± 0	56.4 ± 2.7	117.0 ± 0.0
TL / B	8	23.4 ± 9.8	39.3 ± 0.1	273 ± 0	234 ± 0	57.6 ± 0.2	97.5 ± 0.0
TL / C	10	24.5 ± 10.3	39.0 ± 1.2	273 ± 0	234 ± 0	57.5 ± 0.2	78.0 ± 0.0
TL / D	2	39.2 ± 0.1	39.2 ± 0.6	273 ± 0	234 ± 0	77.2 ± 0.0	117.0 ± 0.0
RL (all)	**25**	25.7 ± 10.5	39.3 ± 0.3	273 ± 0	234 ± 0	59.0 ± 5.5	95.2 ± 16.2
TL (all)	**25**	25.7 ± 10.4	39.2 ± 0.8	273 ± 0	234 ± 0	58.9 ± 5.6	95.2 ± 16.2

3.1.4 Tensile Test (TT) - Parallel and Perpendicular to Grain

A simple tensile test with rectangular samples was carried out to obtain a high-level estimate of tensile strength parallel and perpendicular to the grain. Four specimens were tested: three parallel to the grain (113-115) and one radial (116). The parallel batch supplies the $n = 3$ mean reported in §3.2.4. The single radial specimen is reported as a single-specimen estimate, not a sample mean. Tests were performed on an Instron 5985 machine under displacement control at 1 mm/min for the parallel (L) specimens and 0.3 mm/min for the radial (R) specimen. The test served primarily to calibrate the FEM model and to confirm the applicability of literature values. More tests were done but these are the only ones with valid results.

3.1.5 Splitting Capacity Test

Rather than deriving material properties, the splitting capacity test aims to measure the splitting resistance of beams with dowel-type connection, loaded perpendicular to the grain. The setup for this study follows established research practice for timber [33, 36]. The Eurocode 5 Gen 1 equation 8.4 was calibrated with this kind of test, as elaborated on section 2.2.1.

The test is carried out on two beam geometries: a) 1200 x 200 x 40 mm RL (flatwise section build-up) and b) 960 x 161 x 51 mm TL (edgewise section build-up). The first dimension is the support span S, set as $S = 6h$ on the flatwise specimens (exact). On the edgewise specimens the target $6h = 966$ mm is rounded down to the nearest 20 mm rig increment, giving $S = 960$ mm; all reported edgewise calibrations use this as-built span. The total beam length is $L = 8h$ in both cases (1600 mm flatwise, 1288 mm edgewise). The orientation of the lamellae relative to the loaded edge for each build-up is shown in Figure 2.1. The test setup, common to both geometries, is shown in Figure 3.5.

Both geometries have the dowel placed at an α-value (edge distance over total beam height) of 0.32, taken directly from Gómez-Royuela *et al.* [13] (European beech, splitting capacity at varied α) and close to the 0.33 used by Leijten [23] for multiple-connection splitting in timber. It also represents the limit set by timber edge spacing rules. 0.32 sit comfortably below the 0.7 splitting-governs threshold. Only single dowel connections were tested. Multi-row and column connections as well as multi-location connections were not tested. A 16 mm dowel of 8.8 grade steel was used, to ensure that the beam fails in splitting and no plastic deformation in the dowel takes place. Four tests were carried out for both variants respectively. Tests were performed on an Instron 5985 machine under displacement control at a rate of 1 mm/min. The samples were placed in the climate chamber for 24h before testing. The beam geometries, dowel diameter, and edge-distance ratio per section are summarised in Table 3.3.

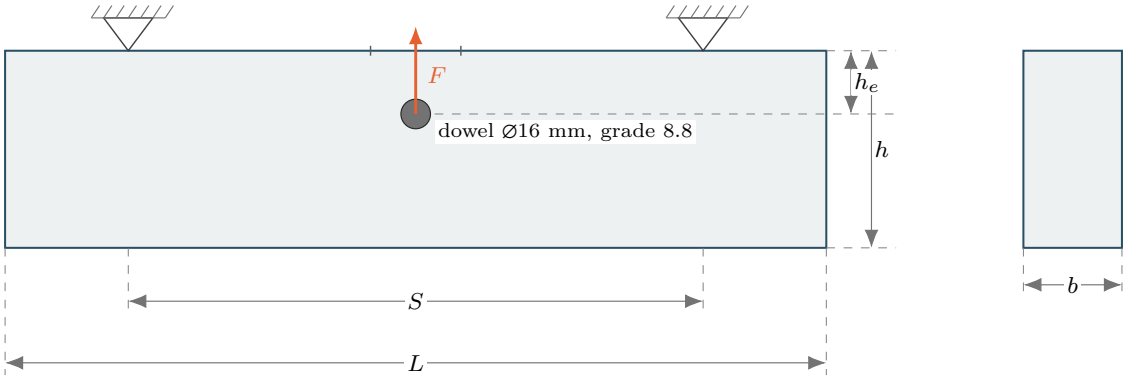

Figure 3.5: Splitting test setup. Inverted three-point bend with a single dowel at edge-distance h_e, $\alpha = h_e/h = 0.32$. Two specimen geometries: $1200 \times 200 \times 40$ mm flatwise (RL) and $960 \times 161 \times 51$ mm edgewise (TL).

Table 3.3: Splitting capacity test setup beam geometry, dowel diameter, and edge-distance ratio per section

Section	n	b [mm]	h [mm]	L [mm]	S [mm]	d [mm]	α	h_e [mm]
Flatwise (RL)	4	40.0 ± 0.0	200.0 ± 0.0	1600 ± 0	1200 ± 0	16	0.32	64.0
Edgewise (TL)	4	51.0 ± 0.0	161.0 ± 0.0	1288 ± 0	960 ± 0	16	0.32	51.5

3.1.6 Finite Element Method (FEM) Analysis

The role of FEM in this work is to support and validate the experimental tests, not to predict where a crack will form in LBL. All three models use a prescribed crack path: cohesive elements are placed only along the experimentally observed crack, so the simulations reproduce the load required to drive a crack along a fixed path rather than the path itself. Earlier exploratory runs that distributed cohesive elements throughout the mesh, letting the solver choose where the crack would initiate, produced fracture in locations that did not match the experimentally observed crack and were not used in the final results. Predictive (non-prescribed-path) modelling of LBL splitting is identified as future work in section 5.3.

Within these limits, finite element analysis was carried out for all three experimental studies. The solver used was LS-Dyna. The pre- and post-processor come from the Oasys LS-Dyna environment. Quad meshing was employed to mesh the geometry. The models were run under displacement control with full Newton solvers. An arc-length indirect method was attempted in order to track the post-peak snap-back regime but the solver could not follow the equilibrium path past peak load, so the snap-back behaviour is not captured experimentally nor numerically. The models were calibrated using the experimental results and mechanical properties derived from the literature (see section 2.1). The cohesive interface takes its critical Mode I energy release rate G_{IC} directly from the SENB experimental measurements (§3.2.2) without further tuning, so the FEM input that drives fracture is the same number that the chapter 4 EC5 Gen 1 calibration consumes.

All three models use a structured quad shell mesh with cohesive interface elements placed only along the experimentally observed crack path. The SENB mesh (Figure A.54) has a vertical cohesive ligament above the central notch and is meshed at a 0.5 mm element edge length on the depth-code 2 specimen geometry. The ENF mesh (Figure A.55) has an L-shaped cohesive interface, a horizontal pre-crack plane from the beam end to a point one beam height before midspan, then a 45 degree wedge rising to the loading point, meshed at a 1 mm element edge length. The two splitting models (Figure A.56 for the $1200 \times 200 \times 40$ mm RL geometry and Figure A.57 for the $960 \times 161 \times 51$ mm TL geometry) carry a horizontal cohesive band at the loaded-edge distance h_e and use an unstructured ring transitioning the structured grid to the 16

mm dowel hole at midspan. The splitting runs use a 5 mm mesh size. The mesh figures referenced here are reproduced at full size in Appendix~A.

3.2 Results and Analysis

In this section, the results from the experiments conducted are elaborated and further analysed, along with the FEM simulation. Throughout the results tables that follow, only ρ, MC, force, displacement, time, and specimen geometry are measured directly. Every fracture quantity (G_{IC}, G_{IIC}, K_{IC}, K_{IIC}), every modulus ($E_{\parallel}$, $E_{\perp}$), and every strength ($f_{t,\parallel}$, $f_{t,\perp}$, F_{split}) is derived from those measurements via the equations in chapter 2. Tables therefore do not flag each cell individually as measured or derived.

3.2.1 Density and Moisture Content Characterisation

The density and moisture content distributions are shown in Figure 3.6a and Figure 3.6b. Density was determined on $n = 10$ cubes, yielding a mean of 669.08 kg/m^3 (SD = 63.98 kg/m^3, CoV = 9.6%). Moisture content was determined on $n = 61$ samples, yielding a mean of 4.55% (SD = 0.98%, CoV = 21.6%).

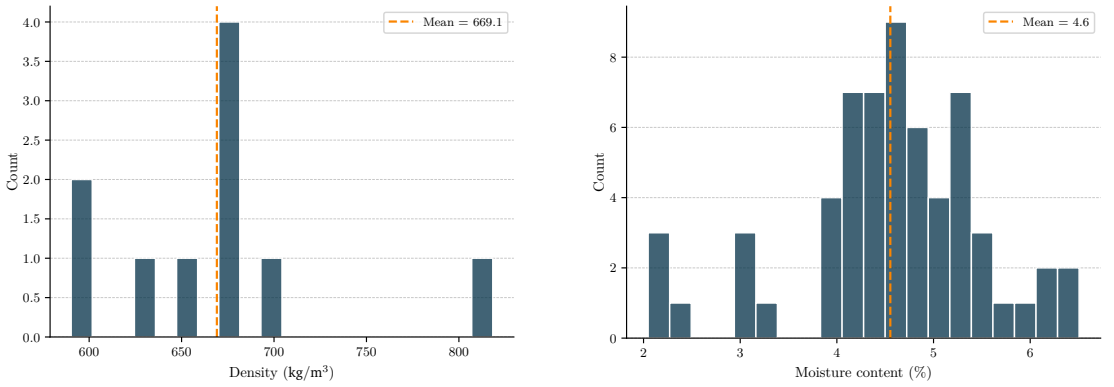

(a) Density across all specimens ($n = 10$, mean = 669.1 kg/m^3, $\sigma = 64.0$ kg/m^3).

(b) Moisture content across all specimens ($n = 61$, mean = 4.6 %, $\sigma = 1.0$ %).

Figure 3.6: Density and moisture content distributions of the LBL test material.

The average mean density is slightly below the manufacturer-published density of 700 kg/m^3. The measured MC of 4.55% is well below every documented LBL or timber reference point. AlRukaibawi *et al.* [2] tested the same MOSO N-finity product to ISO 23478-2022 and reported $\approx$ 7% MC at 65% RH. The wood-standard window for timber-fracture testing is 8-10% MC at the same climate. The MOSO N-finity datasheet itself (Appendix C, [28]) lists 10% MC at 20,°C / 65% RH and 8% MC at 20,°C / 50% RH. The samples in this study were drier than each of these baselines.

The 4.55% reflects the storage and lab climate. From delivery through cutting and testing, the SENB and ENF stock remained in the same uncontrolled indoor lab air, reaching equilibrium with the lab-average 35% RH (§3.1.2). Linear interpolation between the two MOSO N-finity datasheet anchors (8% MC at 50% RH and 10% MC at 65% RH) gives a hygroscopic slope of roughly 0.13 percentage-points of MC per 1% RH and extrapolates to about 6% MC at 35% RH. AlRukaibawi *et al.* [2] measured $\approx$ 7% MC at 65% RH on the same product, about 3 percentage-points below the datasheet, so an experimentally-implied equilibrium at 35% RH would sit lower still. The measured 4.55% sits inside this band.

Not conditioning the material has some advantages. 35% RH represents a more natural indoor environment and real-world service conditions, rather than the 65% RH of the test standards. To make the SENB results comparable with literature data measured at 65% RH, the Mode I fracture energies were corrected by applying the slope $dG_{IC}/d\mathrm{RH} = +7.6$ J/m^2 per percentage-point of relative humidity reported by Chen Qi *et al.* [9]. The Chen Qi slope is fitted to Mode I only, so no analogous correction is applied to the ENF (Mode II) data. Both uncorrected and corrected G_{IC} values are reported in section 3.2.2. The ENF results in section 3.2.3 are uncorrected. The calibration in chapter 4 uses the uncorrected dataset and inherits its conservatism (more brittle behaviour) (§3.3).

3.2.2 Single-edged Notched Beam (SENB) Test - Mode I

In Table 3.4, critical energy release rates and stress intensity factors for Mode I are given by the different calculation methods. Table 3.5 shows the results of different fracture systems as well as the two beam thickness. It can be seen that the Nordtest method (NT BUILD 422) calculation results for G_{IC} gives the lowest mean. There is quite a significant difference between applying orthotropic calculation and isotropic assumptions. The crack system has a larger effect on the results than the thickness (size) of the beam. RL has a higher mean G_{IC} compared to TL. The detailed calculation table can be found in Table A.1 in Appendix~A.

Table 3.4: Mode I method comparison

Property	Method	Unit	n	Mean	Std	CoV	Min	Max	$f_{0.05}$
G_{IC}	NT BUILD 422	J/m^2	62	200.98	57.49	28.6%	39.96	527.29	121.11
G_{IC}	LEFM SENB	J/m^2	62	376.10	150.65	40.1%	15.20	763.55	129.78
G_{IC}	LEFM SENB (Ortho)	J/m^2	62	239.21	94.03	39.3%	9.83	480.65	83.71
K_{IC}	LEFM SENB	MPa·m$^{1/2}$	62	0.722	0.138	19.1%	0.163	0.978	0.461
K_{IC}	Simplified	MPa·m$^{1/2}$	62	0.540	0.075	13.9%	0.264	0.813	0.419
K_{IC}	Orthotropic	MPa·m$^{1/2}$	62	0.676	0.093	13.7%	0.328	1.024	0.527

Table 3.5: Mode I by depth code and crack system

Group	n	G_{IC} NT (J/m^2)	G_{IC} LEFM (J/m^2)	G_{IC} LEFM Ortho (J/m^2)	K_{IC} LEFM	K_{IC} simpl.	K_{IC} ortho.
2_RL	23	208.48 ± 75.70	472.49 ± 150.79	297.42 ± 94.92	0.760 ± 0.124	0.505 ± 0.077	0.637 ± 0.097
2_TL	23	186.92 ± 40.60	310.42 ± 108.25	200.74 ± 70.00	0.719 ± 0.156	0.565 ± 0.076	0.703 ± 0.094
4_RL	8	229.98 ± 52.77	450.20 ± 55.72	283.39 ± 35.07	0.750 ± 0.046	0.534 ± 0.058	0.673 ± 0.073
4_TL	8	190.81 ± 30.26	213.75 ± 72.74	138.23 ± 47.04	0.598 ± 0.126	0.574 ± 0.048	0.714 ± 0.060
RL	31	214.03 ± 70.31	466.73 ± 132.28	293.80 ± 83.27	0.757 ± 0.108	0.513 ± 0.072	0.646 ± 0.091
TL	31	187.92 ± 37.76	285.47 ± 108.06	184.61 ± 69.88	0.687 ± 0.157	0.568 ± 0.069	0.706 ± 0.086
2	46	197.70 ± 61.04	391.45 ± 153.49	249.08 ± 95.86	0.739 ± 0.141	0.535 ± 0.081	0.670 ± 0.100
4	16	210.40 ± 46.21	331.97 ± 137.21	210.81 ± 85.01	0.674 ± 0.121	0.554 ± 0.055	0.693 ± 0.068

Table 3.6 shows the relative humidity corrected G_{IC} values. The Chen Qi +7.6 J/m^2 per percentage-point correction, applied across the ≈ 30 percentage-point gap between the lab climate (35% RH) and the literature reference (65% RH), shifts the SENB Mode I means from roughly 200 J/m^2 uncorrected to roughly 430 J/m^2 corrected. The corrected values land inside the literature window for LBL Mode I (§2.1.2, ≈ 508 J/m^2 RL, 338 TL).

Figure 3.7 shows the data cleaning result for SENB specimen. The initial slack on the machine is removed and the curve is shifted to the left. The plateau at around 10 N is completely removed. All calculated results are based on cleaned data.

Figure 3.8 shows the mean curves for RL and TL as well as the standard deviation band. It can be seen that the stiffness (the pre-peak slope) is almost identical in the two systems. The mean curves also largely overlap, although as has been mentioned before, the average G_{IC} value for RL is higher than TL, which can also be seen on the figure.

Table 3.6: RH-corrected G_{IC}

Parameter	Method	n	Mean (J/m^2)	Std	CoV	Min	Max	$f_{0.05}$
$G_{IC,TL}$	NT BUILD 422	31	415.92	37.76	9.1%	267.96	466.85	351.05
$G_{IC,RL}$	NT BUILD 422	31	442.03	70.31	15.9%	374.69	755.29	353.00
G_{IC}	NT BUILD 422	62	428.98	57.49	13.4%	267.96	755.29	349.53
$G_{IC,TL}$	LEFM SENB	31	513.47	108.06	21.0%	243.20	735.39	344.76
$G_{IC,RL}$	LEFM SENB	31	694.73	132.28	19.0%	457.52	991.55	501.80
G_{IC}	LEFM SENB	62	604.10	150.65	24.9%	243.20	991.55	381.86
$G_{IC,TL}$	LEFM SENB (Ortho)	31	412.61	69.88	16.9%	237.83	556.12	303.86
$G_{IC,RL}$	LEFM SENB (Ortho)	31	521.80	83.27	16.0%	372.48	708.65	398.69
G_{IC}	LEFM SENB (Ortho)	62	467.21	94.03	20.1%	237.83	708.65	326.83

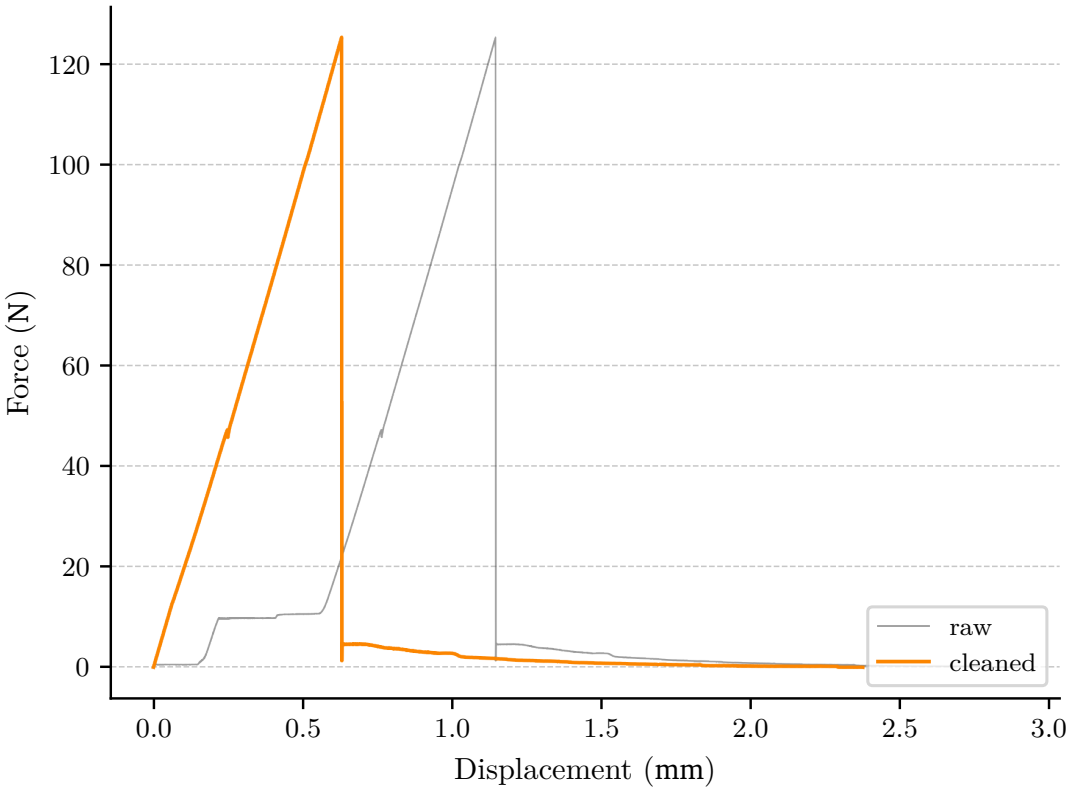

Figure 3.7: Example raw vs. cleaned data for SENB specimen.

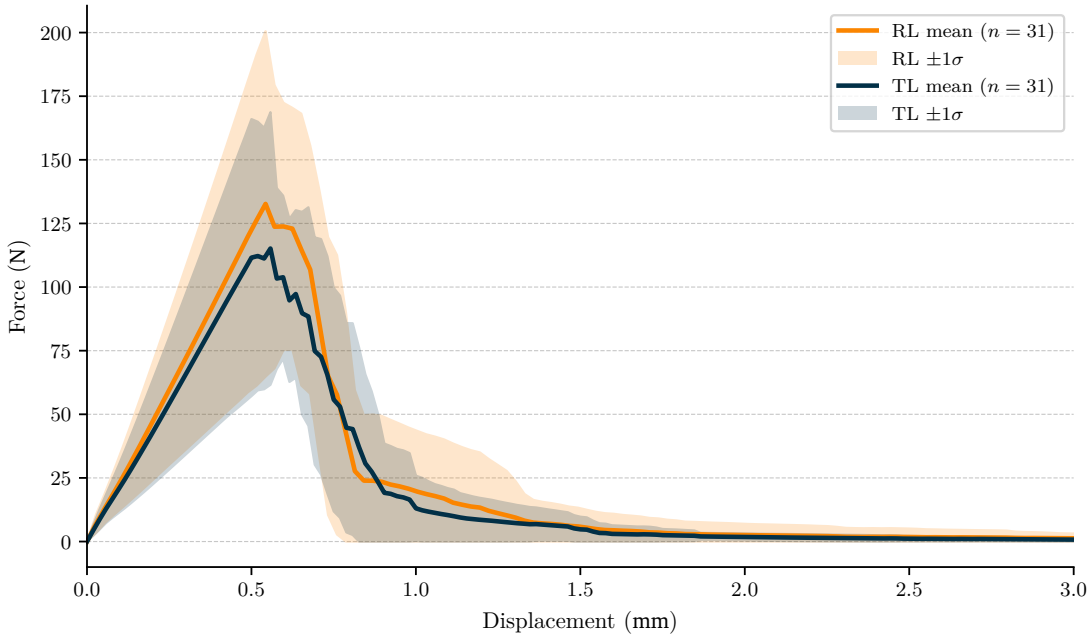

Figure 3.8: SENB load-displacement curves, all batches (cleaned), $n = 62$.

Lastly, Figure 3.9 shows the fail state of an SENB specimen after testing, as an example. The full set of fractured specimens is reproduced in Figure A.2 in Appendix~A. No glue-line separation was observed in any of the SENB specimens. The fracture surface ran through the bamboo fibres rather than along the lamella interfaces.

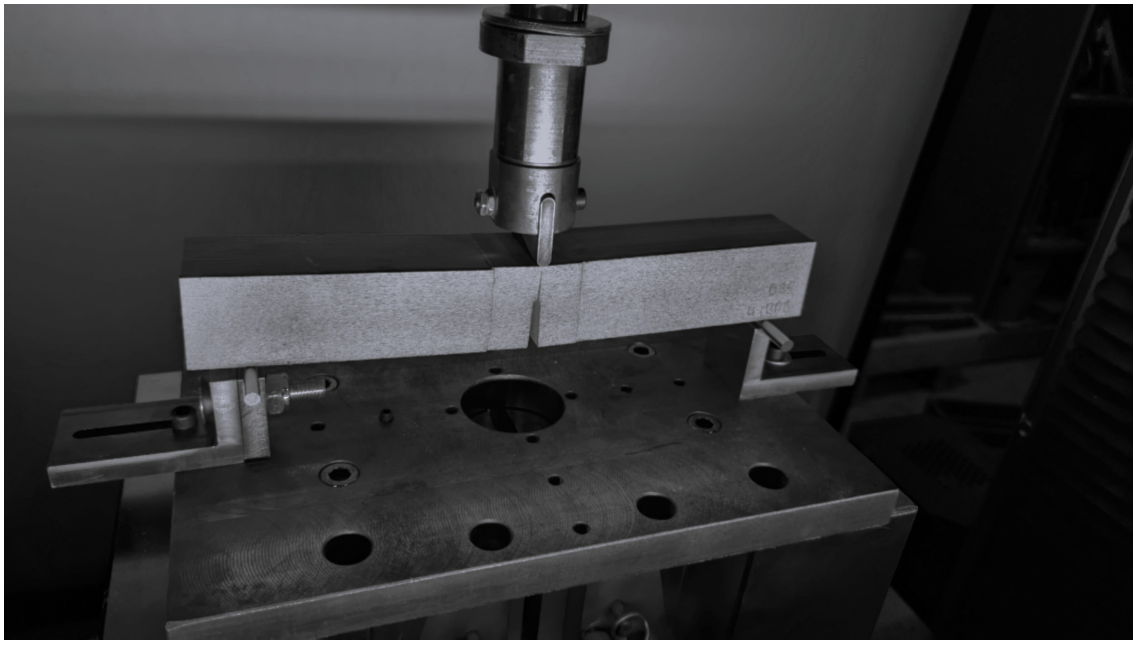

Figure 3.9: Representative fractured SENB specimen after a Mode I test.

3.2.3 End-Notched Flexure (ENF) Test - Mode II and Mixed Mode

Table 3.7 and Table 3.8 show the method calculations as well as crack system and beam thickness comparison for Mode II. It can be noted that the different calculation methods for Mode II result in much larger differences compared to Mode I. This can be explained with the fact that SENB test fails in a very clean Mode I results. On the other hand, ENF tests were all failed in Mixed Mode, not only Mode I or II. This means assumptions had to be made on the ratio between Mode I and II to calculate the values for only Mode II. The different calculation approaches all have different assumptions baked in. Similarly to Mode I, the results for RL are higher than the results for TL. The detailed calculation table can be found in Table A.4 in Appendix~A.

The spread between Mode II reduction methods, and the difficulty of separating Mode I from Mode II in the first place, both trace back to the underlying fracture mechanism. Mode I fracture in LBL is clean inter-fibre delamination: the crack runs as a near-planar surface between the bamboo fibres without rupturing them. Mode II loading instead forces the crack to break individual fibres and step between them, producing a rougher, non-planar fracture surface and routinely transitioning into mixed-mode failure. The extra energy spent on fibre breakage and the geometric tortuosity of the surface are part of why the four reduction methods of section 2.3.4 disagree on the ENF specimens but agree closely on SENB.

Table 3.7: Mode II method comparison

Property	Method	Unit	n	Mean	Std	CoV	Min	Max	$f_{0.05}$
G_{IIC}	CBBM	J/m^2	50	8687.46	3507.49	40.4%	2254.54	16315.66	3779.24
G_{IIC}	SBT	J/m^2	50	1148.38	277.95	24.2%	565.76	2214.67	767.51
G_{IIC}	TBT	J/m^2	50	2110.35	526.08	24.9%	1115.55	3225.16	1346.92
G_{IIC}	CCM	J/m^2	50	9423.22	2433.33	25.8%	4966.35	14790.57	5940.48
K_{IIC}	Orthotropic	MPa·m$^{1/2}$	50	1.754	0.253	14.4%	1.393	2.368	1.387

Further figures below illustrate and underline the results shown in the tables.

The final state of the test can be seen below in Figure 3.12. The full set of fractured specimens is reproduced in Figure A.22 in Appendix~A. As in the SENB tests, no glue-line separation was

Table 3.8: Mode II by depth code and crack system

Group	n	G_{IIC} CBBM (J/m^2)	G_{IIC} SBT (J/m^2)	G_{IIC} TBT (J/m^2)	G_{IIC} CCM (J/m^2)	K_{IIC} ortho.
2_RL	16	9336.42 ± 3779.55	1154.66 ± 189.10	2132.49 ± 359.61	9462.41 ± 1595.14	1.629 ± 0.134
2_TL	16	8355.18 ± 3587.07	1078.44 ± 374.01	2022.18 ± 671.63	8997.60 ± 3003.09	1.850 ± 0.312
4_RL	9	8830.76 ± 3280.67	1256.87 ± 220.36	2261.23 ± 436.26	10193.31 ± 2212.16	1.676 ± 0.156
4_TL	9	7981.15 ± 3468.76	1153.05 ± 268.67	2076.83 ± 610.85	9340.15 ± 2941.41	1.882 ± 0.277
RL	25	9154.38 ± 3546.42	1191.46 ± 202.59	2178.84 ± 385.02	9725.53 ± 1830.23	1.646 ± 0.141
TL	25	8220.53 ± 3476.53	1105.30 ± 335.89	2041.86 ± 637.99	9120.92 ± 2923.82	1.862 ± 0.294
2	32	8845.80 ± 3658.77	1116.55 ± 294.09	2077.33 ± 532.90	9230.00 ± 2377.14	1.740 ± 0.262
4	18	8405.95 ± 3304.27	1204.96 ± 244.28	2169.03 ± 523.60	9766.73 ± 2562.63	1.779 ± 0.242

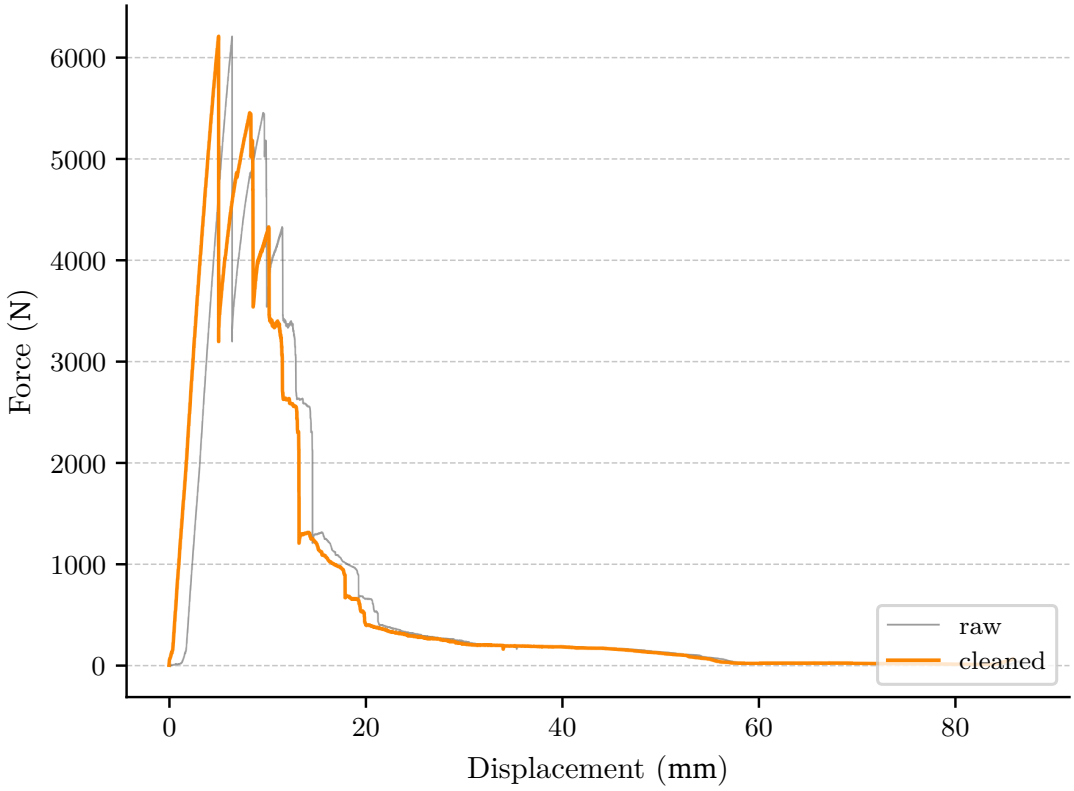

Figure 3.10: Example raw vs. cleaned data for ENF specimen.

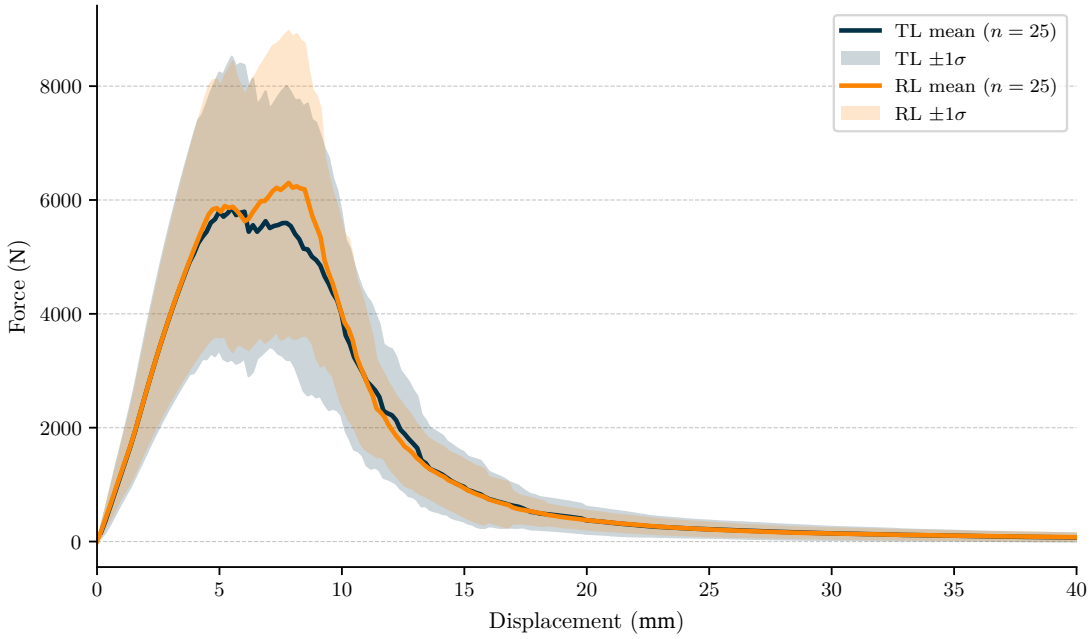

Figure 3.11: ENF load-displacement curves, all batches (cleaned), $n = 50$.

observed in any of the ENF specimens. The fracture surface ran through the lamellae rather than along the lamella interfaces.

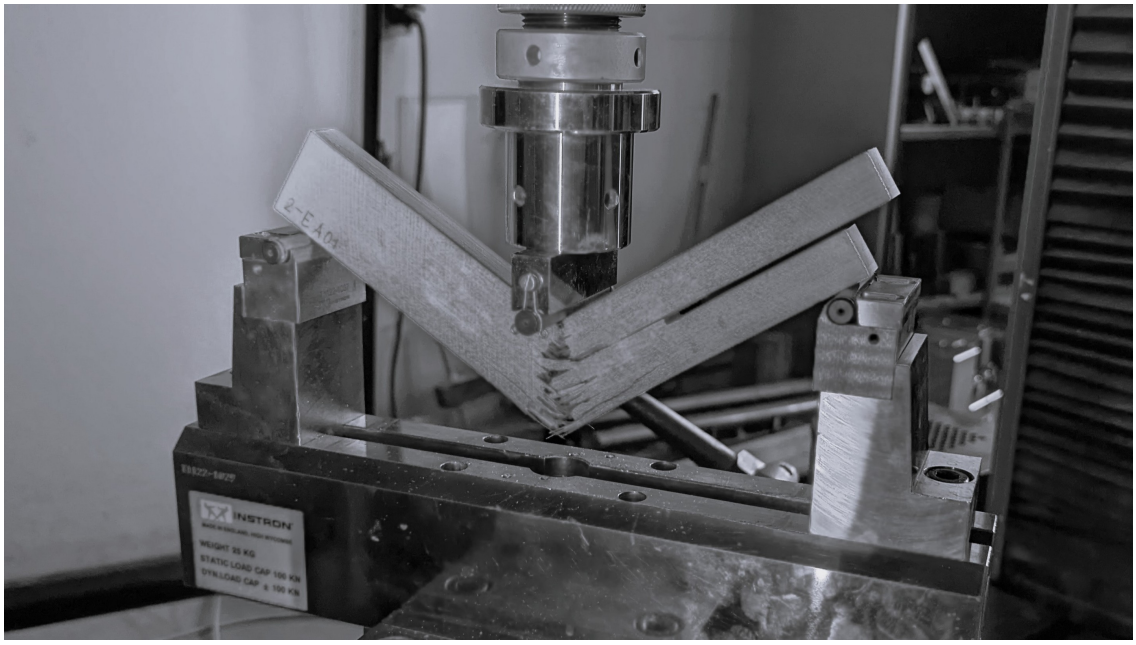

Figure 3.12: Representative fractured ENF specimen after a Mode II test.

3.2.4 Tensile Test (TT)

The tensile test setup is shown in Figure 3.13, with the rectangular LBL specimen clamped between the Instron grips. Tensile test results are shown in Figure 3.14.

The test results suggest a mean tensile strength of 65 MPa. These results are very similar to the 70 MPa derived from the literature [38, 39]. The test only produced one valid radial tensile strength result with a value of 2.7 MPa. This is significantly below the literature mean, and should be taken with a grain of salt. Since the size of the test specimens was limited to the size of the sample beam (approx. 8 x 8 cm), the radial and tangential tests were difficult to execute. Because of this, the values from the literature are used as the radial and tangential strengths in the FEM simulation.

Figure 3.13: Tensile test setup. Rectangular LBL specimen clamped between Instron grips for the parallel-to-grain (TT-L) test.

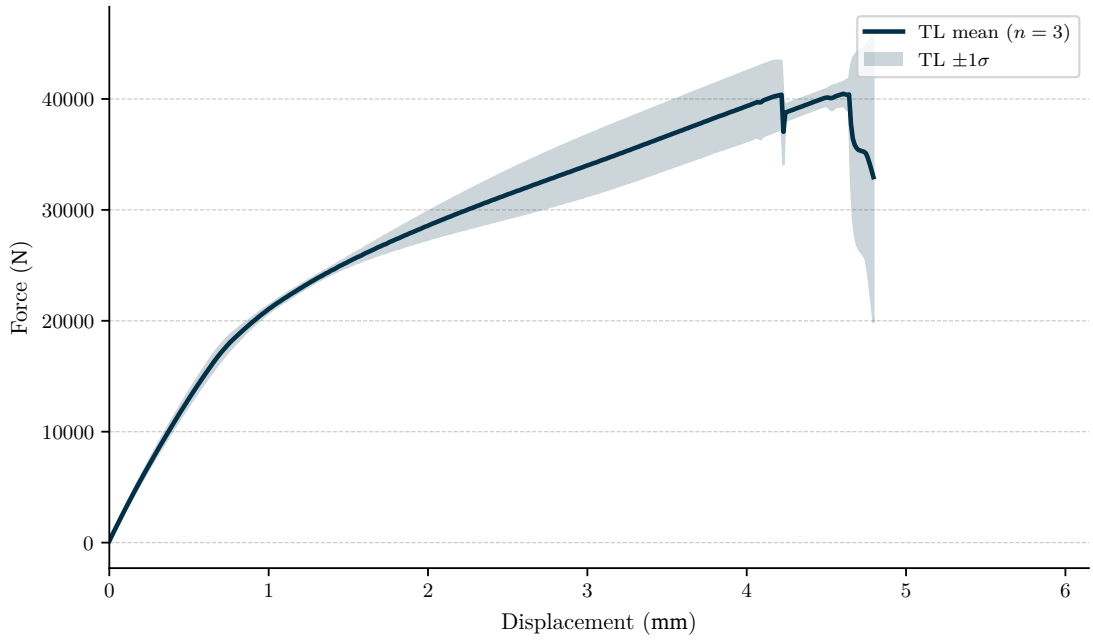

Figure 3.14: tensile load-displacement curves, batch TT-L (cleaned), $n = 3$.

3.2.5 Splitting Capacity Test

Although the splitting test was conducted with only four samples per test, they showed clear results. The coefficient of variation (CoV) of the tests was around 13%, indicating low spread of results. Table 3.9 shows the same result overview as was originally given in the work from Van der Put and Leijten [33]. The shear force applied is calculated as half of the force applied on the dowel. The difference between flatwise (RL) and edgewise (TL) can be seen in the result, supporting the fracture tests. The $C_{\text{mean}} = \sqrt{GG_c}$ fracture parameter can be calculated from the result to be around 16.9 for flatwise (RL) and 12.5 for edgewise (TL). The detailed calculation is shown in Table A.7 in Appendix~A. It has to be noted that for the dowel connection loaded perpendicular to the grain, the splitting behaviour was clearly dominated by Mode I splitting, rather than Mixed Mode or Mode II splitting. The connection first shows embedment (mean 0.81 mm, SD 0.23 mm across the eight specimens) before splitting starts. The 16 mm (Grade 8.8) dowel showed no deformation during the test.

Table 3.9: Splitting tests results per section build-up

Section	n	d (mm)	α	h_e (mm)	$F_{\text{max,mean}}$ (N)	$F_{\text{max},k}$ (N)	V_{mean} (N)	V_k (N)	$F/(b\alpha h)$ (MPa)	$\eta = S/h$	$\sqrt{GG_c}_{,\text{mean}}$	$\sqrt{GG_c}_{,k}$
Flatwise (RL)	4	16	0.32	64.0	16902	13300	8451	6650	6.60	6.00	16.869	13.274
Edgewise (TL)	4	16	0.32	51.5	14298	10360	7149	5180	5.44	5.96	12.475	9.038

Machine slack removal from the data is shown in Figure 3.15. The deformation is also corrected by embedment.

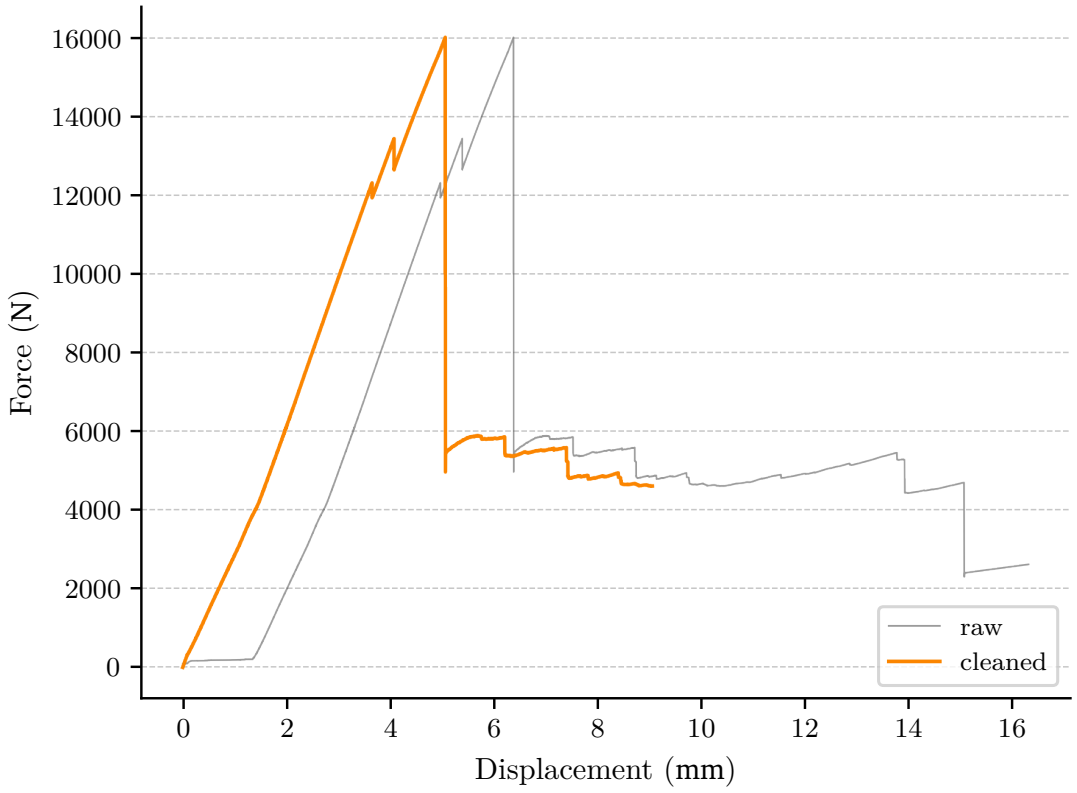

Figure 3.15: Example raw vs. cleaned data for splitting specimen.

The experimental results of the splitting can be seen in Figure 3.16. Consistently with the fracture test results, the flatwise (RL) mean is higher than the edgewise (TL) mean.

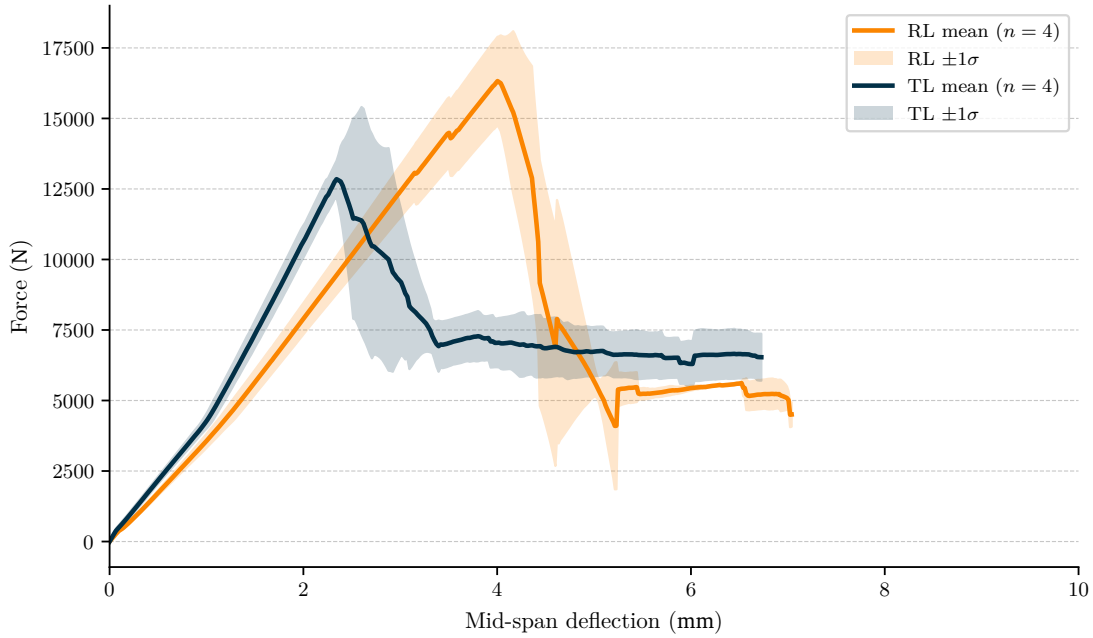

Figure 3.16: splitting force vs. mid-span deflection, all batches (cleaned), $n = 8$.

The crack opening was measured alongside the mid-span deflection. Figure 3.17 shows how the total measured displacement breaks down across the four LVDT-derived channels: the at-dowel sensor, the top of the beam, the crack opening, and the cumulative embedment derived from |LVDT-07| − LVDT-09 (truncated at peak force).

Figure 3.18 and Figure 3.19 show the clean horizontal splitting found in all eight test specimens. The full-beam view of a fractured specimen is reproduced in Figure A.40 in Appendix~A. The fibres clearly delaminated. The splitting happened inside the lamellae rather than at the lamella interfaces.

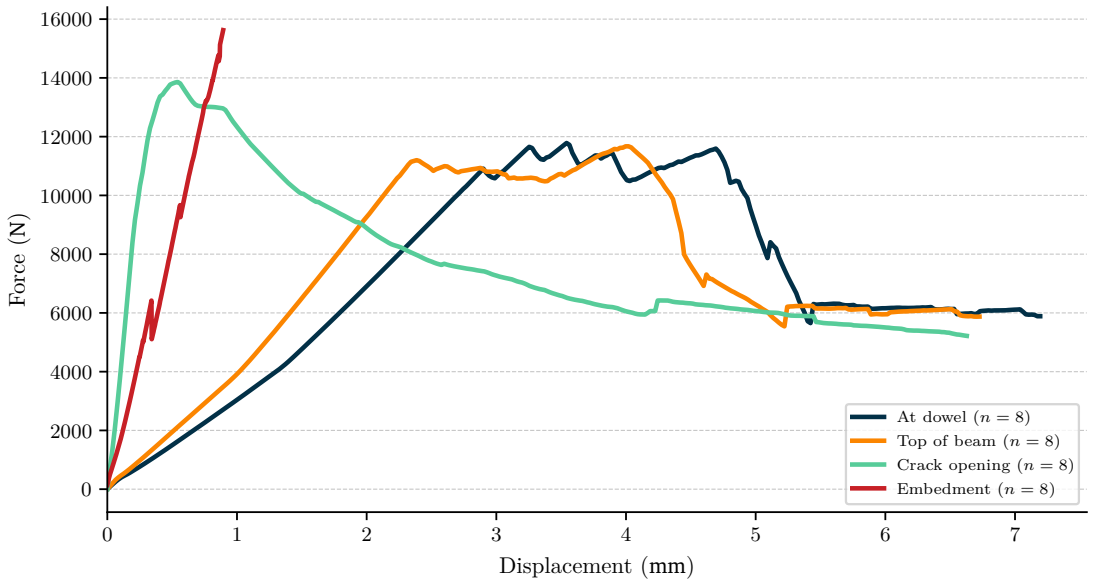

Figure 3.17: Splitting displacement decomposition: channel-mean force vs. displacement for the four LVDT-derived channels (all batches (cleaned), $n = 8$).

Figure 3.18: Representative fractured splitting specimen, edgewise 960 x 161 x 51 mm TL geometry.

Figure 3.19: Detail view of the fracture surface at the dowel hole.

3.2.6 Finite Element Method (FEM) Analysis

With the crack path fixed by the prescribed cohesive layer (section 3.1.6), the FEM simulations reproduce the measured force-displacement response across all three test types. They do not predict crack initiation or location. SENB and splitting match the experimental F/d curves best. ENF follows the same general shape but with a large deviation.

The SENB simulations overlaid on the experimental curves are shown in Figure 3.20 (TL) and Figure 3.21 (RL). For both crack systems the simulated F/d response, pre-peak stiffness, displacement at peak, and the area under the curve up to the first major drop, falls within the experimental scatter band given the prescribed crack path.

The ENF overlays are shown in Figure 3.22 (TL) and Figure 3.23 (RL). The simulated curves deviate from the experimental range. Because the prescribed crack path approximates the real fracture as a single planar surface, which is a good approximation of the clean inter-fibre delamination seen in SENB and splitting (section 3.2.3) but a rough one for ENF: in the real ENF specimens, the Mode II / mixed-mode crack ruptures individual fibres and steps between them, producing a complex, non-planar fracture surface that a single planar cohesive layer cannot represent. SENB and splitting setup reproduce well precisely because the prescribed-path assumption matches the clean Mode I delamination they exhibit. Post-peak results for ENF are limited and unreliable for the same reasons.

The splitting capacity simulations reproduce the measured F/d curves closely on both geometries. Figure 3.24 shows the flatwise (RL) configuration and Figure 3.25 the edgewise (TL). Pre-peak stiffness, displacement at peak, and the area under the F/d curve up to the first major drop all remain within the experimental scatter band, given the prescribed crack path.

The methodology behind these results (prescribed crack path along the experimentally observed crack, the failed exploratory runs with distributed cohesive elements, and the unsuccessful arc-length attempt at tracking post-peak snap-back) is documented in section 3.1.6. The simulated F/d curves therefore stop short of the snap-back regime, and any deviation from the experimental

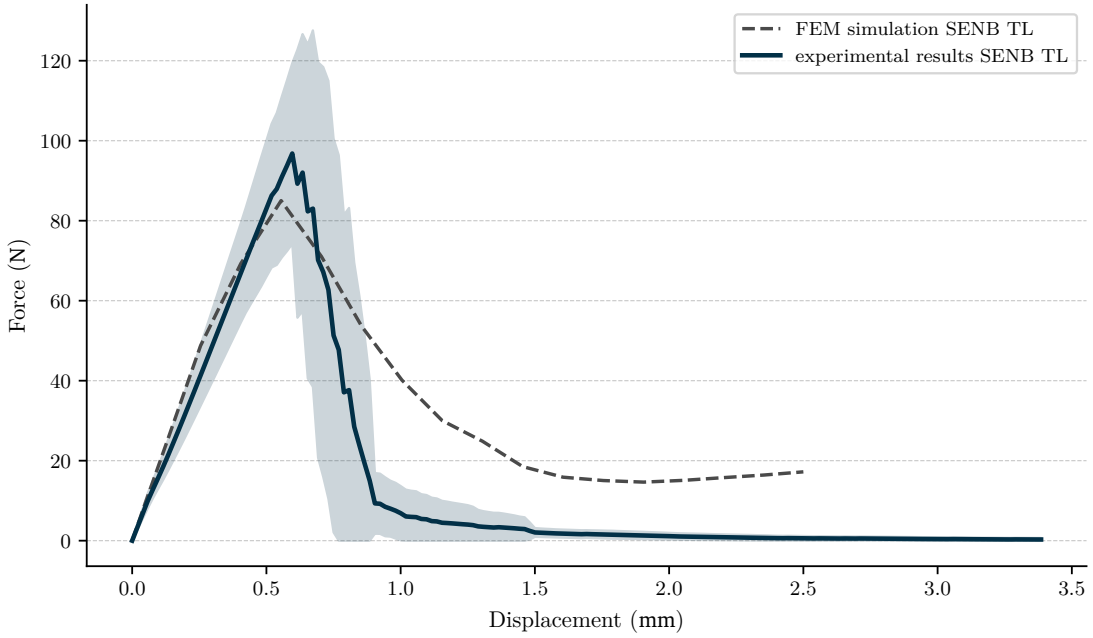

Figure 3.20: FEM vs. experimental mean SENB TL.

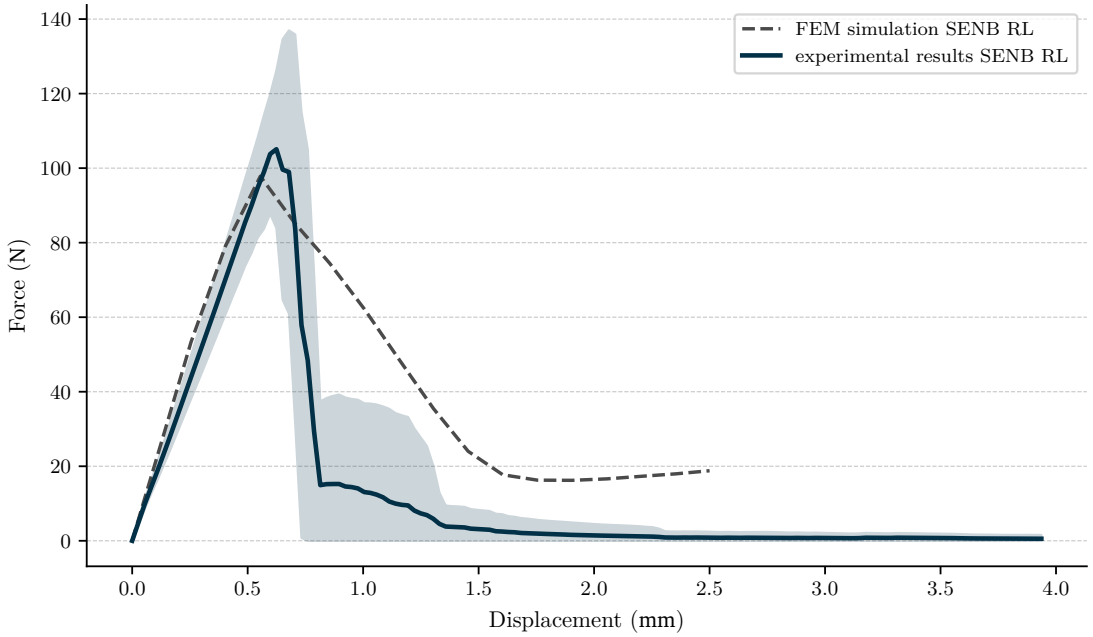

Figure 3.21: FEM vs. experimental mean SENB RL.

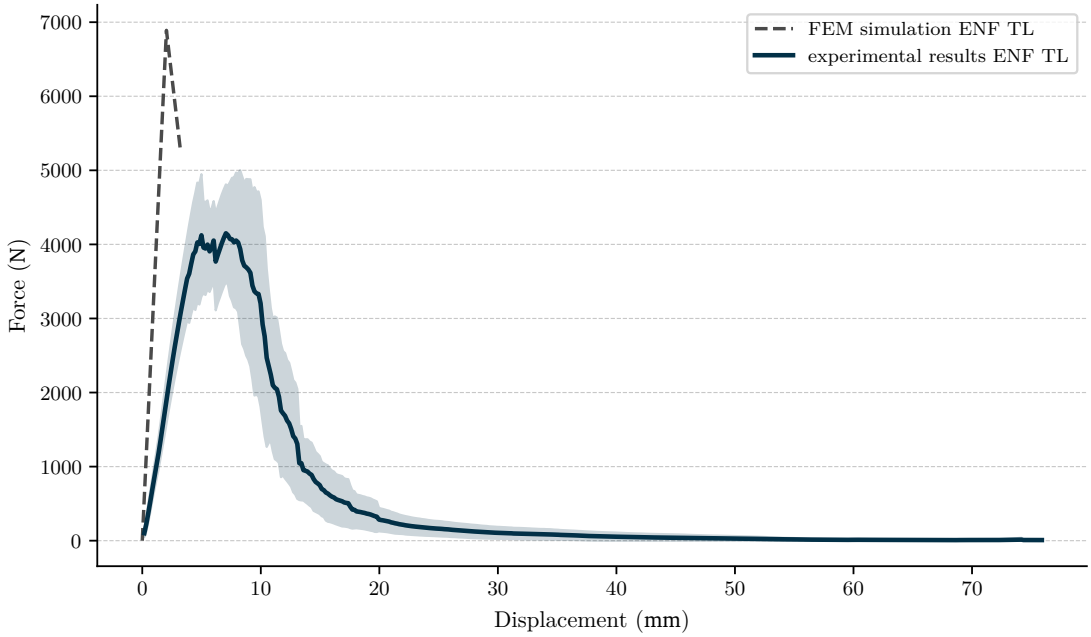

Figure 3.22: FEM vs. experimental mean ENF TL.

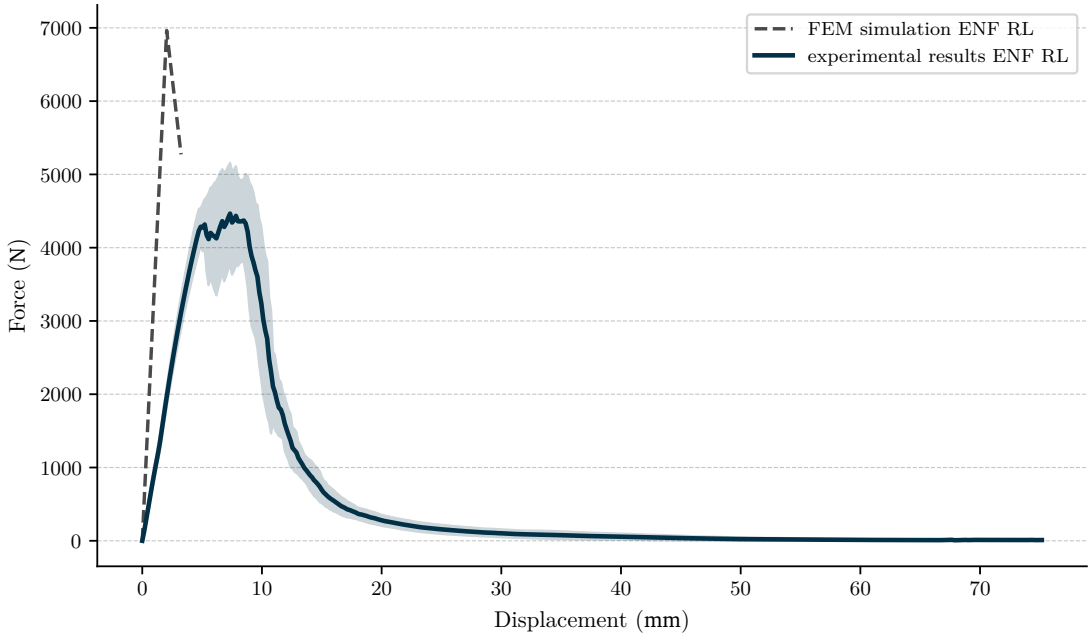

Figure 3.23: FEM vs. experimental mean ENF RL.

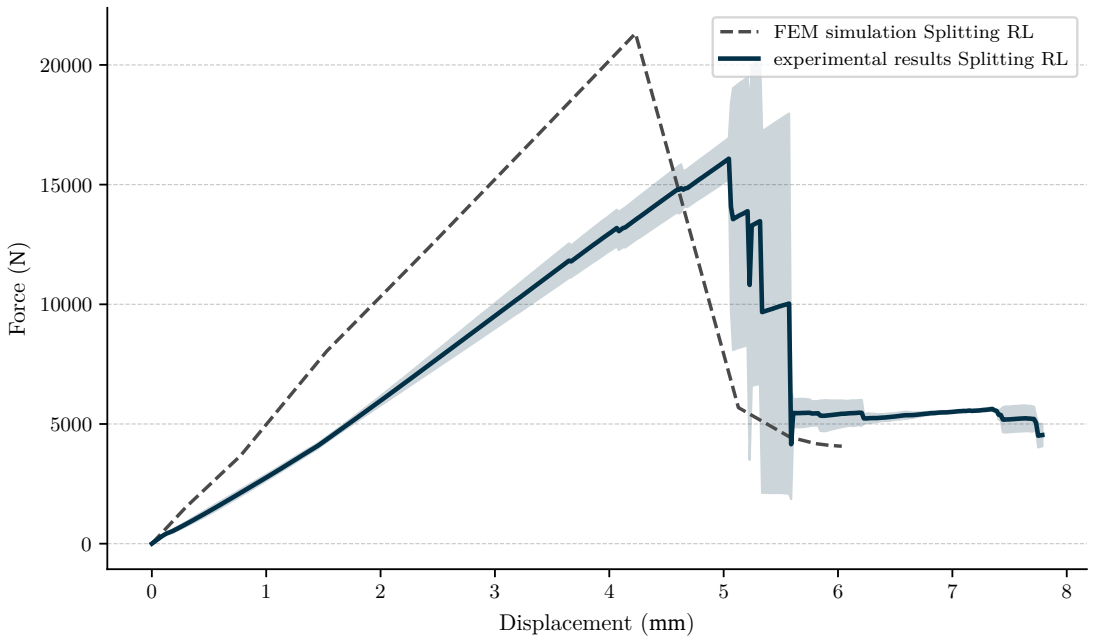

Figure 3.24: FEM vs. experimental mean Splitting RL.

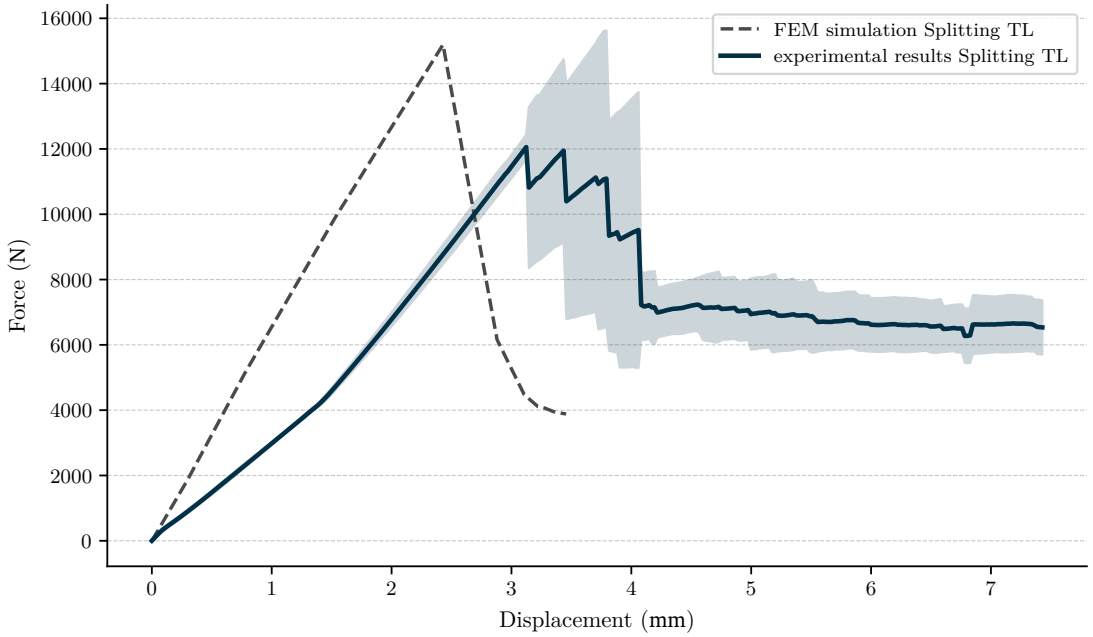

Figure 3.25: FEM vs. experimental mean Splitting TL.

curves is read here as an FEM-vs-experiment validation result, not as a prediction error of the crack location.

Representative FEM result displacement fields per test type and crack systems are shown in Figure 3.26 and Figure 3.27 for SENB, Figure 3.28 and Figure 3.29 for ENF, and Figure 3.30 and Figure 3.31 for the splitting capacity test.

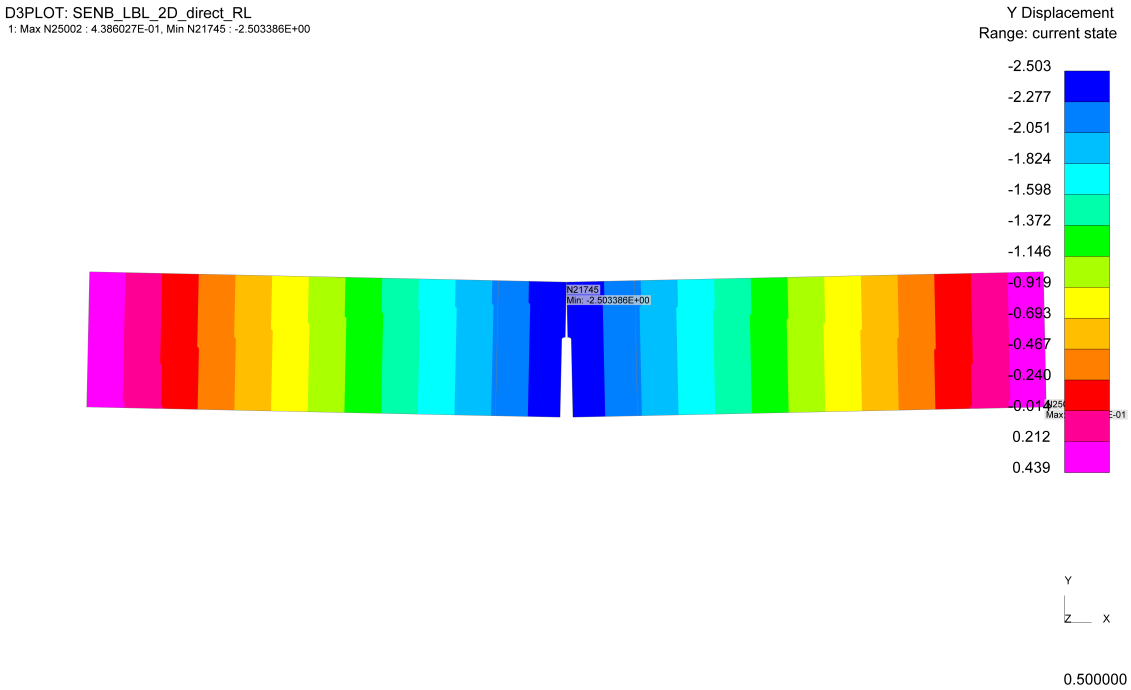

Figure 3.26: FEM result displacement field for SENB, RL crack system. Displacements in [mm].

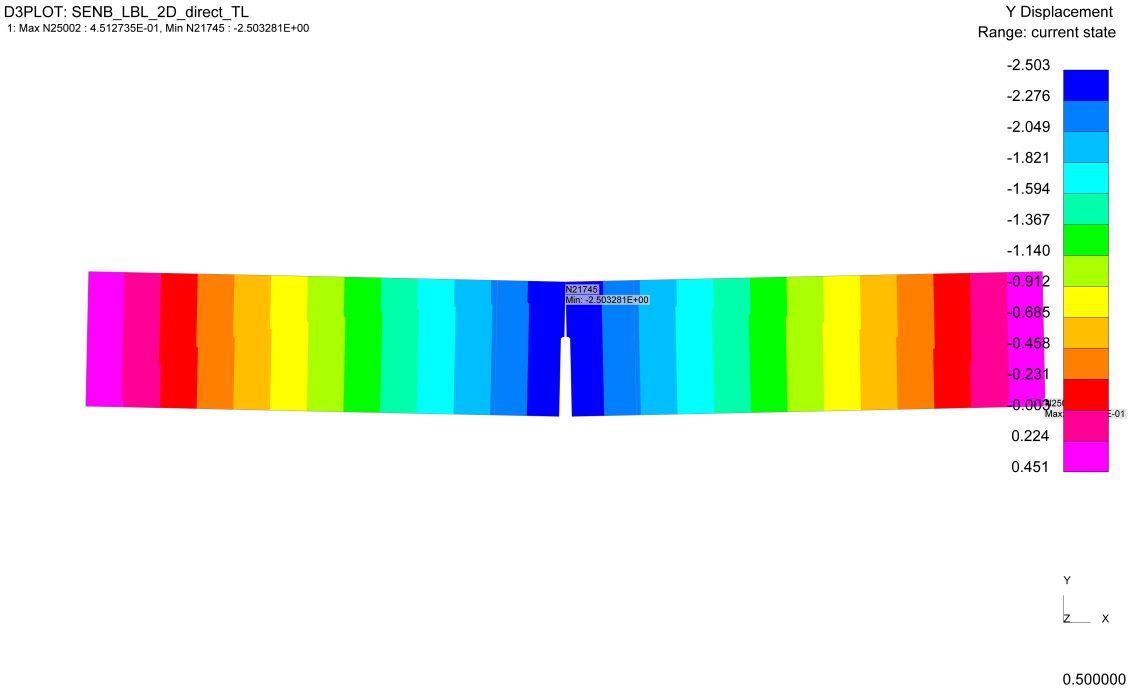

Figure 3.27: FEM result displacement field for SENB, TL crack system. Displacements in [mm].

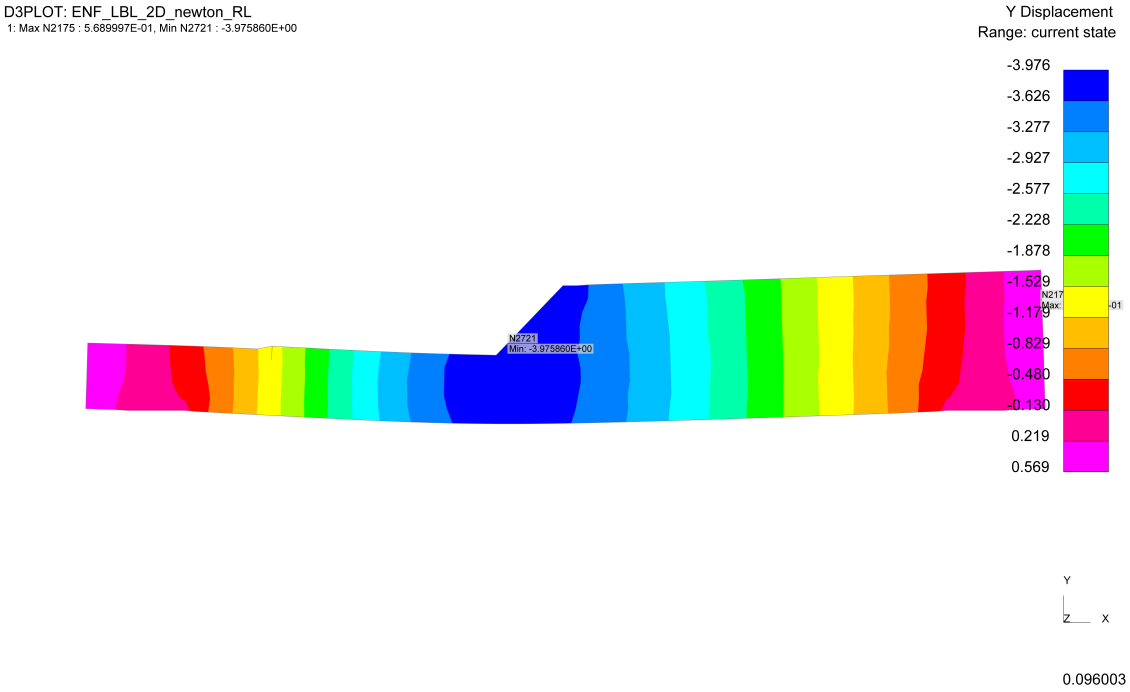

Figure 3.28: FEM result displacement field for ENF, RL crack system. Displacements in [mm].

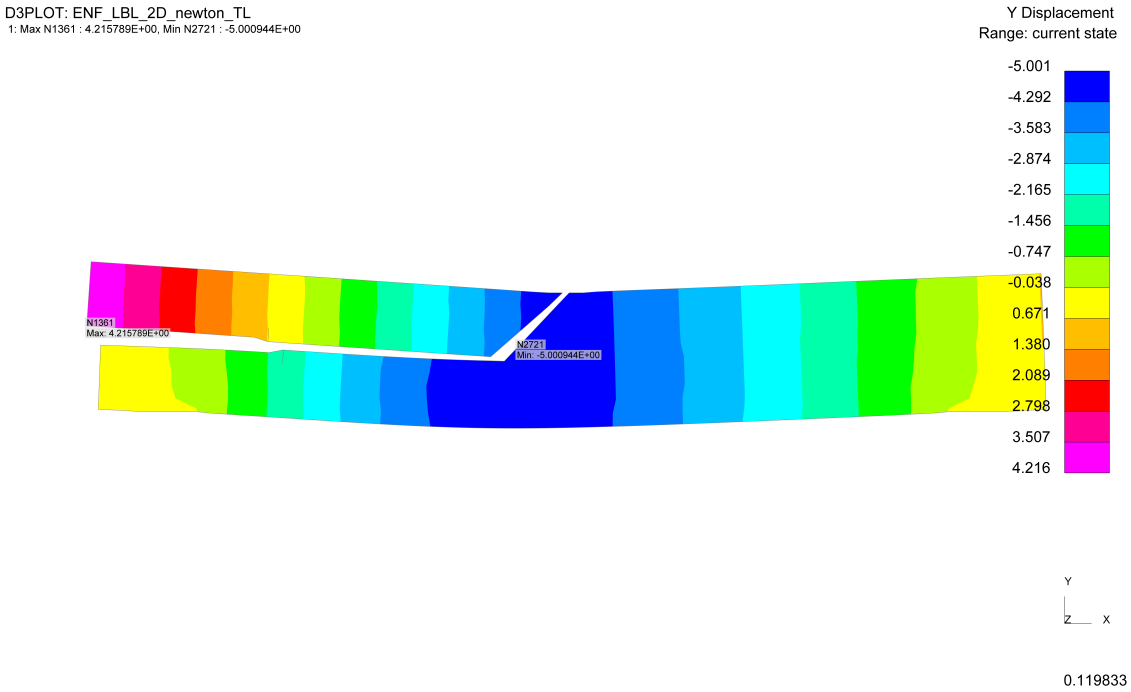

Figure 3.29: FEM result displacement field for ENF, TL crack system. Displacements in [mm].

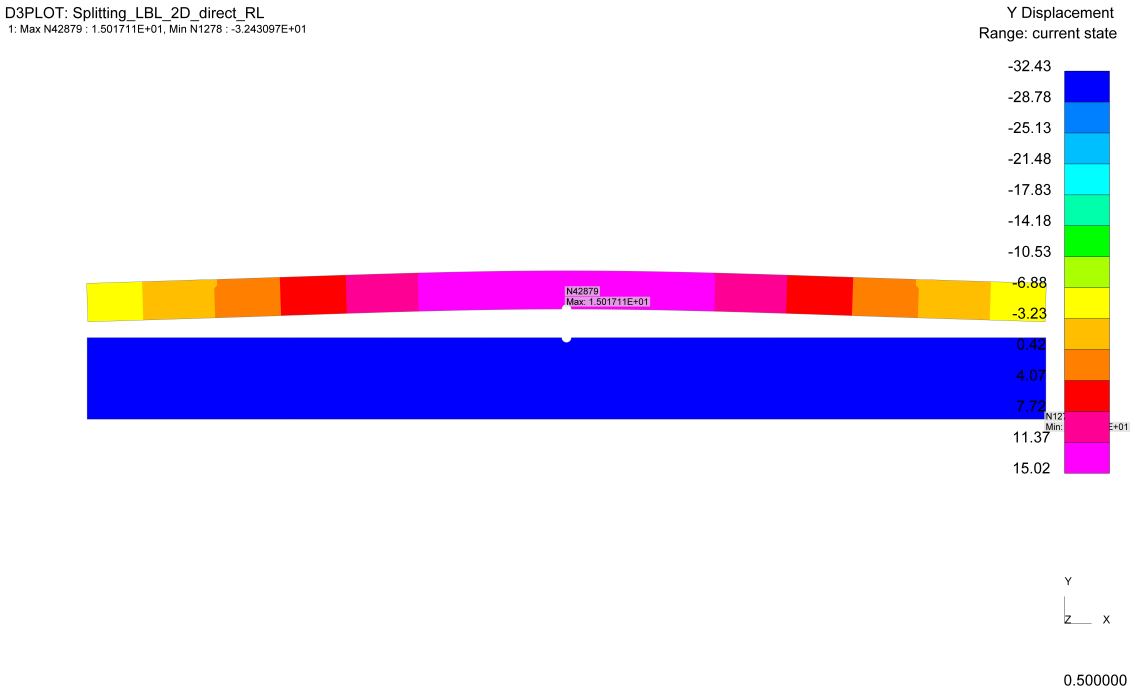

Figure 3.30: FEM result displacement field for the splitting test, RL crack system, 1200 x 200 x 40 mm geometry. Displacements in [mm].

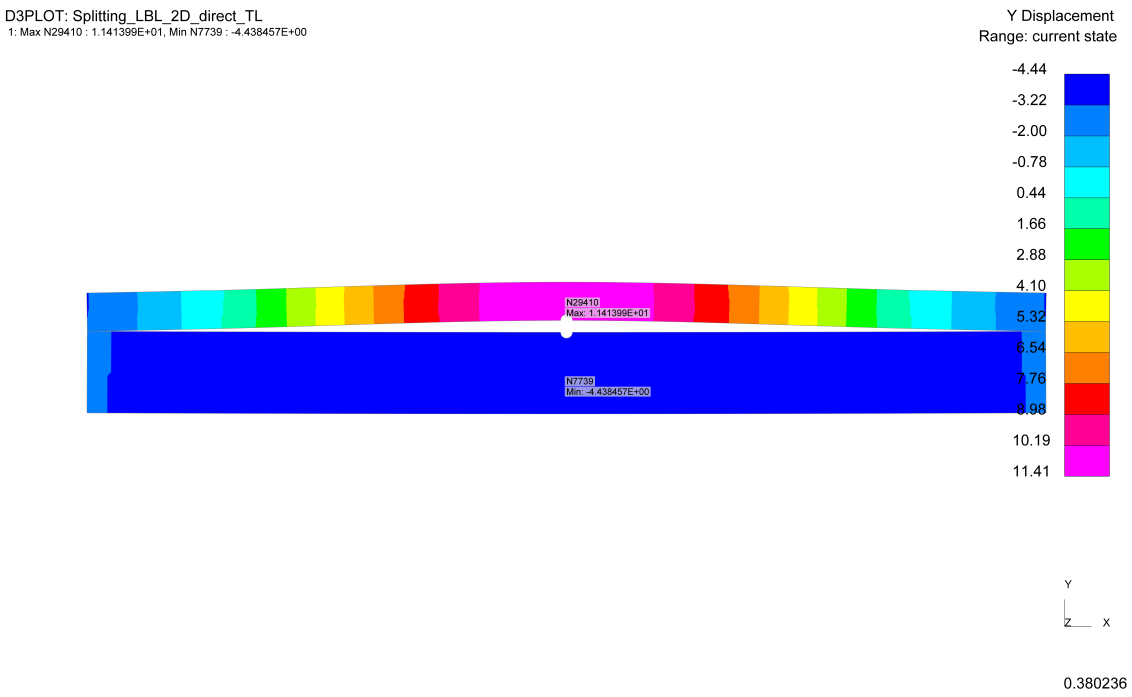

Figure 3.31: FEM result displacement field for the splitting test, TL crack system, 960 x 161 x 51 mm geometry. Displacements in [mm].

3.3 Discussion - Experiments and Simulation

This section discusses the experimental and numerical findings of section 3.2, and answers the chapter's six research questions.

The chapter 4 EC5 calibration takes its inputs from §3.2: full-scale splitting capacities, SENB G_{IC} values, and supporting elastic and tensile parameters. Gen 1 uses both the splitting capacities and the SENB G_{IC}, Gen 2 uses the splitting capacities alone, and ENF feeds neither calibration. RL > TL across SENB, ENF, and full-scale splitting, so the same crack-system asymmetry carries from small-scale fracture to engineering-scale splitting capacity. Splitting under perpendicular-to-grain dowel load is Mode I dominated, with intra-lamella fibre delamination and no glue-line separation observed in any test. The intra-lamella result means the EC5 constants $C_{LBL,k}$ and $k_{\text{mat},LBL}$ encode bamboo-fibre fracture rather than adhesive failure.

The dataset was relatively dry. Specimens were tested at 35% RH (MC 4.55%) against the 65%-RH literature baseline of [2]. The Chen Qi correction (§3.2.2) lifts the SENB Mode I means into the literature window of §2.1.2 but the chapter 4 calibration uses the uncorrected dataset and inherits its conservatism (more brittle behaviour). The proposed $C_{LBL,k}$ (§4.1) and $k_{\text{mat},LBL}$ (§4.2) therefore represent lower-bound values.

The FEM validates the experimental interpretation in energy terms (pre-peak stiffness, displacement at peak, work of fracture) rather than as a peak-load match (§3.1.6, §3.2.6). SENB and splitting reproduce all three features within an acceptable range. ENF diverges more substantially because the prescribed simplified crack path cannot capture the more complex Mode II and mixed-mode fracture seen experimentally.

Summary of findings:

- RL > TL across SENB, ENF, and full-scale splitting: the same crack-system asymmetry carries from small-scale fracture to engineering-scale splitting capacity.
- Splitting under perpendicular-to-grain dowel load is Mode I dominated, with $C_{\text{mean}} \approx 16.9$ N/mm$^{1.5}$ on RL and 12.5 on TL.

- Intra-lamella fibre fracture governs in every test, with no glue-line separation observed.
- The dataset was relatively dry (4.55% MC vs the 8-10% timber-test window). The Chen Qi RH correction lifts SENB Mode I into the literature range (§3.2.2).
- The chapter 4 EC5 calibration uses the uncorrected dataset and inherits its conservatism (more brittle behaviour).
- FEM with prescribed crack path reproduces SENB and Splitting in pre-peak stiffness, displacement at peak, and work of fracture. ENF diverges because the simplified crack-path and complex Mode II and mixed-mode behaviour.
- Splitting and SENB routes converge on flatwise and diverge on edgewise.

RQ-4 - What are the experimental Mode I fracture characteristics of laminated bamboo lumber? - SENB returned higher mean G_{IC} in RL than in TL. - Derivation methods (NT BUILD 422 work-of-fracture, isotropic LEFM, orthotropic LEFM) give different absolute values. The orthotropic form runs higher than the isotropic form because LBL is strongly anisotropic. - Crack system has a larger effect on G_{IC} than specimen thickness, so the calibration is not overly sensitive to specimen geometry. - Tested at 35% RH against the 65%-RH literature baseline. Chen-Qi-corrected values land in the literature range ($\approx$ 508 J/m^2 RL, 338 TL). The chapter 4 EC5 calibration uses the uncorrected dataset, inheriting a conservative fracture-energy floor (§3.3). - No glue-line separation was observed in any SENB specimen. The fracture surface ran through the bamboo fibres rather than along the lamella interfaces.

RQ-5 - What are the experimental Mode II fracture characteristics of laminated bamboo lumber? - ENF returned higher means in RL than in TL, mirroring the SENB ranking. - Four derivation methods (SBT, TBT, CBBM, CCM) gave a wider spread than the SENB Mode I methods because ENF specimens routinely failed in mixed-mode rather than pure Mode II, and each approach holds a different mode-split assumption. - CBBM is reported as the primary method because it tracks an equivalent crack length over the full F/d curve rather than reading only an initiation point. - No glue-line separation was observed in any ENF specimen. - Mode II results are reported for completeness and physical interpretation. They do not feed any chapter 4 calibration since EC5 eq. 8.4 / 11.54 is a Mode I splitting dominated.

RQ-6 - What is the fracture behaviour of laminated bamboo lumber for connections loaded perpendicular to the grain? - Mode I dominated fracture in the splitting tests, with little observed Mode II contribution. - Fracture parameter $C_{\text{mean}} = \sqrt{GG_c}$ at $\approx$ 16.9 N/mm$^{1.5}$ in flatwise (RL) and $\approx$ 12.5 in edgewise (TL), a ratio close to the SENB Mode I asymmetry. - Coefficient of variation $\approx$ 13% across the eight specimens, a tight distribution for the small sample size. - Embedment under the 16 mm grade-8.8 dowel preceded splitting (mean 0.81 mm, SD 0.23 mm) but did not progress to full embedment failure. The dowel showed no plastic deformation. - No glue-line separation was observed. Fracture ran through the lamellae.

RQ-7 - Can the experimental results be numerically reproduced? - Yes for SENB and splitting, partially for ENF. - The FEM uses a prescribed crack path with cohesive elements placed only along the experimentally observed fracture plane (§3.1.6), so it reproduces the load-displacement response rather than predicting where the crack will form. - The cohesive interface takes its mode I and mode II results directly from the experiments.

RQ-8 - How do experimental results compare to literature values? - Uncorrected SENB Mode I means sit below the literature range for LBL ($\approx$ 508 J/m^2 RL, 338 TL) because specimens were tested at 35% RH rather than the 65%-RH literature reference. - After the Chen Qi correction (+7.6 J/m^2 per percentage-point), means shift from $\approx$ 200 to $\approx$ 430 J/m^2 and land inside the literature window. - ENF Mode II values are sparser in the literature ($\approx$ 967 J/m^2 TL only). The comparison is less anchored. - Tensile testing confirmed the literature parallel-to-grain strength on the three specimens. The single radial specimen is reported as a single-specimen estimate, not a sample mean (§3.2.4). - The chapter 4 calibration uses the RH-uncorrected dataset, inheriting a conservative input.

RQ-9 - How do fracture properties derived from small-scale testing translate to full-scale splitting capacity? - Small-scale SENB G_{IC} feeds the EC5 Gen 1 splitting equation through $C = \sqrt{GG_c/0.6}$ (Route B). - Full-scale splitting tests independently solve for $C_{LBL,k}$ from the

measured $F_{\max}$ (Route A). - Both routes are evaluated against the same target in chapter 4. They agree on flatwise and diverge on edgewise. The divergence is attributed in §4.1 to the literature shear modulus used. - The translation from small-scale fracture energy to full-scale splitting capacity therefore works on flatwise and is bounded by the literature G_{shear} assumption on edgewise.

Chapter 4

Regulatory and Design Implications

In this chapter, the regulatory and design implications for splitting capacity of dowel-type connection loaded perpendicular to the grain are discussed based on the experimental results presented in Chapter 3. This chapter addresses RQ-10 (EC5 Gen 1 calibration), RQ-11 (EC5 Gen 2 calibration), and RQ-12 (practical design learning).

4.1 EC5 Gen 1 - Equation 8.4 Calibration

The splitting tests of this study return a characteristic $C_{LBL,k} \approx 14.4$ for laminated bamboo lumber, within 3 % of the EC5 timber value $C_{1,k} = 14$. The mean $C_{LBL,\text{mean}} = 18.94$ sits within 10 % of Leijten's original timber mean of 21 [33]. Based on this dataset, LBL is not resistant to splitting than softwood timber, despite its higher density and the literature G_{IC} values. The single-parameter design rule appears to apply to LBL connections without a separate material factor, but four splitting specimens per section is a small sample to base that equivalence on. The rest of this section elaborates further on how the result is reached.

The derivation underlying eq. 8.4 [33] is reviewed in section 2.2.1. The calibration here uses two independent routes to C_k and compares them section-by-section. Route A calculates from splitting tests and route B from G_{IC} fracture properties.

EC5 eq. 8.4 for splitting capacity in its codified form:

$$F_{90,Rk} = C_k \cdot b \cdot w \cdot \sqrt{\frac{h_e}{1 - h_e/h}}, \tag{8.4}$$

The above formula uses $C_k = 14$ N/mm$^{3/2}$ for softwood timber and $w = 1$ for connections other than punched-plate fasteners. The constant C absorbs the fracture-mechanics term of the underlying derivation, so the same equation in its open form is as follows:

$$F_{90,Rk} = \frac{\sqrt{GG_c}}{\sqrt{0.6}} \cdot b \cdot w \cdot \sqrt{\frac{h_e}{1 - h_e/h}}. \tag{8.4 open form}$$

From the experimental study, the eight splitting specimens (four flatwise RL and four edgewise TL) solve this expression for C_k given the measured F_{max}.

The flatwise specimens are $1200 \times 200 \times 40$ mm ($h = 40$ mm) and the edgewise specimens are $960 \times 161 \times 51$ mm ($h = 51$ mm), so the calibration runs per section and the mean is taken on the $\sqrt{GG_c}$ values, not on the dimensions. The edge-distance ratio $\alpha = h_e/h = 0.32$ is common to both. The characteristic value $C_{LBL,k}$ follows the Route B described below.

Route B calculates from fracture properties. An independent value of $\sqrt{GG_c}$ comes from the Mode-I fracture toughness measured by the SENB tests (section 3.2.2) and the in-plane shear modulus of the corresponding crack system. G_{IC} enters in N/mm (converted from the J/m^2 units used in NT BUILD 422). G_{shear} is used on section build-up: G_{LR} for flatwise (RL) specimens

and G_{LT} for edgewise (TL) specimens, as derived in section 2.2.1. The G_{IC} values come from this study (mean of the RL and TL SENB populations, 31 specimens each). The G_{shear} values are adopted from LBL literature [2] (section 2.1.1) because no shear test was run.

The "14" in EC5 eq. 8.4 is a characteristic value, not a mean. Van der Put & Leijten noted that "the experiments at the time indicated a mean value of 21; as characteristic value $\frac{2}{3}$ of $21 = 14$ was assumed, lacking sufficient tests for more info about the variability" [33]. The $\frac{2}{3}$ factor was a path for unknown variability, not a generally valid mean-to-characteristic conversion. For LBL with measured variability the characteristic value is computed in the following manner:

For each sample (V for splitting, G_{IC} for SENB) the log-normal 5%-percentile is

$$x_k = \exp\big(m_y - k_s(n) \cdot s_y\big), \tag{4.1}$$

with m_y and s_y are the sample mean and standard deviation of the log-transformed values and $k_s(n)$ is the sample-size-dependent fractile factor ($k_s(4) = 2.68$ for splitting, $k_s(31) = 1.80$ for SENB). Substituting x_k into the same formula used for the mean gives the characteristic $\sqrt{G \cdot G_c}$.

The following load convention is used. Van der Put's V_f in eq. shown in 2.2.1 is the shear force on one side of the cracked joint, half of the total load applied across the dowel. Beam statics give each reaction $V = P/2$ for a mid-span load P, so $V = F_{max}/2$. The splitting capacity is taken as the peak load F_{max}, not the first-drop minor fracture load: the maximum load before ultimate failure is the quantity consistent with van der Put's ultimate V.

The calibrated $\sqrt{GG_c}$ and C_{LBL} values per section, source, and variant are listed in Table 4.1 and visualised against the EC5 timber characteristic line $C_k = 14$ in Figure 4.1.

Table 4.1: EC5 splitting capacity calibration proposals for LBL (Gen 1, eq. 8.4)

		$\sqrt{GG_c}$		C_{LBL}		V (N)		G_{IC} (J/m^2)		G_{shear} (MPa)		α	statistics		
Source	Section	mean	k	mean	k	mean	k	mean	k	mean	k	(–)	n	k_s	$\text{COV}_{\log}$
Splitting Tests	FW (RL)	16.869	13.274	21.778	17.137	8451	6650	—	—	—	—	0.320	4	2.68	0.009
Splitting Tests	EW (TL)	12.478	9.041	16.109	11.672	7149	5180	—	—	—	—	0.320	4	2.68	0.012
Splitting Tests	Mean	14.674	11.157	18.944	14.404	7800	5915	—	—	—	—	0.320	4	2.68	0.011
SENB Tests	FW (RL)	17.185	13.510	22.186	17.441	—	—	214.0	132.3	1380.0	1380.0	—	31	1.80	0.047
SENB Tests	EW (TL)	19.240	14.268	24.838	18.419	—	—	187.9	103.3	1970.0	1970.0	—	31	1.80	0.060
SENB Tests	Mean	18.212	13.889	23.512	17.930	—	—	200.9	117.8	1675.0	1675.0	—	31	1.80	0.053
Literature	FW (RL)	26.297	23.523	33.949	30.368	—	—	501.1	401.0	1380.0	1380.0	—	—	—	—
Literature	EW (TL)	28.243	22.684	36.461	29.286	—	—	404.9	261.2	1970.0	1970.0	—	—	—	—
Literature	Mean	27.270	23.104	35.205	29.827	—	—	453.0	331.1	1675.0	1675.0	—	—	—	—

Per section, flatwise (RL) gives $C_{LBL,k} \approx 17.14$ and edgewise (TL) gives 11.67. Reporting the mean is more conservative than picking the higher FW value.

The SENB route returns $C_{LBL,k} \approx 17.93$. Both routes yield mean $\sqrt{GG_c}$ in the 14-19 N/mm$^{1.5}$ range. On flatwise (RL) the two routes agree within $\approx$ 5% (17.14 from Splitting vs $\approx$ 17.9 from SENB). On edgewise (TL) they diverge by $\approx$ 54% (11.67 from Splitting vs $\approx$ 17.9 from SENB). The $G_{LT} \approx 1970$ MPa [2] from the literature might be overestimating the actual specimen shear modulus. Because no direct shear test was run, the SENB route carries the uncertainty of the literature shear-modulus values in it. The Splitting route is therefore taken as the primary calibration source for $C_{LBL,k}$ because it integrates the actual specimen shear modulus and fracture toughness into a single measurable quantity, with no need to source G_{shear} externally. SENB serves as a framework cross-check. Limitations on $C_{LBL,k} \approx 14.4$ are a small sample size, the effect of section build-up, and only one tested α.

The LBL-calibrated form of EC5 eq. 8.4 is therefore

$$F_{90,Rk} = 14.4 \cdot b \cdot w \cdot \sqrt{\frac{h_e}{1 - h_e/h}}, \tag{4.2}$$

a 3 % shift on the timber constant.

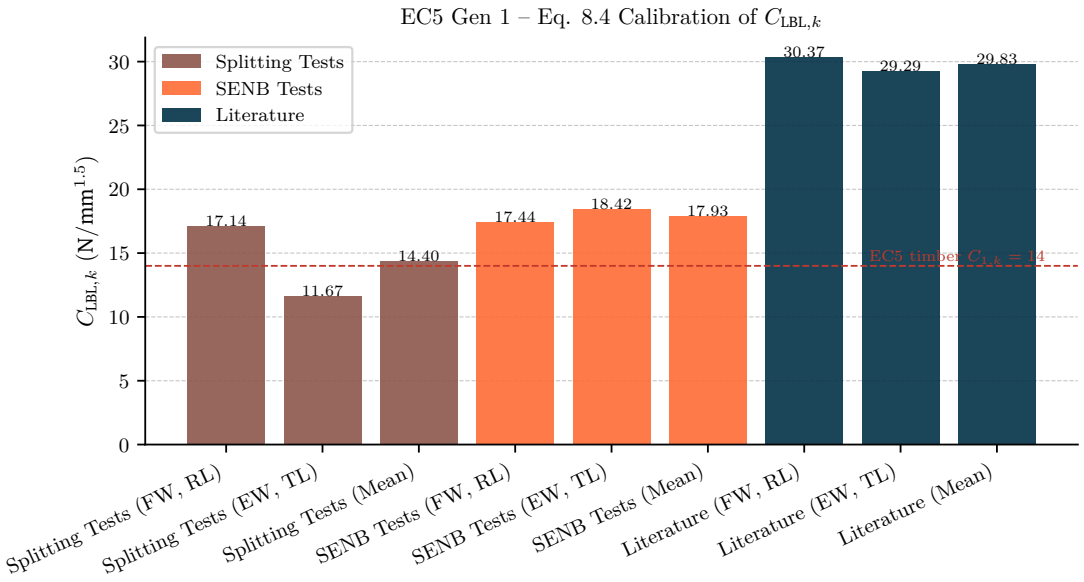

Figure 4.1: Gen 1 EC5 eq. 8.4 characteristic $C_{\mathrm{LBL},k} = \sqrt{GG_c/0.6}$ by source and section ($n = 9$); dashed line is the timber benchmark $C_{1,k} = 14$.

4.2 EC5 Gen 2 - Equation 11.54 Calibration

Gen 2 (FprEN 1995-1-1:2025 §11.6 eq. 11.54 [6]) replaces the single fracture mechanics constant C of Gen 1 with the product $k_{mat} \cdot k_G(\rho_k)$ of a categorical material factor and a density correlation (§2.2.3). The full eq. 11.54 reads

$$F_{sp,Rd} = \frac{k_{mod}}{\gamma_M} \cdot k_{mat} \cdot k_G \cdot b_{ef} \cdot k_{con,0} \cdot k_{con,90} \cdot \sqrt{\frac{h_e}{1 - h_e/h}}. \tag{11.54}$$

For this study's single-dowel single-row splitting test, with laterally loaded fasteners, no reinforcement, $k_{con,0} = k_{con,90} = k_{n,1} = 1$, and $b_{ef} = b$, and with k_{mod}/γ_M set to 1, eq. 11.54 reduces to the form

$$F_{sp,Rk} = k_{mat} \cdot k_G \cdot b \cdot \sqrt{\frac{h_e}{1 - h_e/h}}. \tag{11.54 simplified}$$

Designers apply EC5 Tables 5.4 and 4.4 to convert the characteristic $F_{sp,Rk}$ into the design value $F_{sp,Rd}$ via k_{mod} and γ_M. These are general EC5 design-conversion factors that apply across the code and are not splitting-specific (§1.8). LBL-specific values for k_{mod} and γ_M are not yet calibrated. Designers need to fall back on the timber defaults as a substitute.

Eq. 11.55 lists k_{mat} for example 0.6 for sawn timber. $k_{mat,LBL}$ needs to be calibrated for LBL. The equation needs to be solved for $k_{mat,LBL}$ given the $F_{sp,\mathrm{mean}}$. Eq. 11.54 contains no fracture-mechanics term, so the SENB / ENF / FEM Route B used for Gen 1 has no analogue here for Gen 2. $k_G(\rho_k)$ is computed at the manufacturer-reported nominal characteristic density $\rho_k = 700$ kg/m^3, giving $k_G = 0.05 \cdot 700 + 2 = 37$ N/mm$^{3/2}$. This matches the value a designer would read from a product datasheet when applying eq. 11.54 for LBL.

For Gen 2 the total peak load F_{max} is used, not the per-side internal shear $V = F_{max}/2$ used in Gen 1. This reflects a change in the design code. Solving eq. 11.54 for the material factor k_{mat} at the mean and at the 5%-percentile of the per-specimen F_{max} sample gives the values in Table 4.2. Per crack system, mean and characteristic results are compared against the eq. 11.55 k_{mat} references in Figure 4.2.

The calibration assumptions are again summarized below:

- **Characteristic resistance**: $k_{mod} = \gamma_M = 1$ in eq. 11.54. Design values $F_{sp,Rd}$ require Tables 5.4 and 4.4 modifiers.
- **Single-dowel single-row laterally loaded connection**: $k_{con,0} = k_{con,90} = k_{n,1} = 1$ and $b_{ef} = b$ (eq. 11.57 case 1). No reinforcement.
- **Density from manufacturer**: $\rho_k = 700$ kg/m^3 from the Moso N-finity datasheet, giving $k_G = 0.05 \cdot 700 + 2 = 37$ N/mm$^{3/2}$ via eq. 11.56.
- **Load convention**: $F_{sp,\text{meas}} = F_{max}$, the total peak load, not the per-side shear $V = F_{max}/2$ used by Gen 1.
- **Statistics**: characteristic $k_{mat,k}$ from the lognormal 5%-percentile with $k_s(4) = 2.68$ ($n = 4$ specimens per crack system).
- **Single edge-distance ratio**: $\alpha = h_e/h = 0.32$ for all specimens. Constancy of k_{mat} for different $\alpha < 0.7$ is not verified.

Table 4.2: EC5 Gen 2 ($k_{\text{mat,LBL}}$) calibration

		$k_{\text{mat,LBL}}$		F_{meas} (N)		ρ_k	k_G	k_{mod}	γ_M	b_{ef}	$k_{\text{con},0}$	$k_{\text{con},90}$	$k_{n,1}$	α	Statistics		
Source	Section	mean	k	mean	k	(kg/m^3)	(N/mm$^{1.5}$)	(–)	(–)	(mm)	(–)	(–)	(–)	(–)	n	k_s	$\text{COV}_{\log}$
Splitting Tests	FW (RL)	1.177	0.926	16902	13300	700	37.00	1.00	1.00	40.0	1.00	1.00	1.00	0.320	4	2.68	0.009
Splitting Tests	EW (TL)	0.871	0.631	14298	10360	700	37.00	1.00	1.00	51.0	1.00	1.00	1.00	0.320	4	2.68	0.012
Splitting Tests	Mean	1.024	0.779	15600	11830	700	37.00	1.00	1.00	—	1.00	1.00	1.00	0.320	4	2.68	0.011

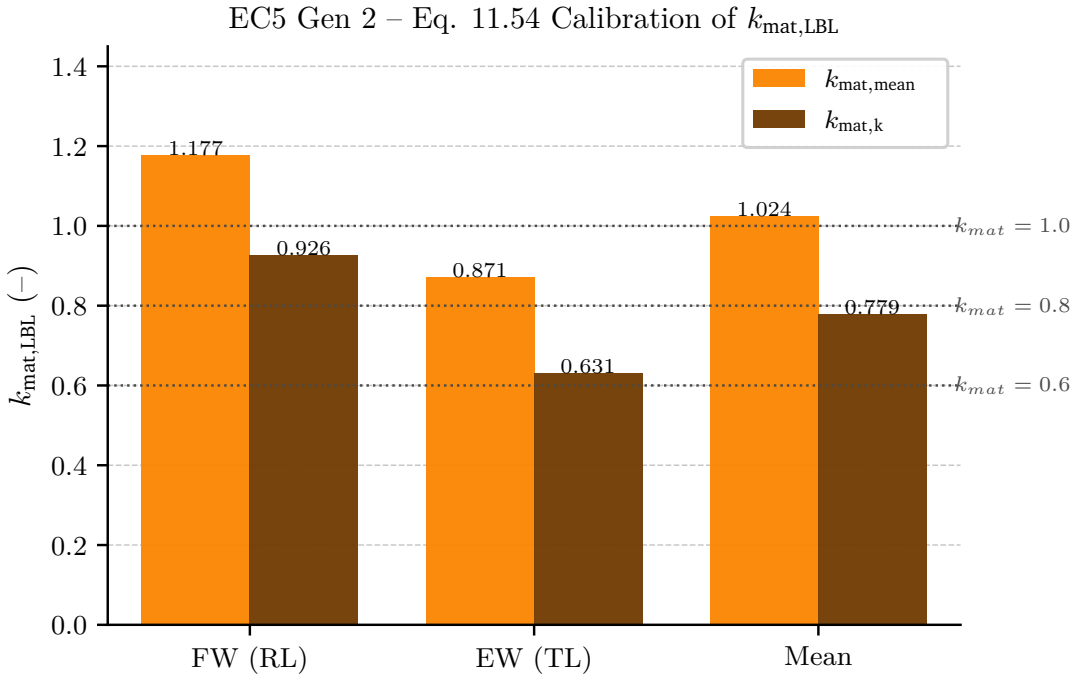

Figure 4.2: Gen 2 EC5 $k_{\text{mat,LBL}}$ (eq. 11.54) per section: $k_{\text{mat,mean}}$ from mean splitting load and $k_{\text{mat,k}}$ from the 5%-percentile.

The conservative single-value choice is the lower of the two crack-system characteristics, $k_{mat,LBL,k} \approx 0.63$ from the edgewise build-up: close to the sawn timber value of 0.6. A conservative recommendation is $k_{mat,LBL} = 0.7$ (section-mean rounded down). LBL with uncontrolled or unknown section orientation should use $k_{mat,LBL,TL} = 0.6$.

Why 0.7 rather than 0.78. The calibrated section-mean $k_{mat,LBL,k} = 0.779$ would round to 0.78 at two decimals. EC5 Gen 2 (eq. 11.55) lists k_{mat} values to **one decimal** for every other material category (sawn timber 0.6, panels 0.8, LVL-P/GLVL-P 1.0). Rounding the LBL value to one decimal therefore matches the existing EC5 k_{mat} values. The choice of 0.7 over 0.8 is rounding **down**, which adds a ≈ 10 % conservative margin on top of the calibration. This asymmetric rounding is intentional and is reflected in the §4.2.1 reconciliation: the calibrated framework is internally consistent ($2C_{LBL,k,\text{calibrated}} = k_{mat,LBL,\text{calibrated}} \cdot k_G$ exactly), while the proposed design pair ($C_{LBL,k} = 14.4$, $k_{mat,LBL} = 0.7$) yields a ≈ 10 % lower Gen 2 capacity than Gen 1 at the same geometry.

Adding LBL to eq. 11.55 gives:

$$k_{mat} = \begin{cases} 0.6 & \text{sawn timber} \\ 0.7 & \text{LBL (proposed)} \\ 0.8 & \text{panels, LVL-C, GLVL-C} \\ 1.0 & \text{LVL-P, GLVL-P (wide face)} \end{cases} . \qquad \text{(11.55 proposed)}$$

4.2.1 Reconciliation between Gen 1 and Gen 2

Gen 1 reports a 3 % shift on C_k and Gen 2 reports a 17 % shift on k_{mat}. The two values describe the same eight specimens, so they must be reconciled. Setting Gen 1 and Gen 2 equal on the same specimen (via $F_{sp,Rk} = 2V_k$) gives the equivalence

$$2C_k = k_{mat} \cdot k_G(\rho_k). \tag{4.3}$$

Substituting the calibrated values from Table 4.1 and Table 4.2 yields identical $F_{sp,Rk}$ for both formulations on every section (top three rows of Table 4.3), as required since the same eight F_{max} values drive both calibrations.

Proposed-for-design values do not reconcile exactly. $C_{LBL,k} = 14.4$ is essentially the calibrated mean (14.404 rounded to 1 d.p., no extra margin). $k_{mat,LBL} = 0.7$ is the calibrated 0.779 rounded **down** to 1 d.p. so that LBL fits EC5's existing one-decimal k_{mat} scale (0.6, 0.8, 1.0). The justification is in §4.2. The asymmetric rounding produces a ≈ 10 % gap between the two formulations at any geometry: $2 \cdot 14.4 = 28.8$ vs $0.7 \cdot 37 = 25.9$ (last row of Table 4.3). Designers applying the Gen 2 recommendation receive a ≈ 10 % lower characteristic splitting capacity than designers applying the Gen 1 recommendation at the same geometry. This margin is the intentional conservatism introduced by the EC5-format rounding. The underlying calibration itself remains internally consistent.

Table 4.3: Gen 1 / Gen 2 reconciliation via $2\,C_k = k_{\text{mat}} \cdot k_G$.

Section	C_k	k_{mat}	k_G	$2\,C_k$	$k_{\text{mat}} \cdot k_G$	Δ (%)
FW (RL)	17.137	0.926	37.00	34.27	34.27	0.00
EW (TL)	11.672	0.631	37.00	23.34	23.34	-0.00
Mean	14.404	0.779	37.00	28.81	28.81	0.00
Proposed	14.400	0.700	37.00	28.80	25.90	-10.07

4.3 Design Implications

The clearest practical implication of these experimental results and calibrations is that the flatwise (RL) section build-up is more resistant to splitting than the edgewise (TL) build-up (see Figure 2.1 for the two build-ups). For dowel connections loaded perpendicular to the height of the beam, the flatwise orientation should be the default for structural use. The edgewise orientation may

be considered only when the connection load is applied perpendicular to the height of the beam rather than to the top or bottom face.

Furthermore, two general points apply to engineers designing bamboo connections. First, the splitting failure case should be understood with the energy-based fracture-mechanics framework, not only with a stress- or strength-based check. For splitting the governing material parameter is fracture energy, not tensile strength perpendicular to the grain. Second, the difference between splitting failure and embedment failure should be made explicit in the design. Embedment failure is ductile and gives a warning. Splitting failure is brittle and the connection should be designed to prevent it. A complete perpendicular-to-grain dowel check is the envelope of the two failure modes: $F_{Rk} = \min(F_{\text{sp},Rk}, F_{\text{emb},Rk})$, with $F_{\text{sp},Rk}$ from EC5 eq.~8.4 / 11.54 (calibrated for LBL in this chapter via $C_{LBL,k}$ / $k_{\text{mat},LBL}$) and $F_{\text{emb},Rk}$ from Johansen's European Yield Model [19] using the embedment strengths $f_{h,0,k}$ / $f_{h,90,k}$. The present work calibrates the splitting branch only. LBL-specific embedment tests (per EN 383) are out of scope, and the EYM inputs $f_{h,0,k}$ / $f_{h,90,k}$ for LBL are not established here. Designers using the splitting calibration of this chapter should pair it with measured or literature embedment values for the specific LBL product they are sourcing. An LBL embedment calibration is identified as future work in §5.3.

4.3.1 Worked example

Both code generations are evaluated for the same dowel connection geometry, for sawn softwood timber and for LBL. The geometry matches the flatwise splitting specimens of this study so the numbers can be cross-checked against Tables 4.1 and 4.2.

Table 4.4: Worked-example geometry.

Parameter	Value
$b = b_{\text{ef}}$	40 mm
h	200 mm
h_e	64 mm
$\alpha = h_e/h$	0.32

Gen 1 (eq. 8.4): $F_{max,k} = 2V_k = 2C_k \cdot b \cdot w \cdot \sqrt{h_e/(1 - h_e/h)}$
For sawn softwood timber ($C_k = 14$ N/mm$^{1.5}$):

$$F_{max,k,\text{timber}} = 2 \cdot 14 \cdot 40 \cdot 1 \cdot \sqrt{64/0.68} = 10{,}866 \text{ N}.$$

For LBL ($C_{LBL,k} = 14.4$ N/mm$^{1.5}$, this study):

$$F_{max,k,\text{LBL}} = 2 \cdot 14.4 \cdot 40 \cdot 1 \cdot \sqrt{64/0.68} = 11{,}176 \text{ N}.$$

Gen 2 (eq. 11.54): $F_{sp,Rk} = k_{mat} \cdot k_G \cdot b \cdot \sqrt{h_e/(1 - h_e/h)}$
For sawn softwood timber ($k_{mat} = 0.6$, $\rho_k = 380$ kg/m^3, $k_G = 0.05 \cdot 380 + 2 = 21$ N/mm$^{1.5}$):

$$F_{sp,Rk,\text{timber}} = 0.6 \cdot 21 \cdot 40 \cdot \sqrt{64/0.68} = 4{,}890 \text{ N}.$$

For LBL ($k_{mat,LBL} = 0.7$, $\rho_k = 700$ kg/m^3 from manufacturer, $k_G = 0.05 \cdot 700 + 2 = 37$ N/mm$^{1.5}$):

$$F_{sp,Rk,\text{LBL}} = 0.7 \cdot 37 \cdot 40 \cdot \sqrt{64/0.68} = 10{,}051 \text{ N}.$$

LBL vs sawn timber with Gen 1 is $11.18/10.87 = 1.03$, the +3 % shift on C_k headlined in §4.1. LBL vs sawn timber with Gen 2 is $10.05/4.89 = 2.06$, a $\approx 2\times$ density gain absorbed into the k_G split. Gen 2 implies LBL has roughly twice the perpendicular-to-grain splitting capacity of sawn softwood at code densities, almost entirely from the density term $k_G(\rho_k)$.

Table 4.5: Worked-example splitting capacities.

Code	Material	Coefficient		$F_{\text{max,k}}$ (kN)
Gen 1	Sawn timber	C_k	= 14	10.87
Gen 1	LBL	$C_{\text{LBL},k}$	= 14.4	11.18
Gen 2	Sawn timber	$k_{\text{mat}} \cdot k_G$	= 12.6	4.89
Gen 2	LBL	$k_{\text{mat}} \cdot k_G$	= 25.9	10.05

The two LBL rows in the worked example do **not** agree exactly. Gen 1 gives 11.18 kN and Gen 2 gives 10.05 kN, a ≈ 10 % gap. This is the rounding asymmetry made explicit in §4.2 and §4.2.1 (see for details). The underlying calibration is internally consistent, but the proposed k_{mat} is rounded down.

The disagreement between Gen 1 and Gen 2 **sawn-timber** capacities at this geometry comes from the load-convention change between the two code generations. The standards committee's reason for the convention change is not documented in the open-literature commentary on FprEN 1995-1-1:2025 and is an open question.

4.4 Discussion - Regulatory and Design Implications

This section discusses the EC5 Gen 1 and Gen 2 calibrations and the design implications of sections 4.1 to 4.3, and answers the chapter's three research questions.

Gen 1 clause 8.1.4 needs no new material factor: the calibrated $C_{LBL,k} \approx 14.4$ N/mm$^{1.5}$ sits within 3% of the softwood value $C_k = 14$, so the existing single-parameter design rule transfers directly. Gen 2 eq. 11.54 needs a new entry in the k_{mat} table at $k_{\text{mat},LBL} = 0.7$, between the sawn-timber 0.6 and the panel / LVL-P 0.8 categories. The four specimen per section sample limits how firmly either calibration can be claimed, and re-testing at additional α values and at 65% RH would refine the values (§5.3).

The two generations agree on the same dowel connection within $\approx 10\%$ of each other, with Gen 2 returning slightly lower characteristic capacities because of the rounding $k_{\text{mat},LBL,k} = 0.779 \rightarrow 0.7$ (§4.3.1). The substantive change between the two is the load convention (per-side shear in Gen 1, total connection load in Gen 2), not the underlying fracture mechanics.

Section build-up matters in both generations. Flatwise (RL) returns higher values across SENB, ENF, and full-scale splitting than edgewise (TL): per-section $C_{LBL,FW,k} \approx 17.1$ vs $C_{LBL,EW,k} \approx 11.7$, and $k_{\text{mat},FW,k} \approx 0.93$ vs $k_{\text{mat},EW,k} \approx 0.63$. Reporting the section-mean is more conservative than picking the flatwise value alone, and is the choice this thesis makes for the recommended $C_{LBL,k}$ and $k_{\text{mat},LBL}$. For dowel connections loaded perpendicular to the grain of the beam, the flatwise orientation should be the default for structural use.

Summary of findings: - EC5 Gen 1 section 8.1.4 applies to LBL with $C_{LBL,k} = 14.4$ N/mm$^{1.5}$, no separate material factor needed. - EC5 Gen 2 eq. 11.54 needs a new entry: $k_{\text{mat},LBL} = 0.7$ (unrounded 0.779, rounded down for design margin). - Section build-up matters: FW returns $\approx 46\%$ higher capacity than EW in both generations. - Use flatwise (RL) as the default build-up for dowel connections loaded perpendicular to the grain. - The complete dowel check is the envelope $F_{Rk} = \min(F_{\text{sp},Rk}, F_{\text{emb},Rk})$. LBL embedment is out of scope here and must be sourced separately. - Both calibrations rest on $n = 4$ per section, a single α, and dry conditioning. They are conservative floors rather than best estimates.

RQ-10 - Is equation 8.4 from Eurocode 5 Gen 1 applicable to laminated bamboo lumber with dowel-type connections loaded perpendicular to the grain? If so, how can it be calibrated with an appropriate fracture parameter $C = \sqrt{GG_c/0.6}$ suitable for laminated bamboo lumber? - Yes, it is applicable. - Route A (full-scale splitting, §4.1) solved eq. 8.4 for $C_{LBL,k} \approx 14.4$ N/mm$^{1.5}$, within 3% of the timber value $C_k = 14$. - Route B (SENB via $C = \sqrt{GG_c/0.6}$) returned $C_{LBL,k} \approx 17.93$ averaged across crack systems. Both routes sit in the 14-19 N/mm$^{1.5}$

range. - Splitting is the primary calibration because it integrates the actual specimen shear modulus and fracture toughness into a single measurable quantity, with no need to source G_{shear} externally. - Per crack system: $C_{LBL,FW/RL,k} \approx 17.14$, $C_{LBL,EW/TL,k} \approx 11.67$. - Recommended LBL-calibrated form: $F_{90,Rk} = 14.4 \cdot b \cdot w \cdot \sqrt{h_e/(1-h_e/h)}$, a 3% shift on the timber constant. - The calibration rests on four splitting specimens per section, a single $\alpha = 0.32$, and indoor lab conditioning (35% RH). The value is a conservative floor rather than a 65%-RH best estimate (§5.3).

RQ-11 - Is equation 11.54 (including sub-equations) from Eurocode 5 Gen 2 applicable to laminated bamboo lumber with dowel-type connections loaded perpendicular to the grain? If so, how can it be calibrated with an appropriate material parameter k_{mat} suitable for laminated bamboo lumber? - Yes, the Gen 2 splitting equation $F_{sp,Rk} = k_{\text{mat}} \cdot k_G(\rho_k) \cdot b_{ef} \cdot k_{\text{con},0} \cdot k_{\text{con},90} \cdot \sqrt{h_e/(1-h_e/h)}$ applies to LBL with a new k_{mat} entry at $k_{\text{mat},LBL} = 0.7$ (§4.2). - Density factor $k_G = 0.05\rho_k + 2$ at the manufacturer-published $\rho_k = 700$ kg/m^3 for MOSO N-finity gives $k_G = 37$ N/mm$^{1.5}$. - Per crack system: $k_{\text{mat},FW,k} \approx 0.93$, $k_{\text{mat},EW,k} \approx 0.63$. Section-mean characteristic 0.779, rounded down to 0.7 to land between the existing sawn-timber (0.6) and panel / LVL-P (0.8) categories and to add a $\approx 10\%$ design margin. - Same $n = 4$ per section and single-α limitations as the Gen 1 calibration. - The general EC5 factors k_{mod} and γ_M are not splitting-specific (§5.3).

RQ-12 - What practical learning can be taken from this research for (perpendicular-to-grain connection) design with Laminated Bamboo Lumber? - Section build-up matters. Flatwise (RL) returns $\approx 50\%$ higher splitting capacity than edgewise (TL) across both EC5 generations and the SENB and ENF small-scale tests, so flatwise should be the default for perpendicular-to-grain dowel connections. - Splitting and embedment are separate failure modes with separate physics and equations. The complete dowel check is the envelope $F_{Rk} = \min(F_{\text{sp},Rk}, F_{\text{emb},Rk})$, with the splitting branch from EC5 eq. 8.4 / 11.54 calibrated here. LBL-specific embedment calibration is out of scope of this thesis and is named as future work (§5.3). Designers using the splitting calibration must pair it with measured or literature embedment values for the specific LBL product. - The splitting check is energy-based (fracture mechanics), not stress-based. The governing material parameter is fracture energy release rate (G_c) rather than tensile strength perpendicular to the grain.

Chapter 5

Conclusions and Recommendations

This chapter consolidates the conclusions, restates each research question with its explicit answer, and lists recommendations for future work.

5.1 Conclusions

This study tested the applicability of EC5 Gen 1 eq. 8.4 and Gen 2 eq. 11.54 to LBL dowel connections loaded perpendicular to the grain, using small-scale fracture tests (SENB, ENF), full-scale splitting tests, and FEM simulation.

The splitting capacity of LBL with dowel-type connections loaded perpendicular to the grain fits the Eurocode 5 framework. Gen 1 applies as-is, while Gen 2 needs a new material-factor entry. Section build-up is important to consider for both code versions.

EC5 Gen 1 section 8.1.4 could be applied to LBL without modification on this dataset. The splitting tests of this work return $C_{LBL,k} \approx 14.4$, within 3 % of the timber value $C_k = 14$. The SENB-based route returns $C_{LBL,k} \approx 17.9$. LBL is not more resistant to splitting than softwood timber, despite what its higher density and literature G_{IC} values might have suggested. EC5 Gen 1 eq. 8.4 may apply without a separate material factor, but four splitting specimens per section is a small sample to base that on definitely.

EC5 Gen 2 eq. 11.55 needs a new entry for LBL. This work proposes $k_{mat,LBL} = 0.7$ as the conservative choice, between sawn timber (0.6) and panels / LVL-C (0.8).

Section build-up matters (see Figure 2.1 for the two orientations): flatwise (RL) returns $k_{mat,FW,k} \approx 0.93$ and $C_{LBL,FW/RL,k} \approx 17.1$, edgewise (TL) returns $k_{mat,EW,k} \approx 0.63$ and $C_{LBL,EW/TL,k} \approx 11.7$.

The flatwise (RL) build-up is more resistant to splitting than the edgewise (TL) build-up across SENB, ENF, and full-scale splitting tests. The same section build-up/crack-system ranking carries from the small-scale fracture tests to the full-scale splitting tests. The flatwise (RL) configuration should be the default for structural use.

Splitting in connections loaded perpendicular to the grain is Mode-I dominated, with clean fibre delamination inside the lamella. No test resulted in any glue-line separation. Intra-lamella splitting is always governing.

The FEM models support and validate the experimental tests. They are not a predictive cracking model. With the crack path fixed by a prescribed cohesive layer along the experimentally observed crack, the simulations reproduce the measured F/d response: SENB and splitting match the experiment well, ENF less so. The ENF gap is explained by an oversimplified prescribed crack path for the more complex Mode II and mixed-mode splitting observed in the ENF experimental results. Predictive (non-prescribed-path) modelling of LBL splitting and the post-peak snap-back regime are not captured by these models and remain open research topic (section 5.3).

Summary of findings: - EC5 Gen 1 section 8.1.4 applies to LBL without modification on this dataset, with $C_{LBL,k} \approx 14.4$ within 3% of the timber value $C_k = 14$. - EC5 Gen 2 eq. 11.54 needs

a new entry: $k_{\text{mat},LBL} = 0.7$, between sawn timber (0.6) and panels / LVL-P (0.8). - Flatwise (RL) > edgewise (TL) across SENB, ENF, and full-scale splitting: per-section $C_{LBL,FW,k} \approx 17.1$ vs 11.7 for EW, $k_{\text{mat},FW,k} \approx 0.93$ vs 0.63 for EW. - Splitting in perpendicular-to-grain dowel connections is Mode I dominated, with intra-lamella fibre delamination and no glue-line separation in any test. - The FEM models support and validate the experimental tests in three energy features (pre-peak stiffness, displacement at peak, work of fracture). They are not predictive cracking models. - Both calibrations rest on $n = 4$ per section, a single α, and dry conditioning. They are conservative floors rather than best estimates. - Predictive (non-prescribed-path) modelling of LBL splitting and the post-peak snap-back regime are open problems for future work (§5.3). - LBL embedment calibration is out of scope of this thesis. The complete dowel check requires the splitting branch (calibrated here) paired with measured or literature embedment values.

5.2 Answers to Research Questions

This section restates the main research question and each of the twelve sub-research questions verbatim, followed by the answer drawn from the chapter that addresses it (§2.4 for RQ-1 to RQ-3, §3.3 for RQ-4 to RQ-9, §4.4 for RQ-10 to RQ-12).

Main research question - How can the splitting capacity of Laminated Bamboo Lumber with dowel-type connections loaded perpendicular to the grain be established under the Eurocode 5 framework?

Yes by calibrating the existing EC5 splitting equations against full-scale LBL splitting tests. EC5 Gen 1 eq. 8.4 transfers to LBL with $C_{LBL,k} \approx 14.4$ N/mm$^{1.5}$ (within 3% of softwood) and no separate material factor. EC5 Gen 2 eq. 11.54 requires a new k_{mat} entry, calibrated here to $k_{\text{mat},LBL} = 0.7$ (between sawn timber 0.6 and panels / LVL-P 0.8). Both routes are based on four splitting specimens per section, a single edge-distance ratio $\alpha = 0.32$, and dry indoor lab conditioning.

RQ-1 - What are the mechanical properties of laminated bamboo lumber found in the literature?

- LBL is orthotropic and bimodular, with longitudinal moduli and strengths an order of magnitude above the across-grain values [2].
- Tensile and compressive responses along the fibres differ, so a single Young's modulus cannot represent both.
- Property values vary by species, by position in the culm, and by processing [34, 35].
- The MOSO N-finity dataset of Al-Rukaibawi *et al.* [2] is the peer-reviewed anchor for the product tested here, with compressive properties in all three orthotropic directions reported to ISO 23478-2022.
- Tensile, bending, and shear values come from the wider LBL literature [7, 24, 38, 39].
- Flatwise and edgewise build-ups carry different elastic and strength values per orientation [38].

RQ-2 - What values for the fracture properties of laminated bamboo lumber can be found in the literature?

- Mode I: ≈ 508 J/m^2 in RL and ≈ 338 J/m^2 in TL [8, 10, 26, 37, 42, 45].
- Mode II: ≈ 967 J/m^2 in TL, no published values in RL [12, 41].
- Most data is on full-culm moso bamboo and engineered LBL, and most covers Mode I rather than Mode II. Both gaps are filled by the SENB and ENF tests of chapter 3.
- Chen Qi *et al.* [9] reported a humidity sensitivity of $+7.6$ J/m^2 per percentage-point RH for G_{IC}. The dry-conditioned chapter 3 specimens (§3.2.1) are corrected against this slope.

RQ-3 - What is the Eurocode framework for Gen 1 and Gen 2 for splitting of connections loaded perpendicular to the grain, and the underlying mechanical theory?

- Gen 1 clause 8.1.4, eq. 8.4: $F_{90,Rk} = C_k \cdot b \cdot w \cdot \sqrt{h_e/(1 - h_e/h)}$ with $C_k = 14$ for softwood timber.
- The constant absorbs van der Put's fracture-mechanics derivation $C = \sqrt{GG_c/0.6}$, coupling the in-plane shear modulus G to the Mode-I critical energy release rate G_c [32, 33].
- Gen 2 clause 11.6 [6] replaces the lumped C with the product $k_{\text{mat}} \cdot k_G(\rho_k)$, where k_{mat} is categorical (0.6 sawn timber, 0.8 plywood, 1.0 LVL-P) and $k_G = 0.05\rho_k + 2$ is a density correlation.
- The two generations agree on the geometric square-root term.
- The substantive change between them is the load convention: Gen 1 checks per-side shear, Gen 2 checks total connection load.
- Splitting and embedment remain separate failure modes with separate test routes (splitting beam vs EN 383 cube) and material parameters [18, 36].

RQ-4 - What are the experimental Mode I fracture characteristics of laminated bamboo lumber?

- SENB returned higher mean G_{IC} in RL than in TL.
- Derivation methods (NT BUILD 422 work-of-fracture, isotropic LEFM, orthotropic LEFM) give different absolute values. The orthotropic form runs higher than the isotropic form because LBL is strongly anisotropic.
- Crack system has a larger effect on G_{IC} than specimen thickness, so the calibration is not overly sensitive to specimen geometry.
- Tested at 35% RH against the 65%-RH literature baseline. Chen-Qi-corrected values land in the literature range ($\approx$ 508 J/m^2 RL, 338 TL). The chapter 4 EC5 calibration uses the uncorrected dataset, inheriting a conservative fracture-energy floor (§3.3).
- No glue-line separation was observed in any SENB specimen. The fracture surface ran through the bamboo fibres rather than along the lamella interfaces.

RQ-5 - What are the experimental Mode II fracture characteristics of laminated bamboo lumber?

- ENF returned higher means in RL than in TL, mirroring the SENB ranking.
- Four derivation methods (SBT, TBT, CBBM, CCM) gave a wider spread than the SENB Mode I methods because ENF specimens routinely failed in mixed-mode rather than pure Mode II, and each approach holds a different mode-split assumption.
- CBBM is reported as the primary method because it tracks an equivalent crack length over the full F/d curve rather than reading only an initiation point.
- No glue-line separation was observed in any ENF specimen.
- Mode II results are reported for completeness and physical interpretation. They do not feed any chapter 4 calibration since EC5 eq. 8.4 / 11.54 is a Mode I splitting dominated.

RQ-6 - What is the fracture behaviour of laminated bamboo lumber for connections loaded perpendicular to the grain?

- Mode I dominated fracture in the splitting tests, with little observed Mode II contribution.
- Fracture parameter $C_{\text{mean}} = \sqrt{GG_c}$ at $\approx$ 16.9 N/mm$^{1.5}$ in flatwise (RL) and $\approx$ 12.5 in edgewise (TL), a ratio close to the SENB Mode I asymmetry.
- Coefficient of variation $\approx$ 13% across the eight specimens, a tight distribution for the small sample size.
- Embedment under the 16 mm grade-8.8 dowel preceded splitting (mean 0.81 mm, SD 0.23 mm) but did not progress to full embedment failure. The dowel showed no plastic deformation.
- No glue-line separation was observed. Fracture ran through the lamellae.

RQ-7 - Can the experimental results be numerically reproduced?

- Yes for SENB and splitting, partially for ENF.
- The FEM uses a prescribed crack path with cohesive elements placed only along the experimentally observed fracture plane (§3.1.6), so it reproduces the load-displacement response rather than predicting where the crack will form.
- The cohesive interface takes its mode I and mode II results directly from the experiments.

RQ-8 - How do experimental results compare to literature values?

- Uncorrected SENB Mode I means sit below the literature range for LBL (≈ 508 J/m^2 RL, 338 TL) because specimens were tested at 35% RH rather than the 65%-RH literature reference.
- After the Chen Qi correction (+7.6 J/m^2 per percentage-point), means shift from ≈ 200 to ≈ 430 J/m^2 and land inside the literature window.
- ENF Mode II values are sparser in the literature (≈ 967 J/m^2 TL only). The comparison is less anchored.
- Tensile testing confirmed the literature parallel-to-grain strength on the three specimens. The single radial specimen is reported as a single-specimen estimate, not a sample mean (§3.2.4).
- The chapter 4 calibration uses the RH-uncorrected dataset, inheriting a conservative input.

RQ-9 - How do fracture properties derived from small-scale testing translate to full-scale splitting capacity?

- Small-scale SENB G_{IC} feeds the EC5 Gen 1 splitting equation through $C = \sqrt{GG_c/0.6}$ (Route B).
- Full-scale splitting tests independently solve for $C_{LBL,k}$ from the measured $F_{\max}$ (Route A).
- Both routes are evaluated against the same target in chapter 4. They agree on flatwise and diverge on edgewise. The divergence is attributed in §4.1 to the literature shear modulus used.
- The translation from small-scale fracture energy to full-scale splitting capacity therefore works on flatwise and is bounded by the literature G_{shear} assumption on edgewise.

RQ-10 - Is equation 8.4 from Eurocode 5 Gen 1 applicable to laminated bamboo lumber with dowel-type connections loaded perpendicular to the grain? If so, how can it be calibrated with an appropriate fracture parameter $C = \sqrt{GG_c/0.6}$ suitable for laminated bamboo lumber?

- Yes, it is applicable.
- Route A (full-scale splitting, §4.1) solved eq. 8.4 for $C_{LBL,k} \approx 14.4$ N/mm$^{1.5}$, within 3% of the timber value $C_k = 14$.
- Route B (SENB via $C = \sqrt{GG_c/0.6}$) returned $C_{LBL,k} \approx 17.93$ averaged across crack systems. Both routes sit in the 14-19 N/mm$^{1.5}$ range.
- Splitting is the primary calibration because it integrates the actual specimen shear modulus and fracture toughness into a single measurable quantity, with no need to source G_{shear} externally.
- Per crack system: $C_{LBL,FW/RL,k} \approx 17.14$, $C_{LBL,EW/TL,k} \approx 11.67$.
- Recommended LBL-calibrated form: $F_{90,Rk} = 14.4 \cdot b \cdot w \cdot \sqrt{h_e/(1 - h_e/h)}$, a 3% shift on the timber constant.
- The calibration rests on four splitting specimens per section, a single $\alpha = 0.32$, and indoor lab conditioning (35% RH). The value is a conservative floor rather than a 65%-RH best estimate (§5.3).

RQ-11 - Is equation 11.54 (including sub-equations) from Eurocode 5 Gen 2 applicable to laminated bamboo lumber with dowel-type connections loaded perpendicular to the grain? If so, how can it be calibrated with an appropriate material parameter k_{mat} suitable for laminated bamboo lumber?

- Yes, the Gen 2 splitting equation $F_{sp,Rk} = k_{\text{mat}} \cdot k_G(\rho_k) \cdot b_{ef} \cdot k_{\text{con},0} \cdot k_{\text{con},90} \cdot \sqrt{h_e/(1 - h_e/h)}$ applies to LBL with a new k_{mat} entry at $k_{\text{mat},LBL} = 0.7$ (§4.2).
- Density factor $k_G = 0.05\rho_k + 2$ at the manufacturer-published $\rho_k = 700$ kg/m^3 for MOSO N-finity gives $k_G = 37$ N/mm$^{1.5}$.
- Per crack system: $k_{\text{mat},FW,k} \approx 0.93$, $k_{\text{mat},EW,k} \approx 0.63$. Section-mean characteristic 0.779, rounded down to 0.7 to land between the existing sawn-timber (0.6) and panel / LVL-P (0.8) categories and to add a $\approx 10\%$ design margin.
- Same $n = 4$ per section and single-α limitations as the Gen 1 calibration.
- The general EC5 factors k_{mod} and γ_M are not splitting-specific (§5.3).

RQ-12 - What practical learning can be taken from this research for (perpendicular-to-grain connection) design with Laminated Bamboo Lumber?

- Section build-up matters. Flatwise (RL) returns $\approx 50\%$ higher splitting capacity than edgewise (TL) across both EC5 generations and the SENB and ENF small-scale tests, so flatwise should be the default for perpendicular-to-grain dowel connections.
- Splitting and embedment are separate failure modes with separate physics and equations. The complete dowel check is the envelope $F_{Rk} = \min(F_{\text{sp},Rk}, F_{\text{emb},Rk})$, with the splitting branch from EC5 eq. 8.4 / 11.54 calibrated here. LBL-specific embedment calibration is out of scope of this thesis and is named as future work (§5.3). Designers using the splitting calibration must pair it with measured or literature embedment values for the specific LBL product.
- The splitting check is energy-based (fracture mechanics), not stress-based. The governing material parameter is fracture energy release rate (G_c) rather than tensile strength perpendicular to the grain.

5.3 Recommendations for Future Research

Conditioning of fracture specimens. SENB and ENF tests should be repeated on LBL conditioned to 65% RH, the service-condition baseline used in earlier studies [2]. This work applied the +7.6 J/m^2 per percentage-point RH correction of [9] to compensate for the dry samples, a quantity originally fitted on full-culm bamboo. Its applicability to engineered LBL is itself an assumption. Re-testing at 65% RH would likely produce higher G_{IC} and a higher splitting capacity (qualitatively), so the $C_{LBL,k}$ and $k_{mat,LBL}$ proposed here sit at the conservative end of the plausible range. A re-test would refine the calibration upward rather than correct an error.

Direct orthotropic shear-modulus tests on LBL. The SENB-based Gen 1 calibration used literature values for G_{LR} and G_{LT} because no direct shear test was run. Dedicated orthotropic shear tests covering both planes would replace the derived literature input by [2].

More edge-distance ratios in splitting tests. All splitting tests in this work used a single $\alpha = h_e/h = 0.32$. Verifying that $C_{LBL,k}$ and $k_{mat,LBL}$ stay constant across the splitting-governs range $\alpha < 0.7$ requires tests at additional α values.

Multi-dowel and multi-row splitting tests. The single-dowel single-row case fixes $k_{con,0} = k_{con,90} = k_{n,1} = 1$ in eq. 11.54. The multi-fastener provisions of eqs. 11.58 and 11.60 are not tested by this work.

Calibration of k_{mod} and γ_M for LBL. Both are general EC5 design-conversion factors (§1.8) and apply across every connection limit state, not just splitting. k_{mod} requires long-duration and creep tests on LBL at multiple service classes, fitted to derive instantaneous, short-term, medium-term, long-term and permanent values populating EN 1995-1-1 Table 3.1 for the new material. γ_M requires a reliability analysis on a statistically significant sample of LBL splitting and other failure-mode tests, following EN 1990 Annex D (design assisted by testing), to fix the partial factor for resistance.

Spacing and edge-distance rules. The minimum-spacing and edge-distance provisions of EC5 are derived from timber. Tests on LBL connections at different spacings and edge distances would verify whether the timber rules transfer to LBL or need an LBL-specific revision.

Other fastener types. This study used 16 mm grade-8.8 steel dowels only. Bolts, screws, and nails should be tested for their splitting behaviour in LBL.

Embedment characterisation of LBL. EC5 takes the connection capacity as the lower of the splitting and embedment branches. This thesis calibrates the splitting branch only. The embedment branch needs its own test series to establish $f_{h,90,k}$ for LBL, combined with EYM mode-by-mode validation against measured single-dowel connection capacities. Until this is done, the present splitting calibration alone cannot answer the design-mode-selection question (which mode governs at a given geometry, dowel diameter, and edge distance).

Manufacturing treatment. Different treatments, and glues produce different LBL products. The effect of these manufacturing variables on splitting capacity has not been measured.

LBL from other bamboo species. This work covers LBL made from moso (*Phyllostachys edulis*) only. LBL produced from other bamboo species should be tested before the calibrated $C_{LBL,k}$ and $k_{mat,LBL}$ values are extended beyond moso-based products.

Build-up variants for splitting resistance. Only the standard flatwise (RL) and edgewise (TL) build-ups were tested. Two manufacturing variants could improve splitting resistance but have not been measured. Raising the internode ratio, or placing internodes strategically during lay-up, would interrupt long-fibre paths and give a more interwoven structure. Cross-laminated LBL (CL-LBL), with alternating fibre directions between lamellae, would distribute splitting resistance across more than one orientation. Both need an experimental study before being recommended for design.

Predictive (non-prescribed-path) modelling of LBL splitting. The FEM in this work uses a prescribed crack path because exploratory runs with distributed cohesive elements did not reproduce the experimental fracture locations. A predictive cracking model for LBL splitting, selecting the crack system from the loading and orthotropic geometry alone, remains an open problem.

Snap-back investigation in SENB and ENF. The arc-length solver in this work could not track the post-peak snap-back portion of the F/d curve. A combined experimental and numerical study of snap-back behaviour in LBL fracture tests would close this gap.

Updated testing standards for SENB and ENF. NT BUILD 422 dates from 1993 and was written for timber. No standard exists for ENF on timber-based materials. An updated standard for both, covering laminated bamboo and other engineered-timber products, would help compare results across studies.

Acknowledgements

This thesis is the product of 8 months of testing, modelling, and reading, and it would not exist without the people who guided, taught, supported, and challenged me along the way.

I am grateful to my graduation committee. **Emanuela Bosco** (TU/e, Associate Professor) stepped up as committee chair and gave essential input on the FEM cohesive-zone modelling. **Arjan Habraken** (TU/e, Assistant Professor) was my guiding supervisor and the constant through the whole project: the bi-weekly design-studio discussions with him and peers kept the structural-engineering perspective in focus, and his decision to connect me with Ad Leijten unlocked the Eurocode 5 splitting story. **Roy Crielaard** (Arup) joined as external supervisor and gave the manuscript its sharpest critical review. The report structure and several reframings in chapters 1 and 5 follow directly from his comments.

The experimental work would not have been possible without the LBL sample donated by **MOSO Bamboo**. I thank **Arjan van der Vegte** (MOSO) for arranging the sample sponsorship.

Several researchers and professionals gave generously of their time outside the formal committee. **Ad Leijten** (retired Professor, TU/e and TU Delft) shared first-hand insight into the original EC5 splitting research that produced equation 8.4 and reviewed the splitting-test setup. **Sebastian Kaminski** (Arup) helped frame the research at the start and made the introduction to David Trujillo. **David Trujillo** (Professor, University of Warwick) sharpened the framing of the bamboo-engineering and code alignment. **Davide Leonetti** (Associate Professor, TU/e) and **Jose Luis Galan Argumedo** (Arup) were generous with fracture-mechanics discussions. **Ron Peerlings** (Associate Professor, TU/e)'s fracture-mechanics lectures shaped the theoretical backbone of chapter 2. **Rianne Luimes** (TNO) advised on the SENB testing and on the snap-back behaviour observed in several specimens, which informed the post-peak interpretation. **Wim de Groot** (Docent, TU/e and SHR) and **Faas Moonen** (retired Associate Professor, TU/e) offered timber-research insights. **Jamie Dennis** (Arup) was the go-to for computational design with LS-DYNA.

In the SED laboratory at TU/e, **Theo van de Loo** prepared the specimens and built up the test setups, **Eric Wijen** ran the calibration, setup and test execution, and **Hans Lamers** organised the test programme and kept the lab discussions lively. The quality of the experimental data is in large part thanks to them.

Several fellow students sharpened the work through conversation. **Ruben Philips** (TU/e and Arup) traded practical and research notes. **Kaj Hasenaar** (TU/e) and **Cas Gansner** gave helpful feedback at Arjan's design-studio. **Bonno van der Horst** (TU/e) shared insights from his own SENB research. **Mees Fabel** (TU/e) was a fellow bamboo researcher and a lively sounding board. **Sten van Meel** (TU/e) was a strong sparring partner in the SED lab.

My wife **Santika Chenderasa** supported me through the entire journey with a patience I did not always deserve. This thesis would not have been possible without her.

References

[1] E. T. Akinlabi, K. Anane-Fenin, and D. R. Akwada. *Bamboo: The Multipurpose Plant*. Cham, Switzerland: Springer International Publishing, 2017. doi: 10.1007/978-3-319-56808-9.

[2] L. S. AlRukaibawi, M. Kachichian, and G. Károly. "Mechanical properties of laminated bamboo lumber N-finity according to ISO 23478-2022". In: *Journal of Wood Science* 70, 1 (2024). doi: 10.1186/s10086-023-02115-z.

[3] M. Ballerini and M. Rizzi. "Numerical analyses for the prediction of the splitting strength of beams loaded perpendicular-to-grain by dowel-type connections". In: *Materials and Structures* 40 (2007), pp. 139–149. doi: 10.1617/s11527-006-9156-2.

[4] H. J. Blass and C. Sandhaas. *Timber Engineering — Principles for Design*. Karlsruhe, Germany: KIT Scientific Publishing, 2017. doi: 10.5445/KSP/1000069616.

[5] CEN. *EN 1995-1-1: Eurocode 5 — Design of timber structures — Part 1-1: General — Common rules and rules for buildings*. Tech. rep. Brussels: European Committee for Standardization, 2004.

[6] CEN. *FprEN 1995-1-1:2025: Eurocode 5 — Design of timber structures — Part 1-1: General rules and rules for buildings*. Tech. rep. Final draft. Brussels: European Committee for Standardization, 2025.

[7] G. Chen, Y. Yu, X. Li, and B. He. "Mechanical behavior of laminated bamboo lumber for structural application: an experimental investigation". In: *European Journal of Wood and Wood Products* 78 (2020), pp. 53–63. doi: 10.1007/s00107-019-01486-9.

[8] Q. Chen, C. Dai, C. Fang, M. Chen, S. Zhang, R. Liu, X. Liu, and B. Fei. "Mode I interlaminar fracture toughness behavior and mechanisms of bamboo". In: *Materials & Design* 183, 108132 (2019). doi: 10.1016/j.matdes.2019.108132.

[9] Q. Chen, B. Fei, J. Qi, S. Zhang, X. Huang, Y. Jiang, J. Xie, and S. Jia. "Effect of moisture content on bamboo's mode I interlaminar fracture toughness: the competition between promoting and impeding crack growth". In: *Construction and Building Materials* 341, 127822 (2022). doi: 10.1016/j.conbuildmat.2022.127822.

[10] Y. Chen, H. Li, L. Gao, W. Xu, R. Lorenzo, and M. Gaff. "A review of experimental research on the mode I fracture behavior of bamboo". In: *Journal of Renewable Materials* 11 (2023). doi: 10.32604/jrm.2023.027634.

[11] J. Ehlbeck and R. Görlacher. "Tension perpendicular to the grain in joints". In: *Timber Engineering STEP 1*. Almere, The Netherlands: Centrum Hout, 1995. Chap. C2.

[12] R. Ellison. "Mode II fracture mechanics of moso bamboo for application in novel engineering materials". MA thesis. Massachusetts Institute of Technology, 2015. url: http://hdl.handle.net/1721.1/98653.

[13] J. L. Gómez-Royuela, A. Majano-Majano, A. J. Lara-Bocanegra, J. Xavier, and M. F. S. F. de Moura. "Experimental and numerical research on the splitting capacity of European beech beams loaded perpendicular to the grain by connections". In: *Applied Sciences* 14.2, 900 (2024). doi: 10.3390/app14020900.

[14] K. A. Harries and D. Trujillo. "Opportunities and limitations for the design of engineered bamboo structures using design standards for wood". In: *Journal of Building Engineering* 114, 114125 (2025). doi: 10.1016/j.jobe.2025.114125.

[15] *ISO 23478:2022 – Bamboo structures – Engineered bamboo products – Test methods for determination of physical and mechanical properties*. Tech. rep. ISO 23478:2022. Geneva, Switzerland: International Organization for Standardization, 2022.

[16] *ISO 554:1976 – Standard atmospheres for conditioning and/or testing – Specifications*. Tech. rep. ISO 554:1976. Geneva, Switzerland: International Organization for Standardization, 1976.

[17] J. J. A. Janssen. *Mechanical Properties of Bamboo*. Vol. 37. Forestry Sciences. Dordrecht: Springer, 1991. doi: 10.1007/978-94-011-3236-7.

[18] R. Jockwer and P. Dietsch. "Review of design approaches and test results on brittle failure modes of connections loaded at an angle to the grain". In: *Engineering Structures* 171 (2018), pp. 362–372. doi: 10.1016/j.engstruct.2018.05.061.

[19] K. W. Johansen. "Theory of timber connections". In: *IABSE Publications* 9 (1949). doi: 10.5169/seals-9703.

[20] J. Jonasson, H. Danielsson, and E. Serrano. "Fracture energy of birch in tension perpendicular to grain: experimental evaluation and comparative numerical simulations". In: *Wood Science and Technology* 58 (2024), pp. 1925–1949. doi: 10.1007/s00226-024-01595-6.

[21] S. Kaminski, A. Lawrence, and D. J. A. Trujillo. "Structural use of bamboo, Part 1: introduction to bamboo". In: *The Structural Engineer* (Aug. 2016).

[22] H. J. Larsen and P. J. Gustafsson. "Design of end-notched beams". In: *Proceedings of CIB-W18 Meeting 23, Paper 23-10-3*. Lisbon, Portugal, 1990.

[23] A. J. M. Leijten. "Splitting of timber beams caused by perpendicular to grain forces of multiple connections". In: *Engineering Structures* 171 (2018), pp. 10–14. doi: 10.1016/j.engstruct.2018.05.059.

[24] H.-t. Li, A. J. Deeks, Q.-s. Zhang, and G. Wu. "Flexural performance of laminated bamboo lumber beams". In: *BioResources* 11.1 (2016), pp. 929–943. doi: 10.15376/biores.11.1.929-943.

[25] W. Liu, Z. Li, and Z. Li. "Mixed-mode I/II fracture performances of glued laminated bamboo in the in-plane longitudinal direction". In: *Engineering Fracture Mechanics* 281, 109080 (2023). doi: 10.1016/j.engfracmech.2023.109080.

[26] Y. Liu, B. Sheng, D. Huang, and A. Zhou. "Mode-I interlaminar fracture behavior of laminated bamboo composites". In: *Advances in Structural Engineering* 24 (2021), pp. 733–741. doi: 10.1177/1369433220965270.

[27] D. Malkowska, T. Laux, D. Trujillo, and J. Norman. "Adaptation of a wood theoretical fracture model for predicting splitting capacity of dowelled connections in bamboo". In: *Construction and Building Materials* 357, 129358 (2022). doi: 10.1016/j.conbuildmat.2022.129358.

[28] MOSO International B.V. *MOSO N-finity indoor beams – product datasheet*. Product datasheet. June 2023.

[29] M. F. S. F. de Moura and A. B. de Morais. "Equivalent crack based analyses of ENF and ELS tests". In: *Engineering Fracture Mechanics* 75.9 (2008), pp. 2584–2596. doi: 10.1016/j.engfracmech.2007.03.005.

[30] F. L. Palombini and F. M. Nogueira, eds. *Bamboo and Sustainable Construction*. Environmental Footprints and Eco-design of Products and Processes. Singapore: Springer Nature Singapore, 2023. doi: 10.1007/978-981-99-0232-3.

[31] N. Perez. *Fracture Mechanics*. 2nd ed. Cham, Switzerland: Springer, 2017. doi: 10.1007/978-3-319-24999-5.

[32] T. A. C. M. van der Put. "Tension perpendicular to the grain at notches and joints". In: *Proceedings of CIB-W18 Meeting 23, Paper 23-10-1*. Lisbon, Portugal, 1990.

[33] T. C. A. M. van der Put and A. J. M. Leijten. "Evaluation of perpendicular to grain failure of beams caused by concentrated loads of joints". In: *Proceedings of CIB-W18 Meeting 33*. Delft, The Netherlands, 2000.

[34] T. Reynolds, B. Sharma, K. Harries, and M. Ramage. "Dowelled structural connections in laminated bamboo and timber". In: *Composites Part B: Engineering* 90 (2016), pp. 232–240. doi: 10.1016/j.compositesb.2015.11.045.

[35] T. P. S. Reynolds, B. Sharma, E. Serrano, P.-J. Gustafsson, and M. H. Ramage. "Fracture of laminated bamboo and the influence of preservative treatments". In: *Composites Part B: Engineering* 174, 107017 (2019). doi: 10.1016/j.compositesb.2019.107017.

[36] J. C. M. Schoenmakers. "Fracture and failure mechanisms in timber loaded perpendicular to the grain by mechanical connections". PhD thesis. Technische Universiteit Eindhoven, 2010. doi: 10.6100/IR673053.

[37] Z.-P. Shao, C.-H. Fang, and G.-L. Tian. "Mode I interlaminar fracture property of moso bamboo (*Phyllostachys pubescens*)". In: *Wood Science and Technology* 43 (2009), pp. 527–536. doi: 10.1007/s00226-009-0265-2.

[38] B. Sharma, H. Bauer, G. Schickhofer, and M. H. Ramage. "Mechanical characterisation of structural laminated bamboo". In: *Proceedings of the Institution of Civil Engineers – Structures and Buildings* 170.4 (2017), pp. 250–264. doi: 10.1680/jstbu.16.00061.

[39] B. Sharma, A. Gatão, M. Bock, and M. Ramage. "Engineered bamboo for structural applications". In: *Construction and Building Materials* 81 (2015), pp. 66–73. doi: 10.1016/j.conbuildmat.2015.01.077.

[40] G. C. Sih, P. C. Paris, and G. R. Irwin. "On cracks in rectilinearly anisotropic bodies". In: *International Journal of Fracture Mechanics* 1.3 (1965), pp. 189–203. doi: 10.1007/BF00186854.

[41] F. Wang, Z. Shao, and Y. Wu. "Mode II interlaminar fracture properties of Moso bamboo". In: *Composites Part B: Engineering* 44 (2013), pp. 242–247. doi: 10.1016/j.compositesb.2012.05.035.

[42] F. Wang, Z. Shao, Y. Wu, and D. Wu. "The toughness contribution of bamboo node to the mode I interlaminar fracture toughness of bamboo". In: *Wood Science and Technology* 48 (2014), pp. 1257–1268. doi: 10.1007/s00226-013-0591-2.

[43] S. Wang, H. Li, G. Cheng, Z. Xiong, and M. Ashraf. "Mechanical behavior of bolted steel laminated bamboo lumber connections loaded perpendicular to grain". In: *Construction and Building Materials* 345, 128302 (2022). doi: 10.1016/j.conbuildmat.2022.128302.

[44] *Wood: Fracture energy in tension perpendicular to the grain*. Tech. rep. NT BUILD 422. Nordtest, 1993.

[45] Y. Wu, Z. Wan, and Z. Li. "Mode I fracture behavior of unidirectional bamboo laminate and its applications to the estimation of bamboo–steel–bamboo connections' bearing capacities". In: *Structures* 45 (2022), pp. 2226–2238. doi: 10.1016/j.istruc.2022.10.050.

Appendix A

Full Results

This appendix collects the full set of results and calculation figures and tables.

A.1 Figures

A.1.1 SENB

Figure A.1: SENB specimen preparation. Bamboo lamellae clamped during glue cure to form the three-element specimen with the central cube rotated to the target crack system.

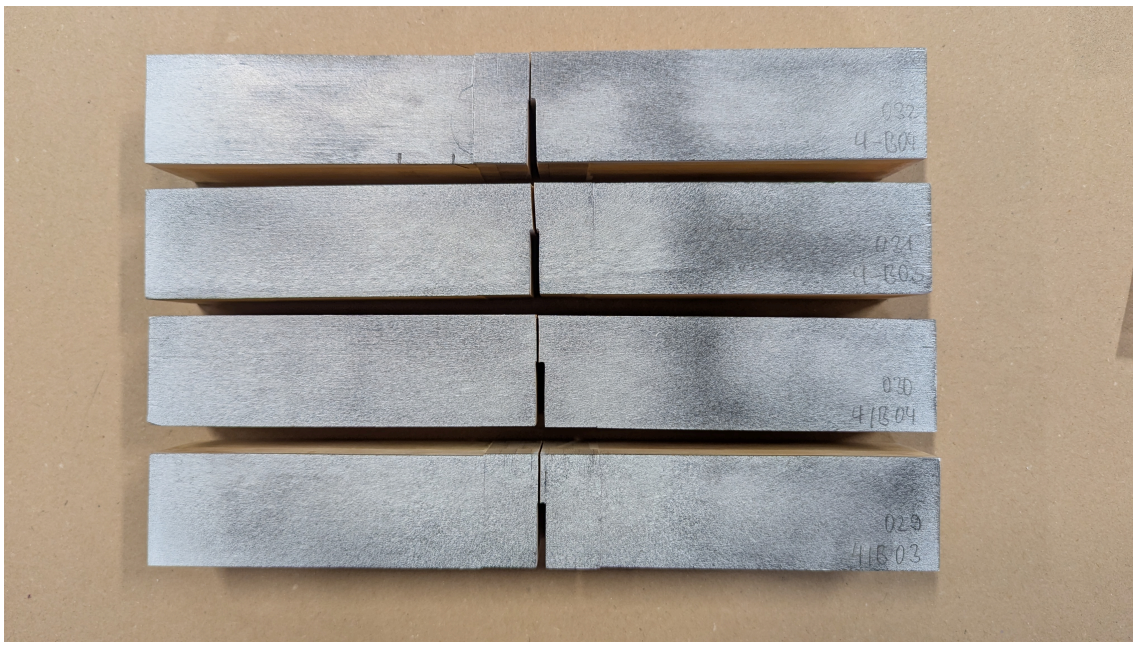

Figure A.2: Fractured SENB specimens after testing, showing the central notch and the Mode I crack.

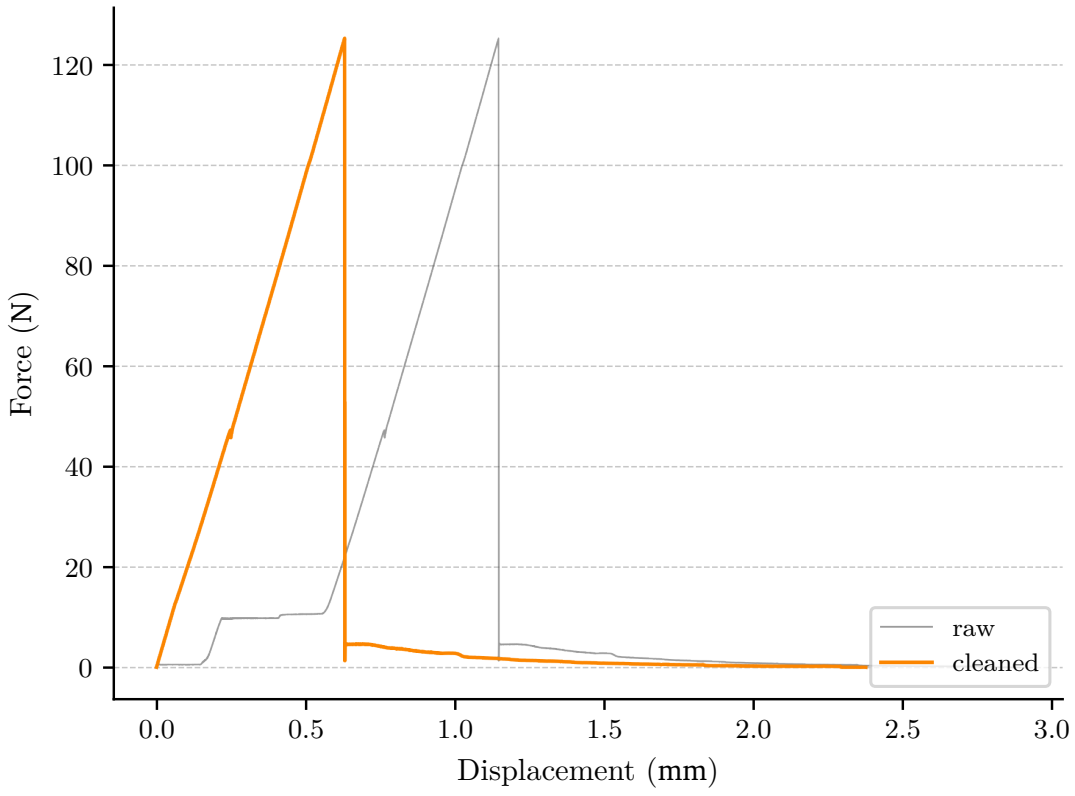

Figure A.3: Example raw vs. cleaned data for SENB specimen.

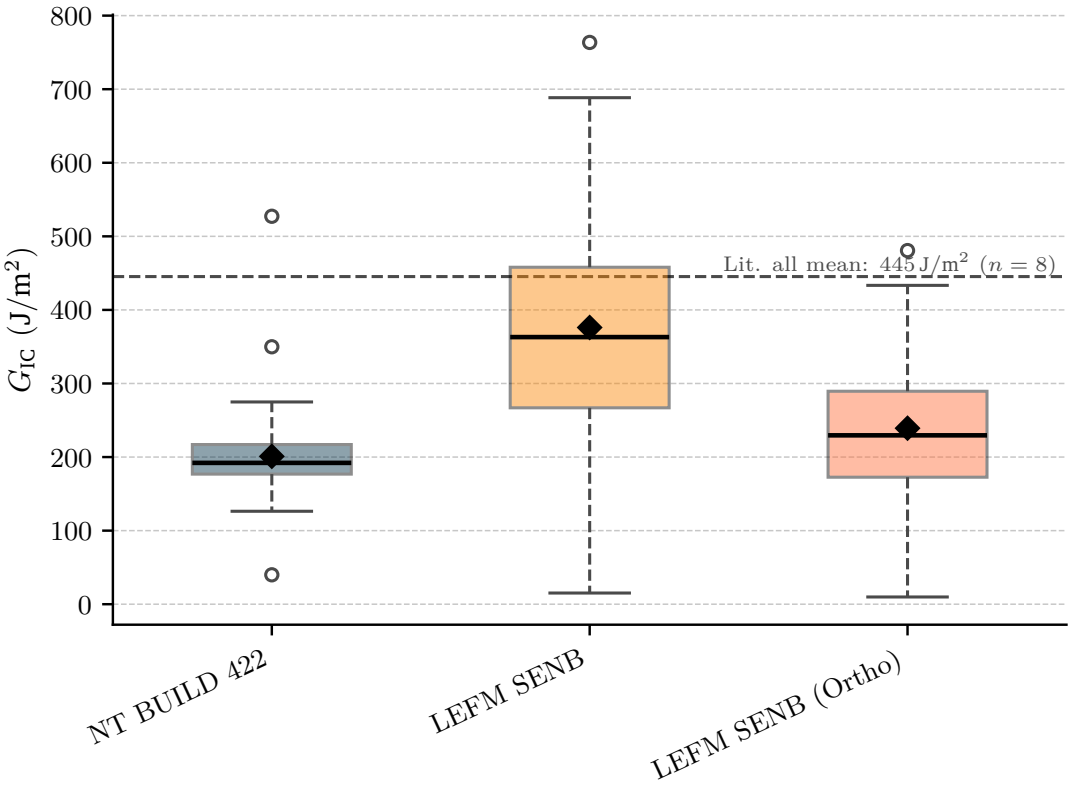

Figure A.4: G_{IC} by calculation method, all batches (cleaned), $n = 62$.

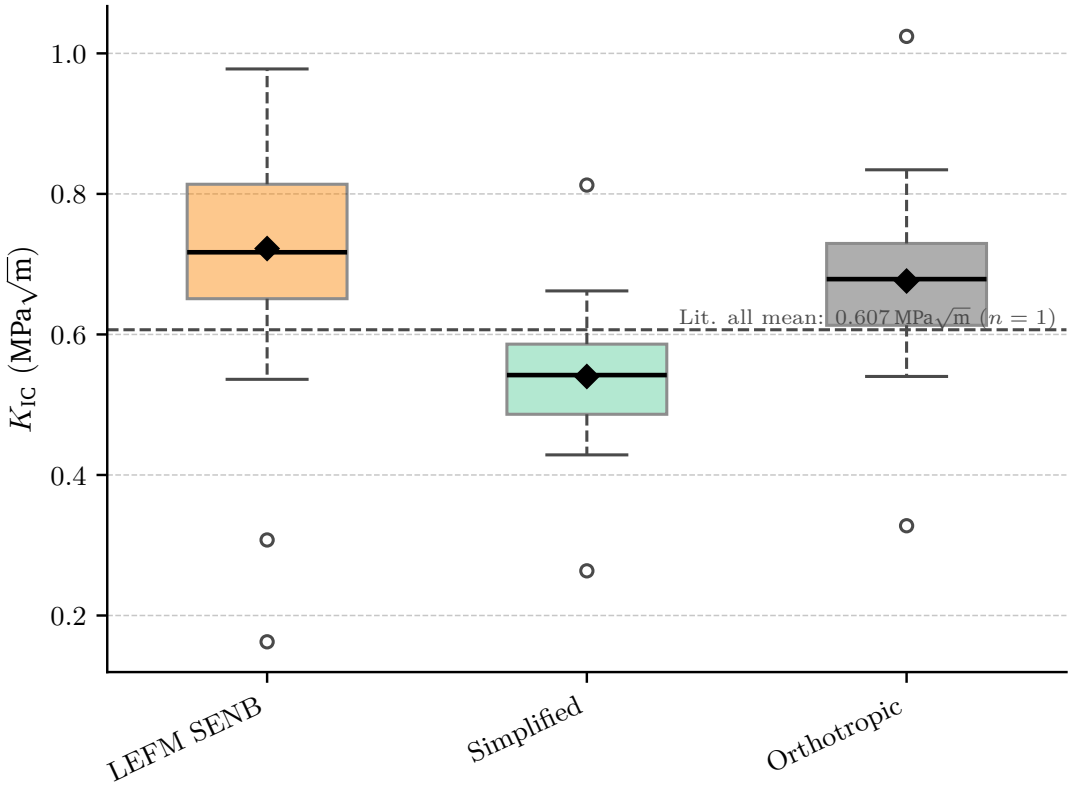

Figure A.5: K_{IC} by calculation method, all batches (cleaned), $n = 62$.

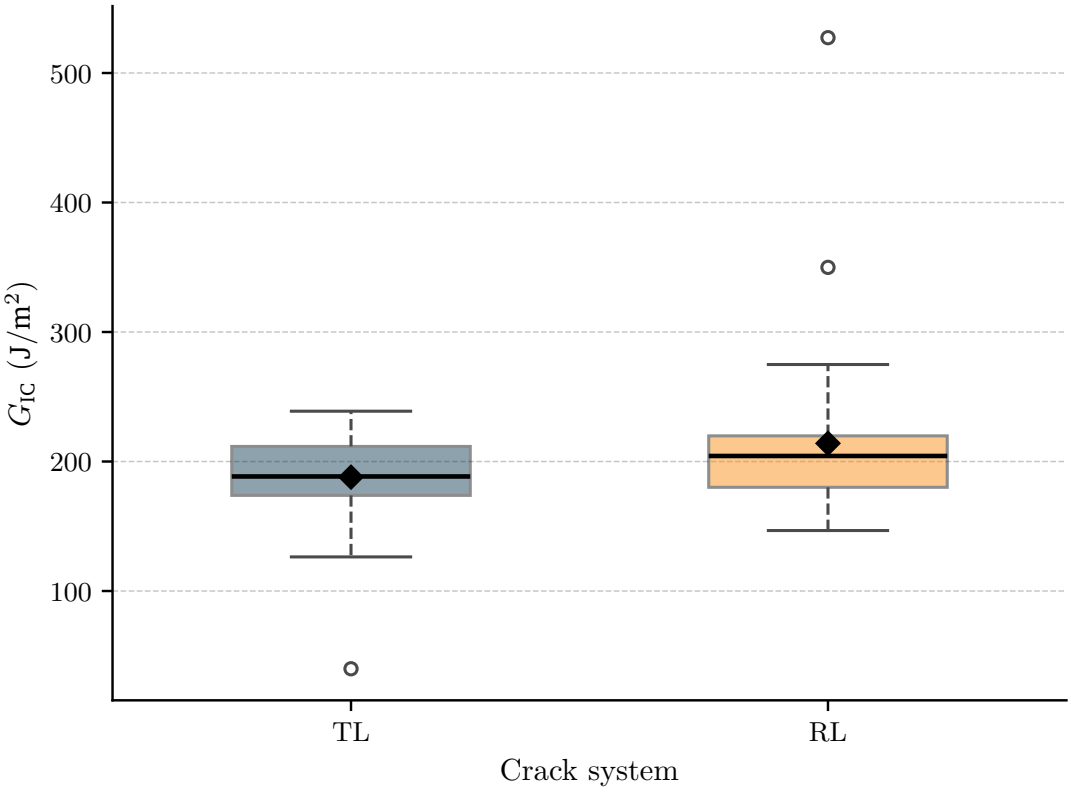

Figure A.6: G_{IC} by crack system, SENB, $n = 62$.

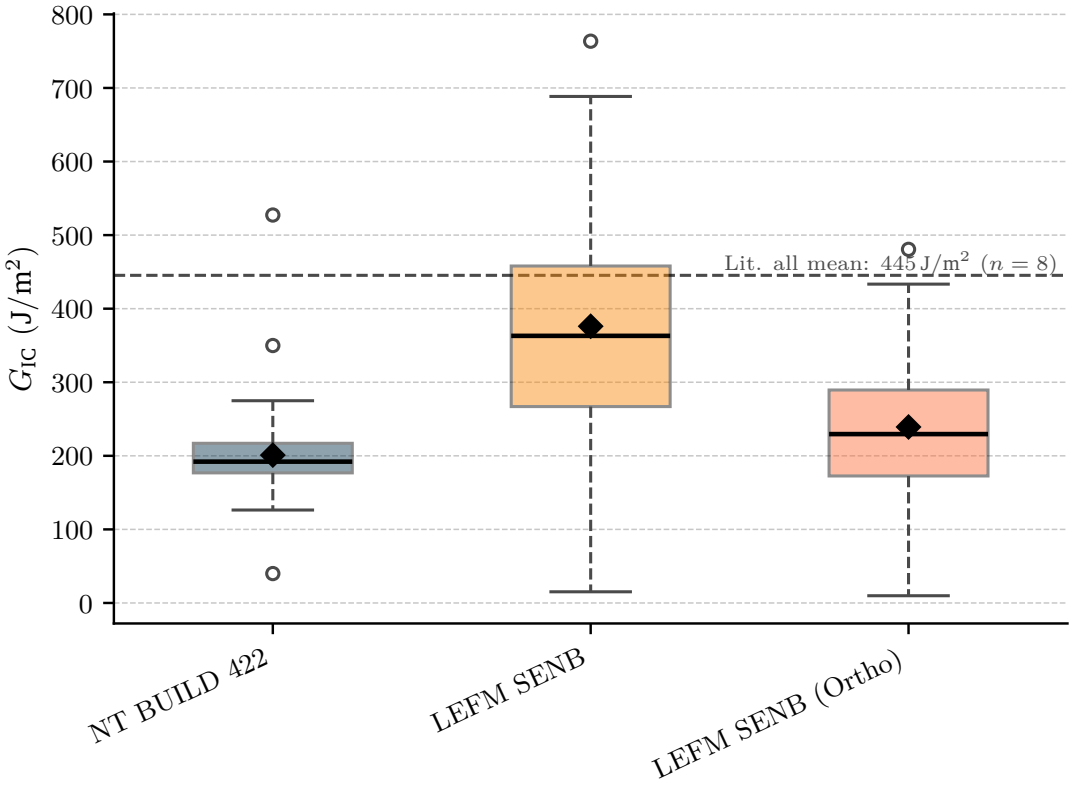

Figure A.7: G_{IC} by calculation method, all batches (cleaned), $n = 62$.

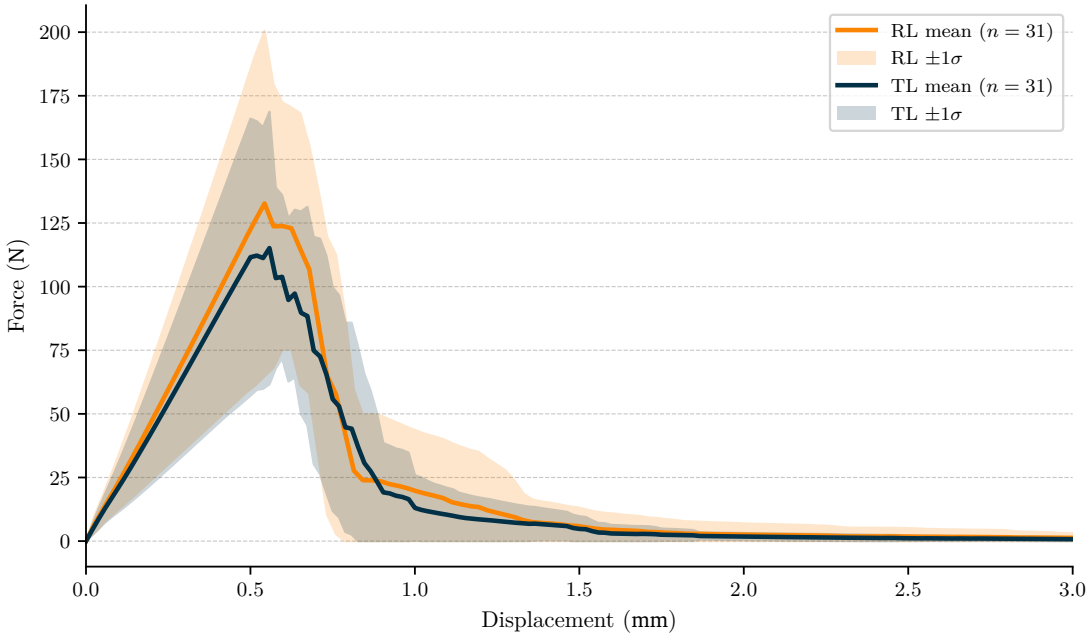

Figure A.8: SENB load-displacement curves, all batches (cleaned), $n = 62$.

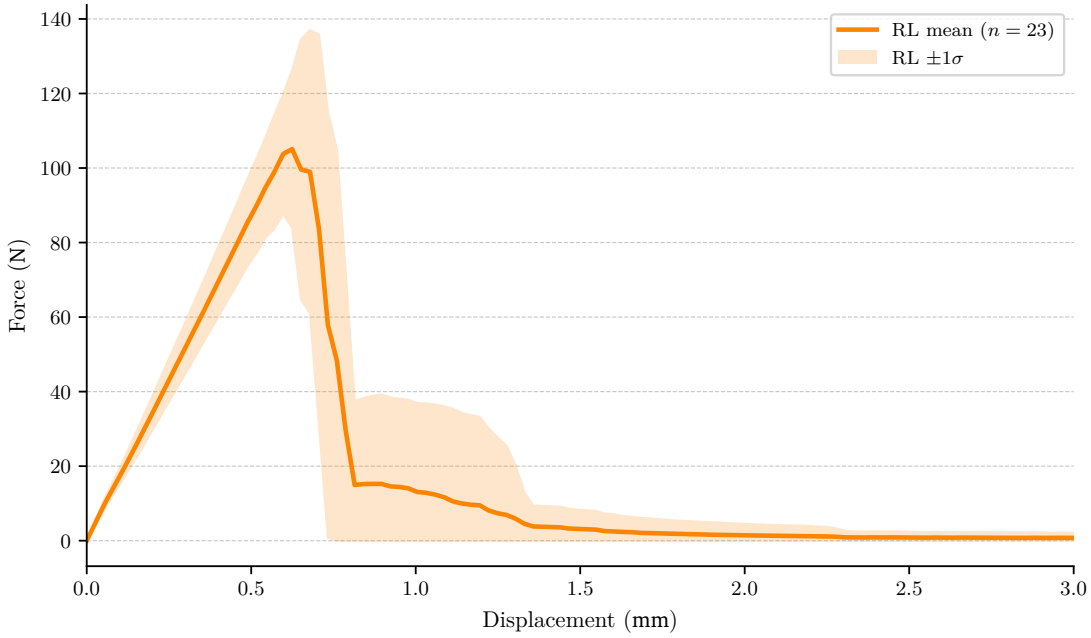

Figure A.9: SENB load-displacement curves, batch SENB-2-RL (cleaned), $n = 23$.

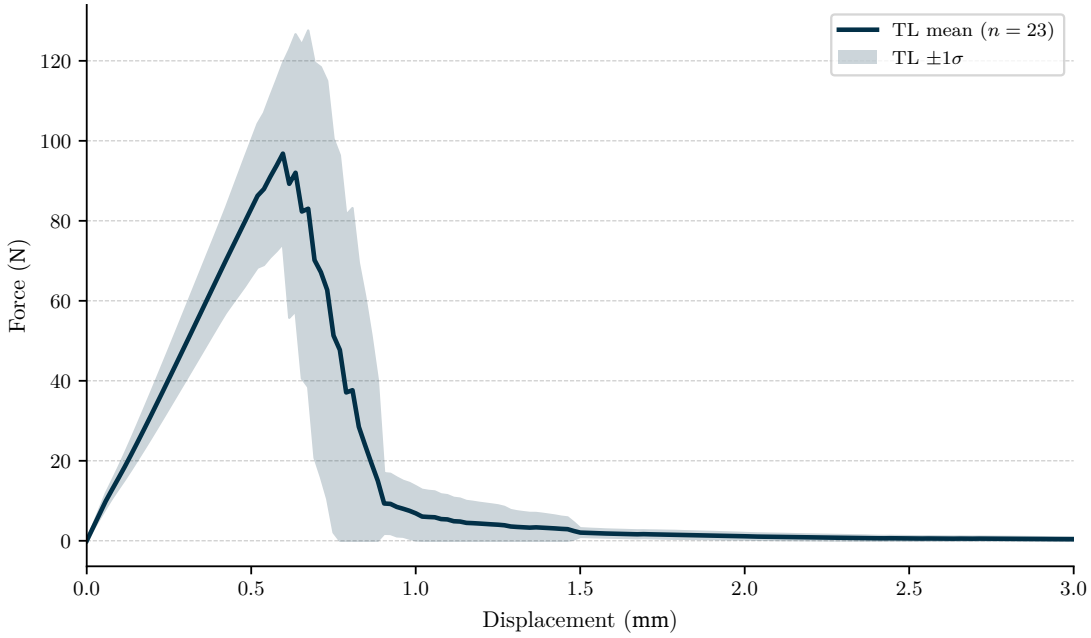

Figure A.10: SENB load-displacement curves, batch SENB-2-TL (cleaned), $n = 23$.

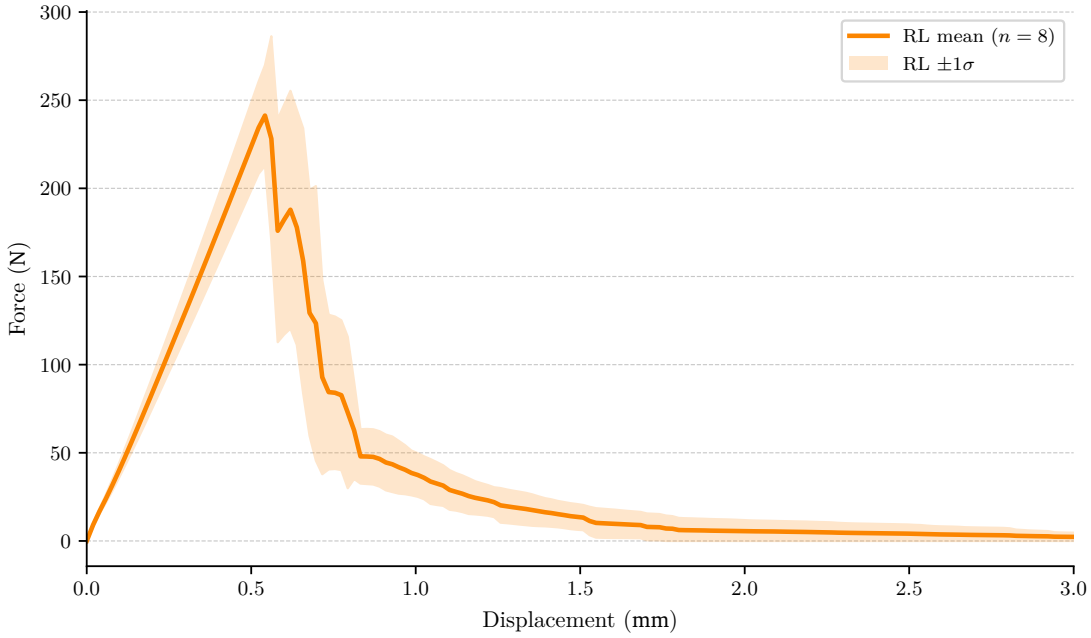

Figure A.11: SENB load-displacement curves, batch SENB-4-RL (cleaned), $n = 8$.

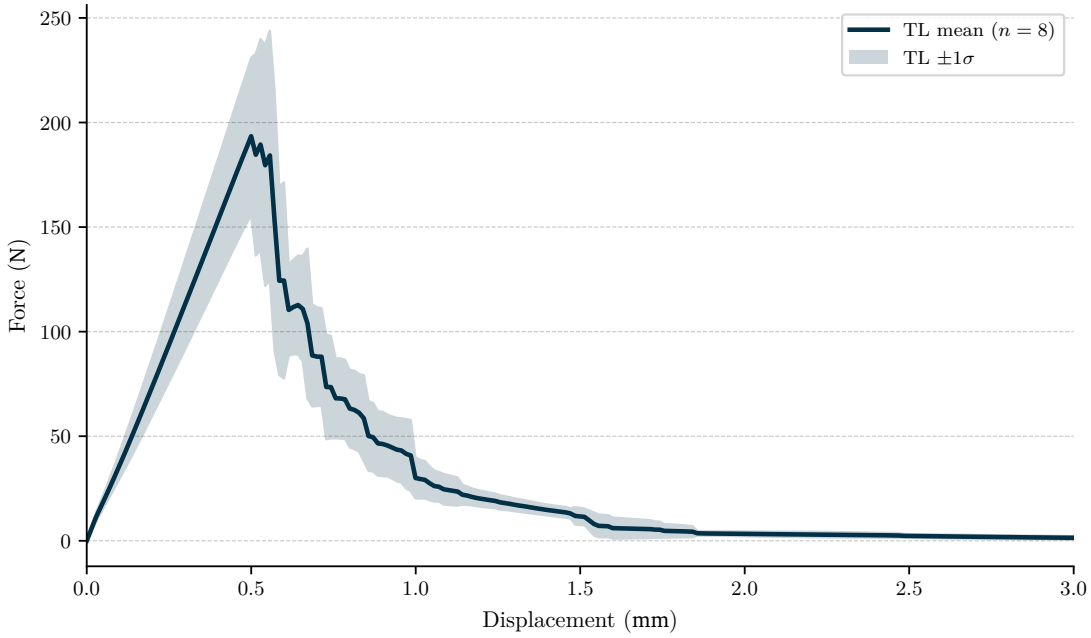

Figure A.12: SENB load-displacement curves, batch SENB-4-TL (cleaned), $n = 8$.

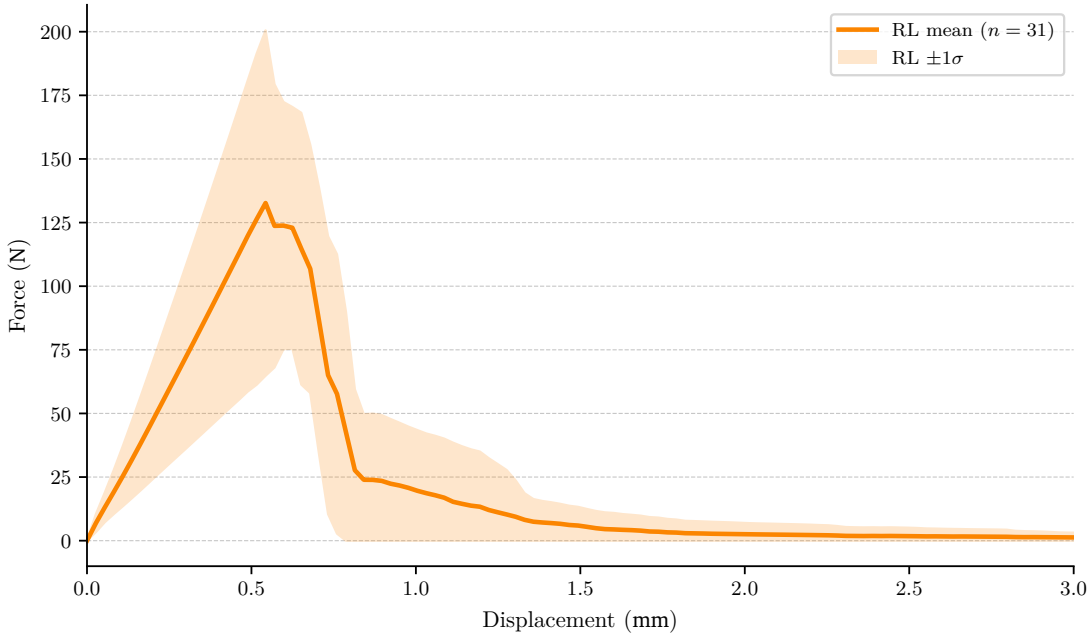

Figure A.13: SENB load-displacement curves, all batches, RL (cleaned), $n = 31$.

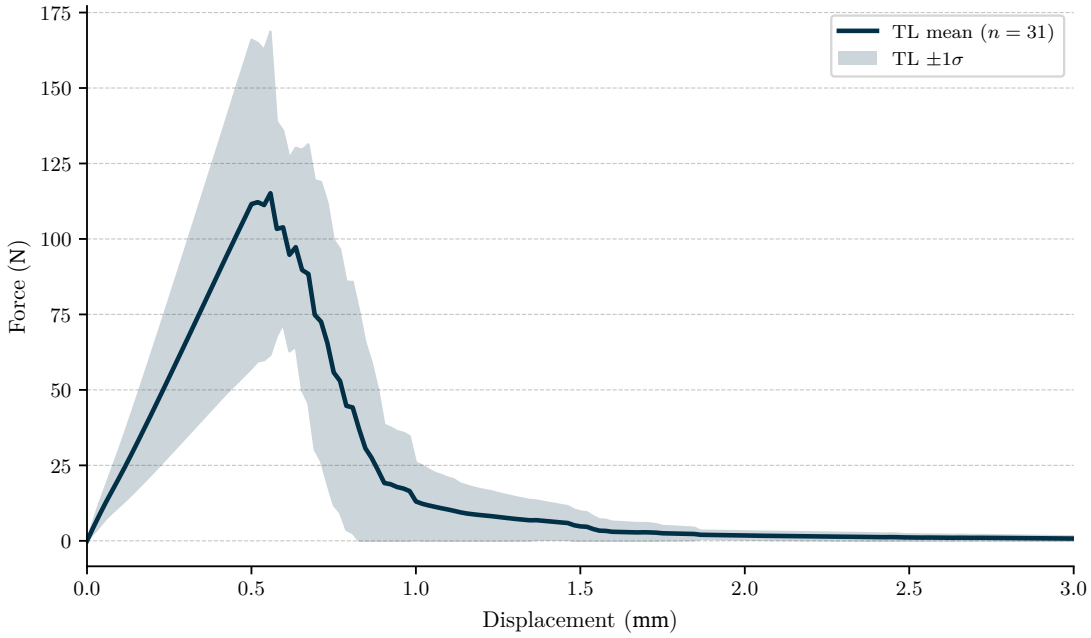

Figure A.14: SENB load-displacement curves, all batches, TL (cleaned), $n = 31$.

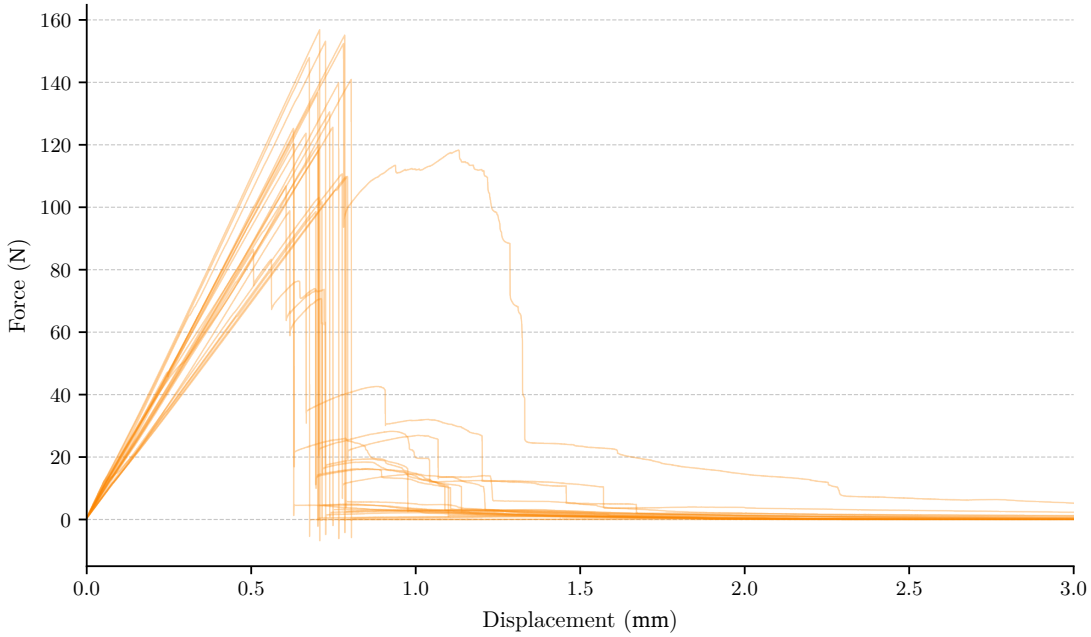

Figure A.15: SENB load-displacement curves, batch SENB-2-RL (cleaned), $n = 23$.

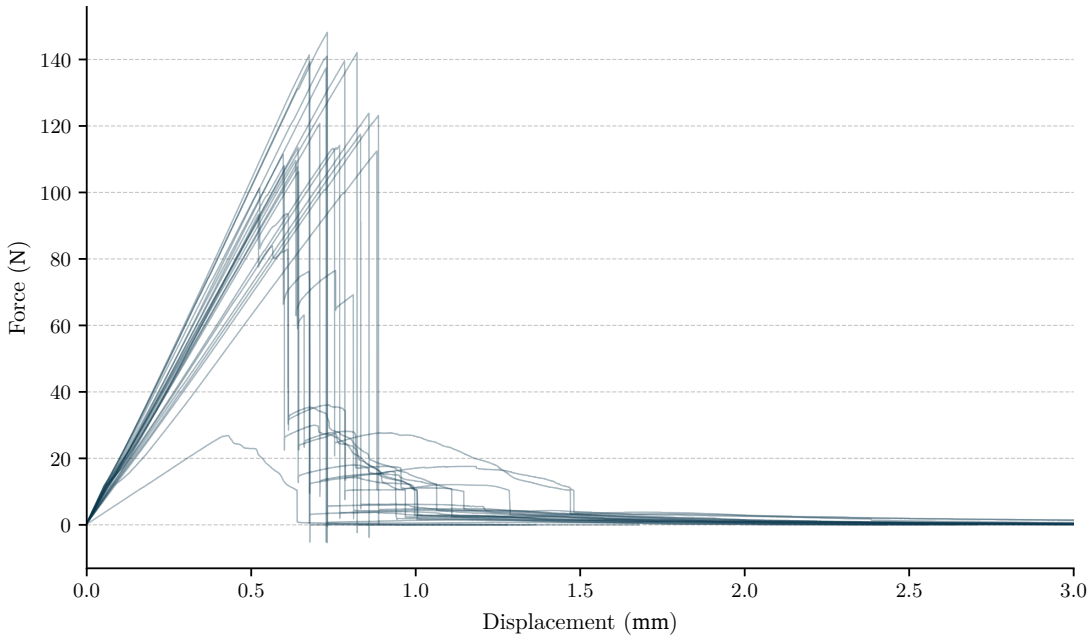

Figure A.16: SENB load-displacement curves, batch SENB-2-TL (cleaned), $n = 23$.

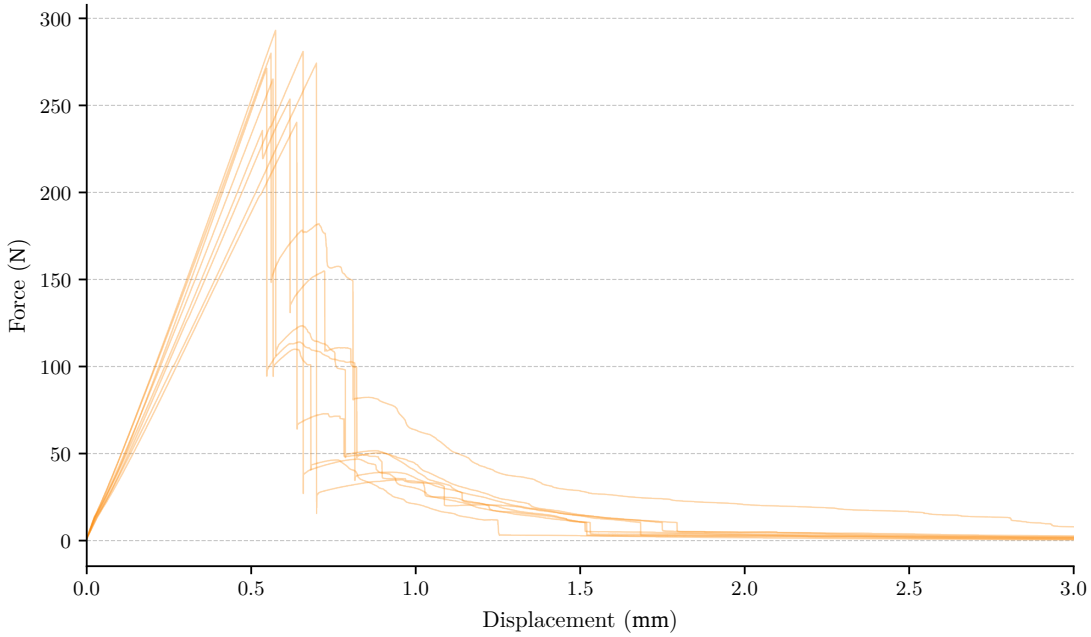

Figure A.17: SENB load-displacement curves, batch SENB-4-RL (cleaned), $n = 8$.

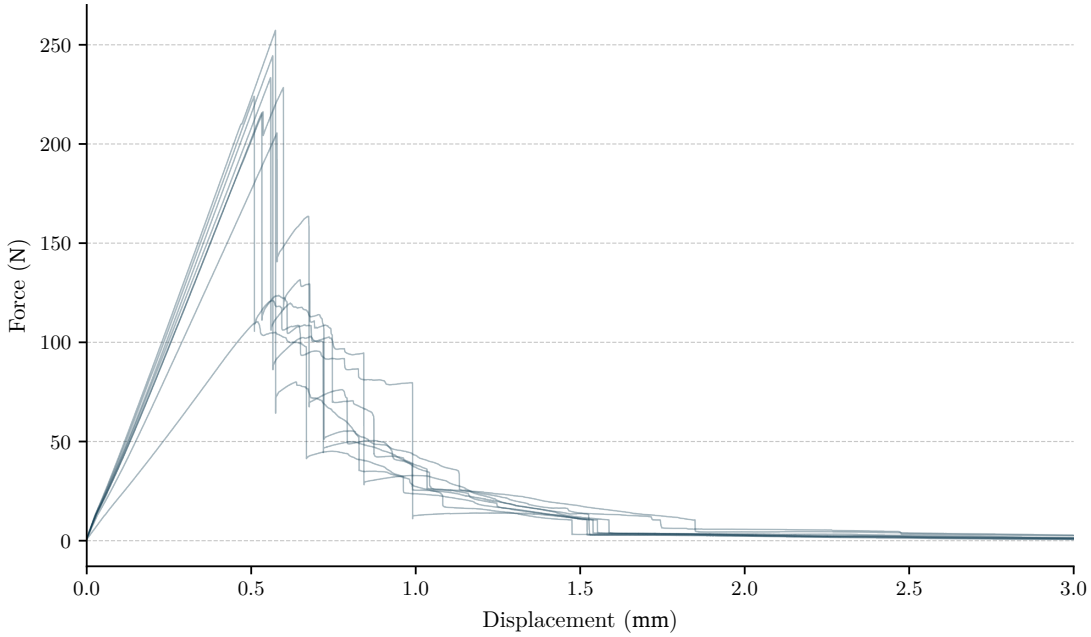

Figure A.18: SENB load-displacement curves, batch SENB-4-TL (cleaned), $n = 8$.

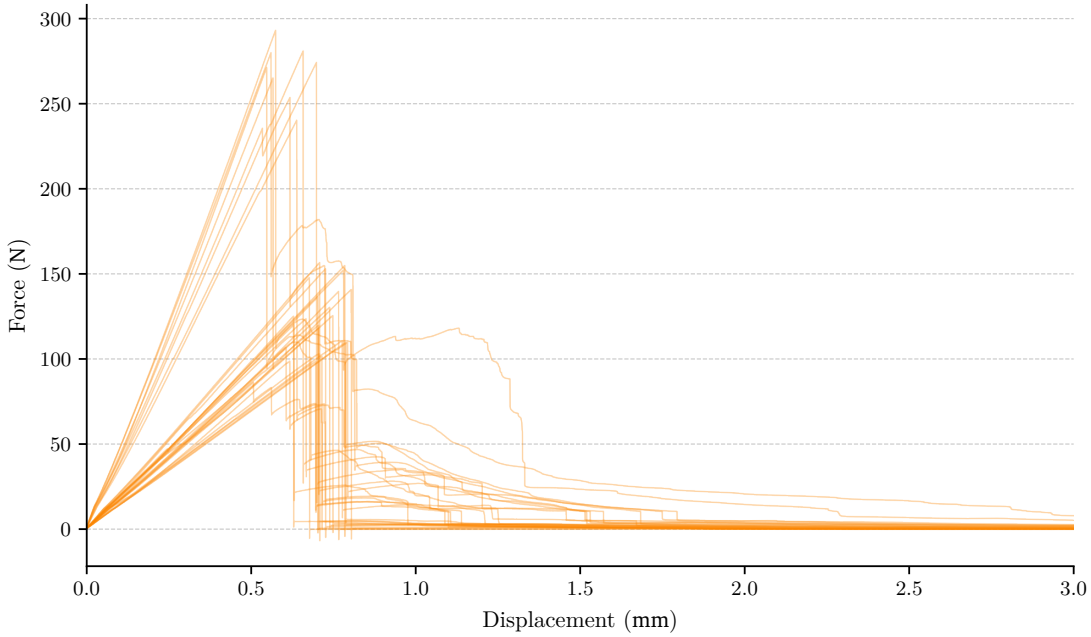

Figure A.19: SENB load-displacement curves, all batches, RL (cleaned), $n = 31$.

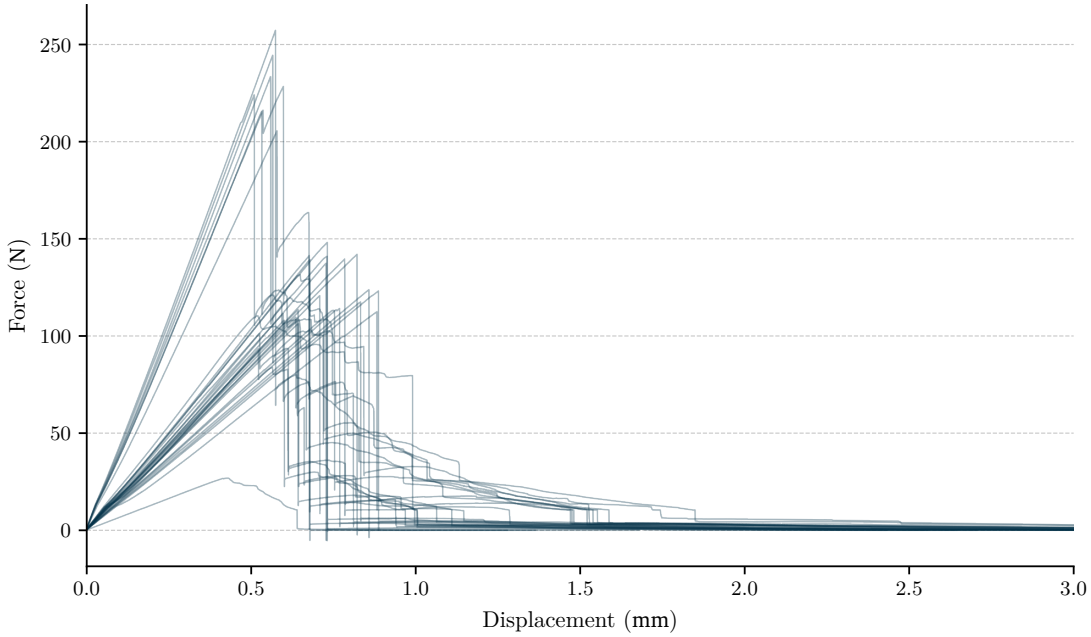

Figure A.20: SENB load-displacement curves, all batches, TL (cleaned), $n = 31$.

A.1.2 ENF

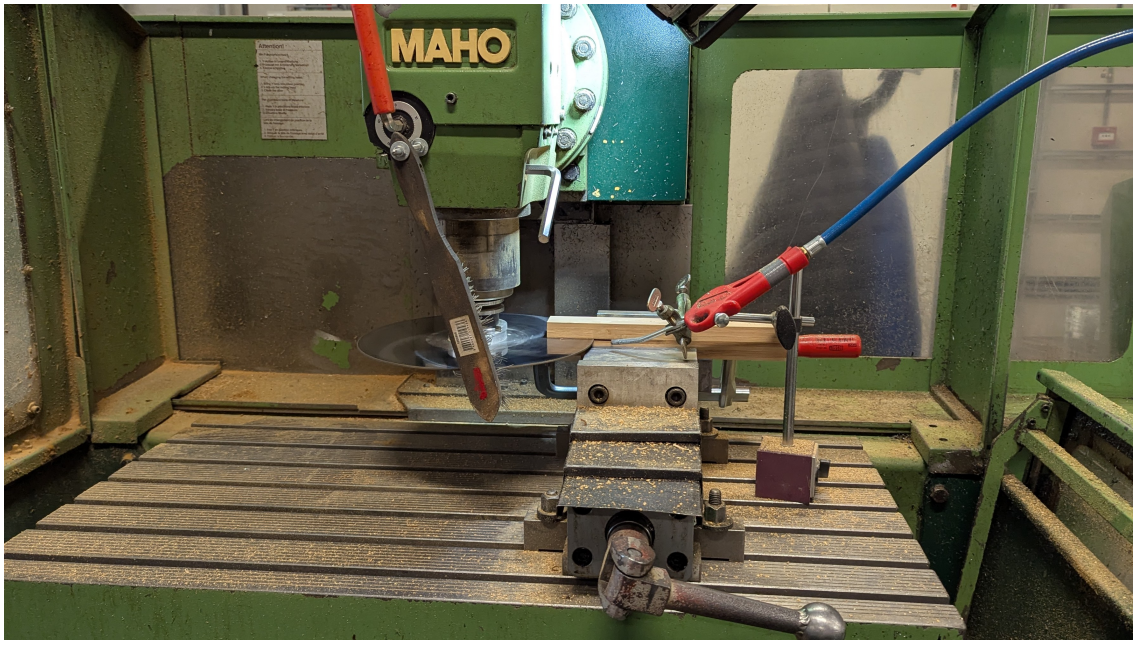

Figure A.21: ENF specimen preparation. Mid-plane pre-crack notch cut on a MAHO milling machine with a circular saw blade, the specimen clamped horizontally on the bed.

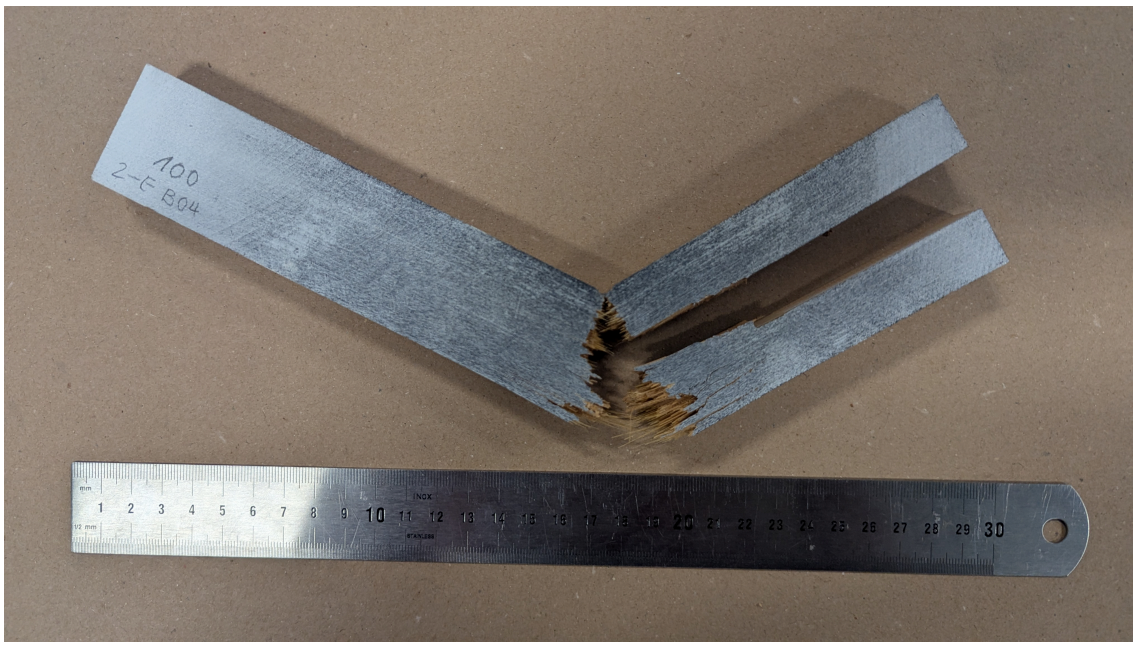

Figure A.22: Fractured ENF specimen after Mode II testing, mid-span V-failure shown with ruler for scale.

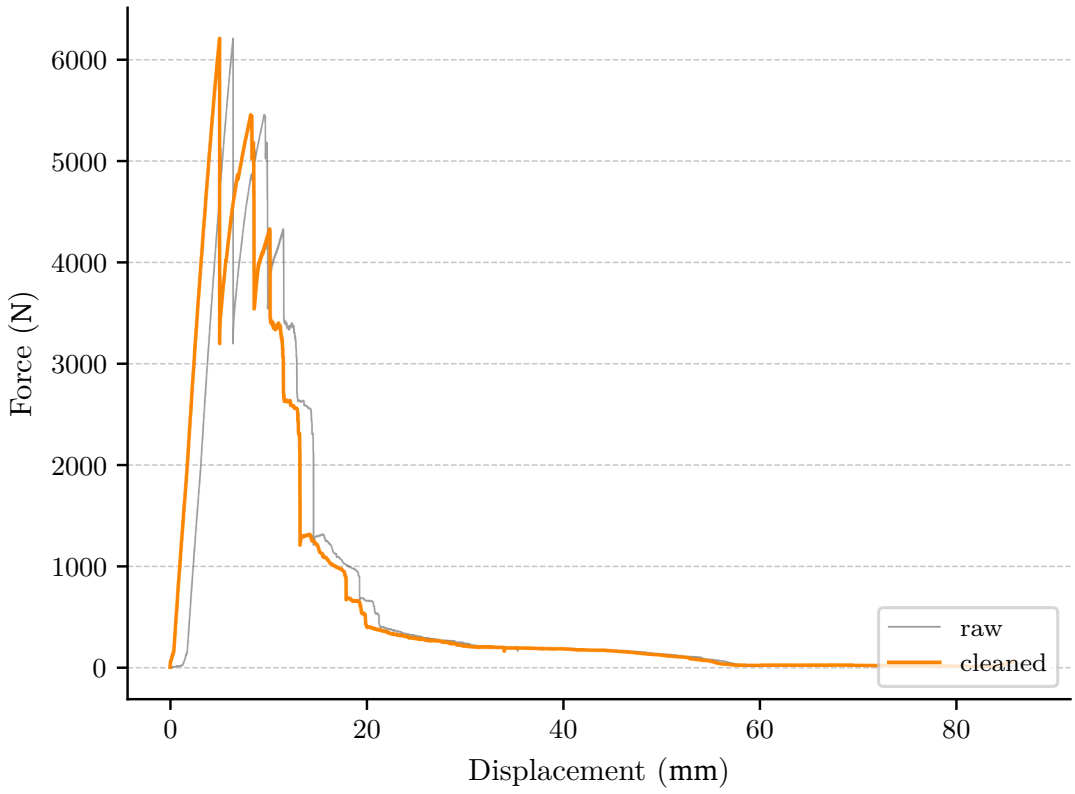

Figure A.23: Example raw vs. cleaned data for ENF specimen.

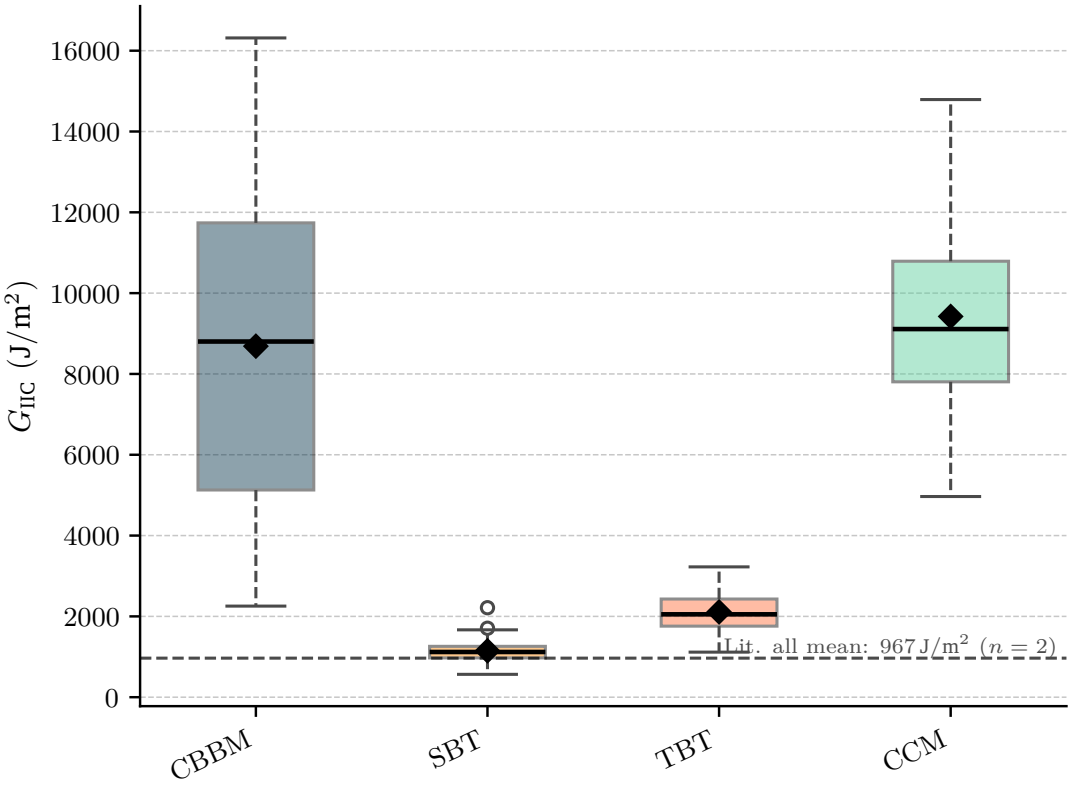

Figure A.24: G_{IIC} by calculation method, all batches (cleaned), $n = 50$.

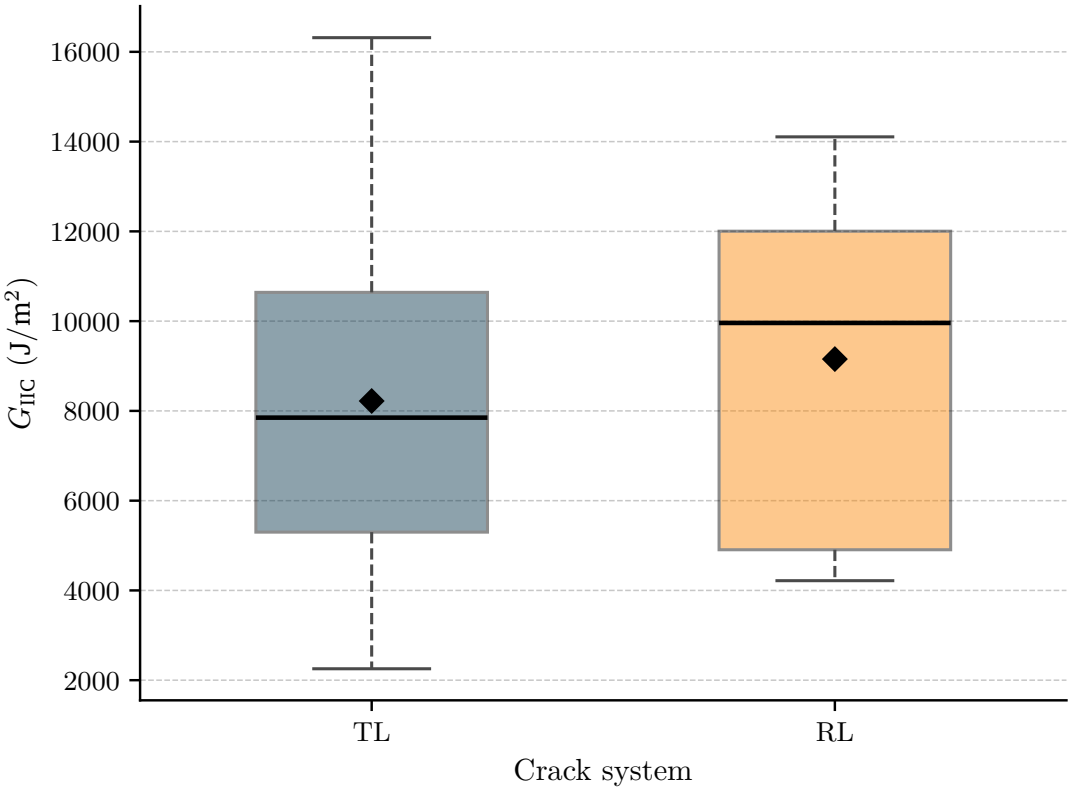

Figure A.25: G_{IIC} by crack system, ENF, $n = 50$.

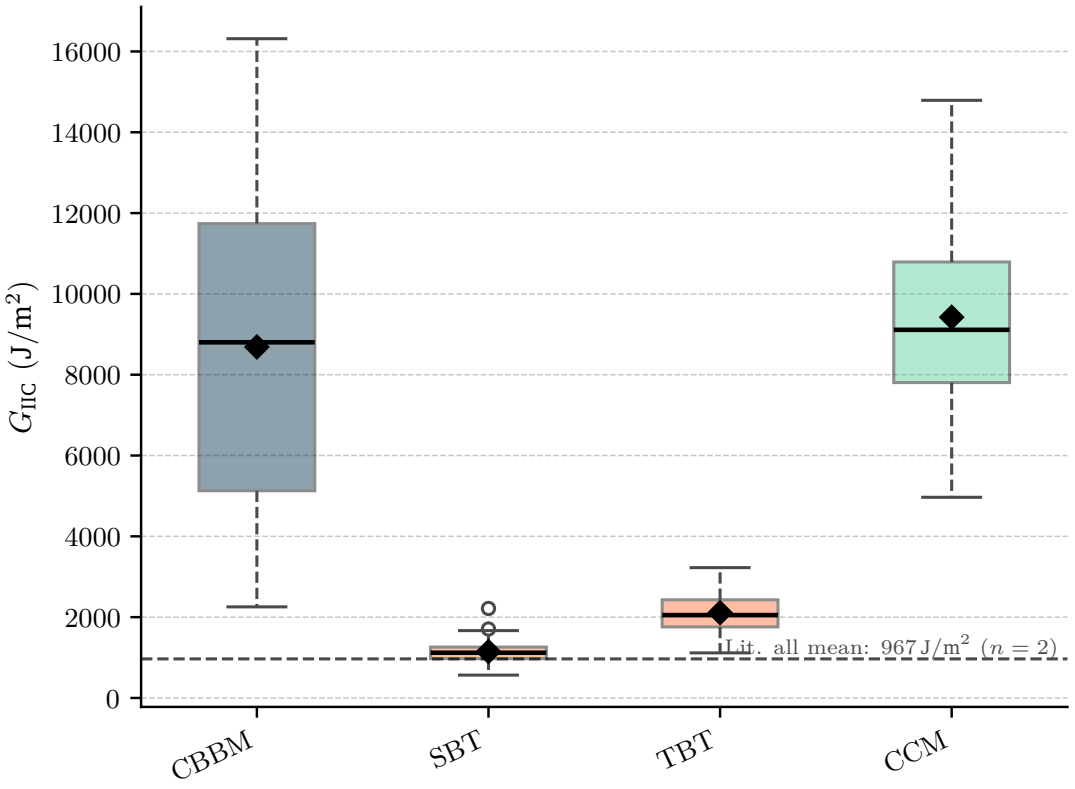

Figure A.26: G_{IIC} by calculation method, all batches (cleaned), $n = 50$.

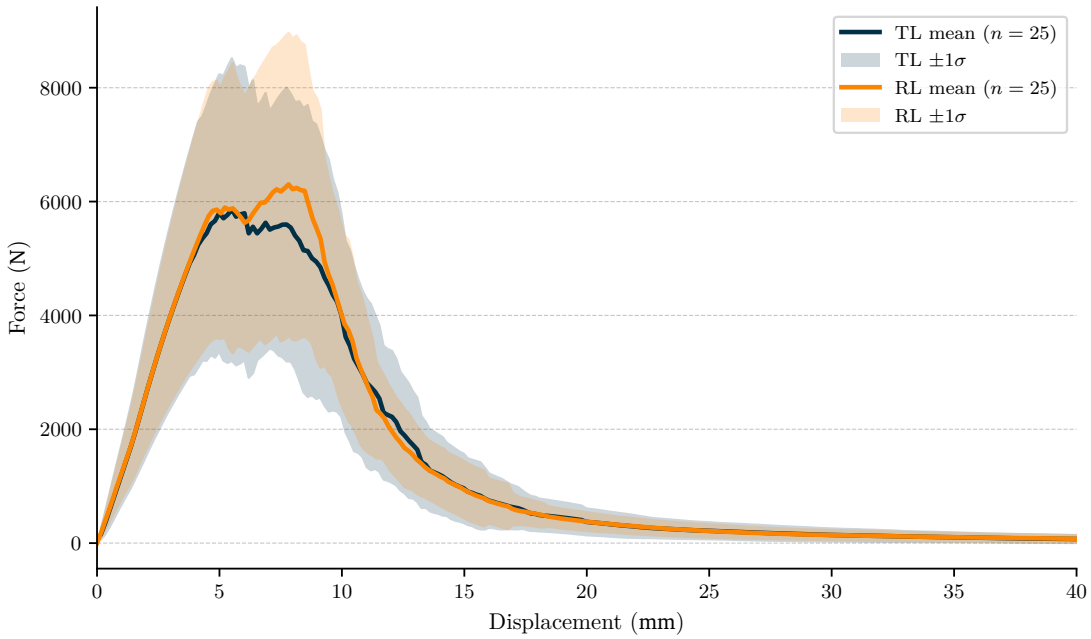

Figure A.27: ENF load-displacement curves, all batches (cleaned), $n = 50$.

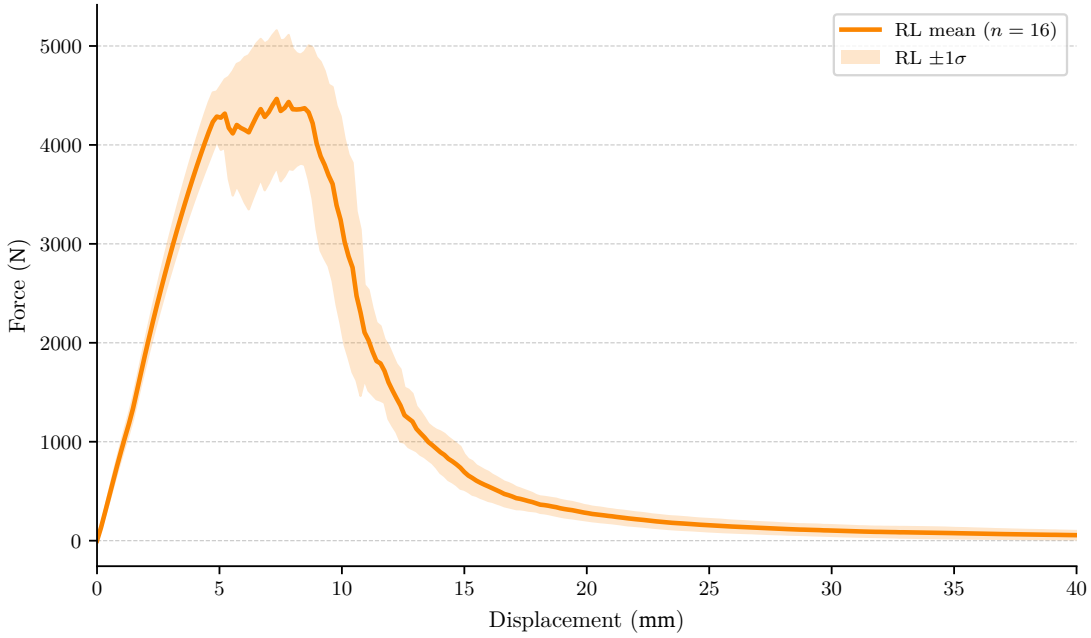

Figure A.28: ENF load-displacement curves, batch ENF-2-RL (cleaned), $n = 16$.

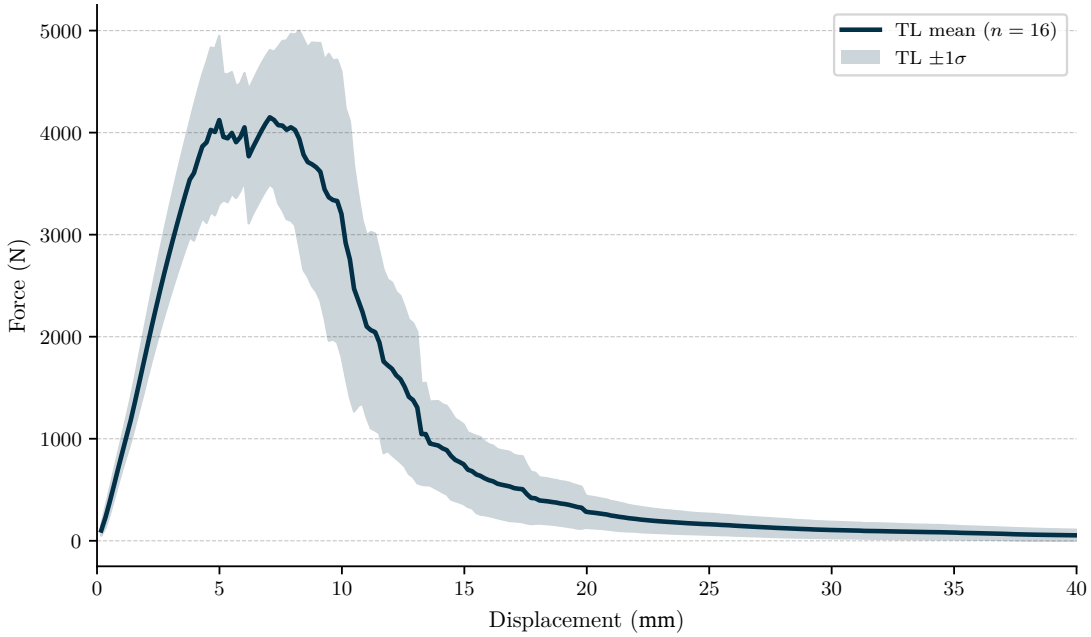

Figure A.29: ENF load-displacement curves, batch ENF-2-TL (cleaned), $n = 16$.

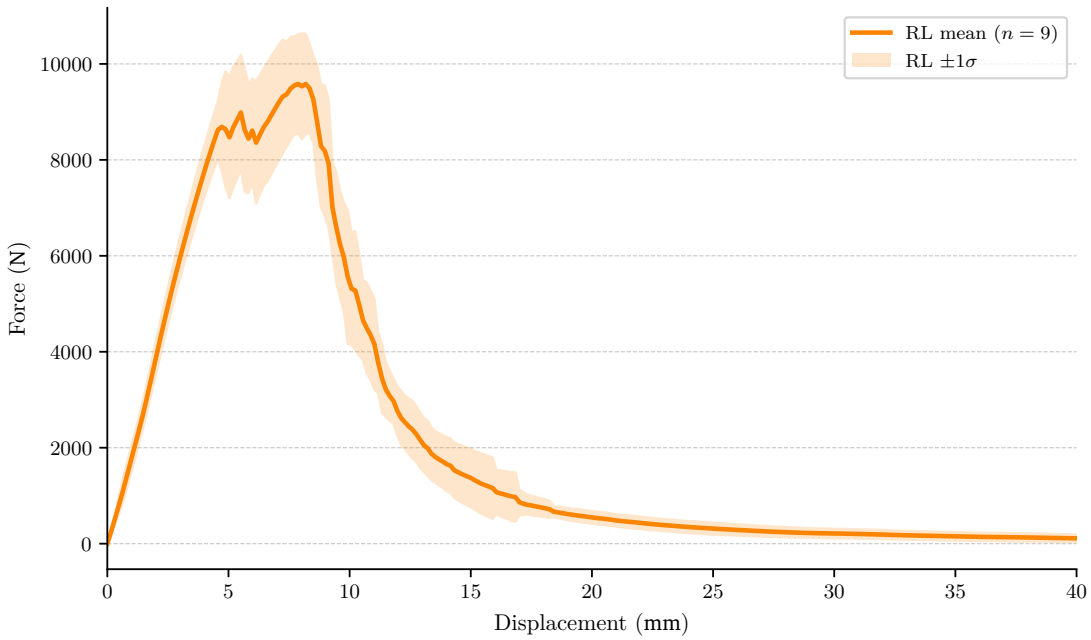

Figure A.30: ENF load-displacement curves, batch ENF-4-RL (cleaned), $n = 9$.

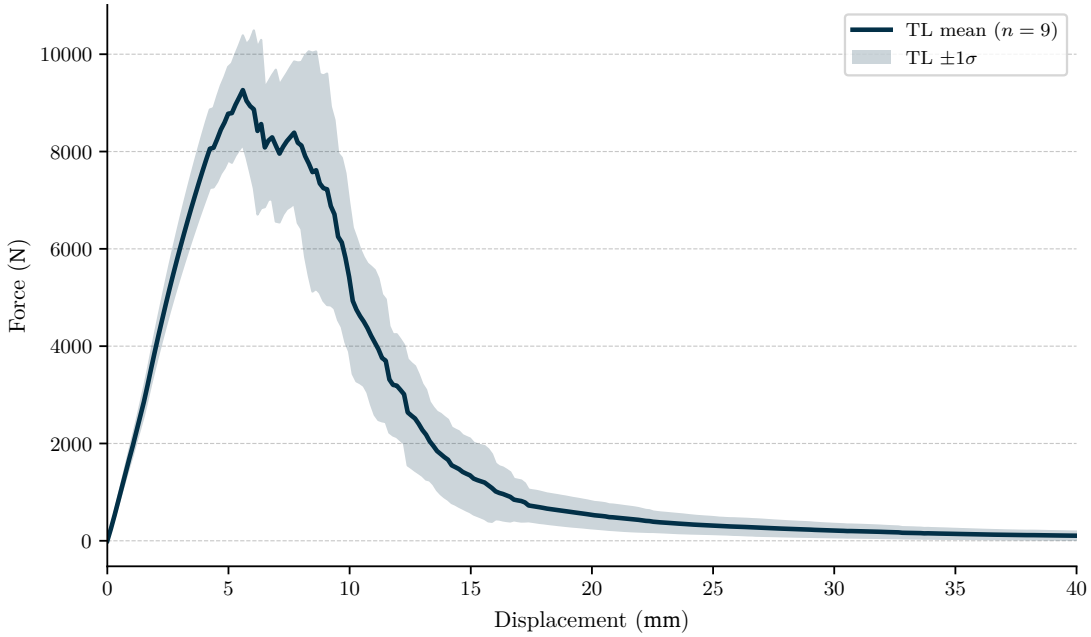

Figure A.31: ENF load-displacement curves, batch ENF-4-TL (cleaned), $n = 9$.

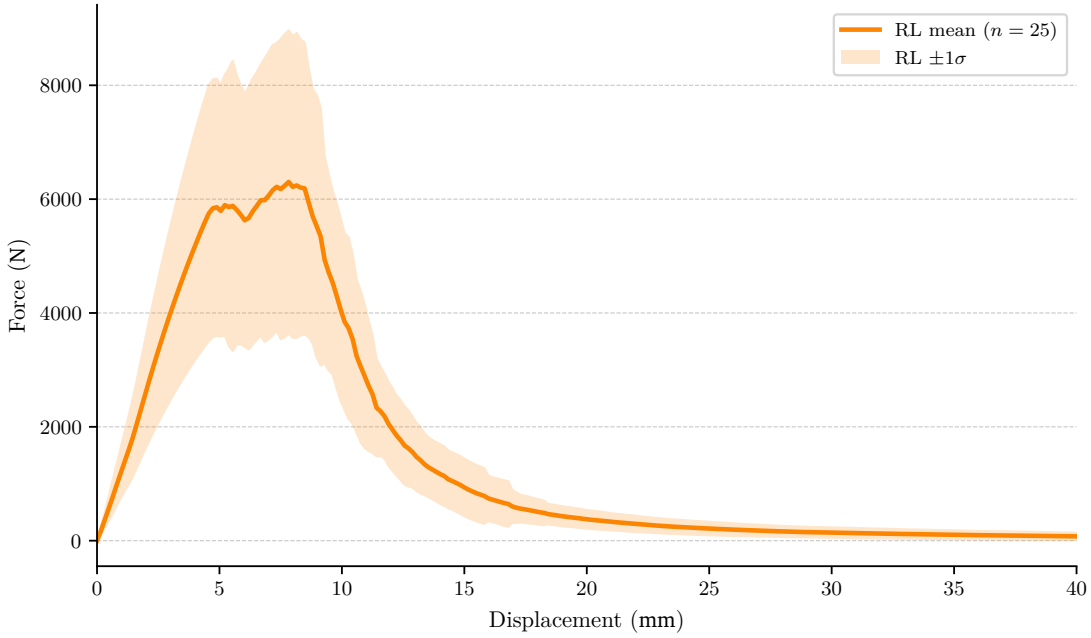

Figure A.32: ENF load-displacement curves, all batches, RL (cleaned), $n = 25$.

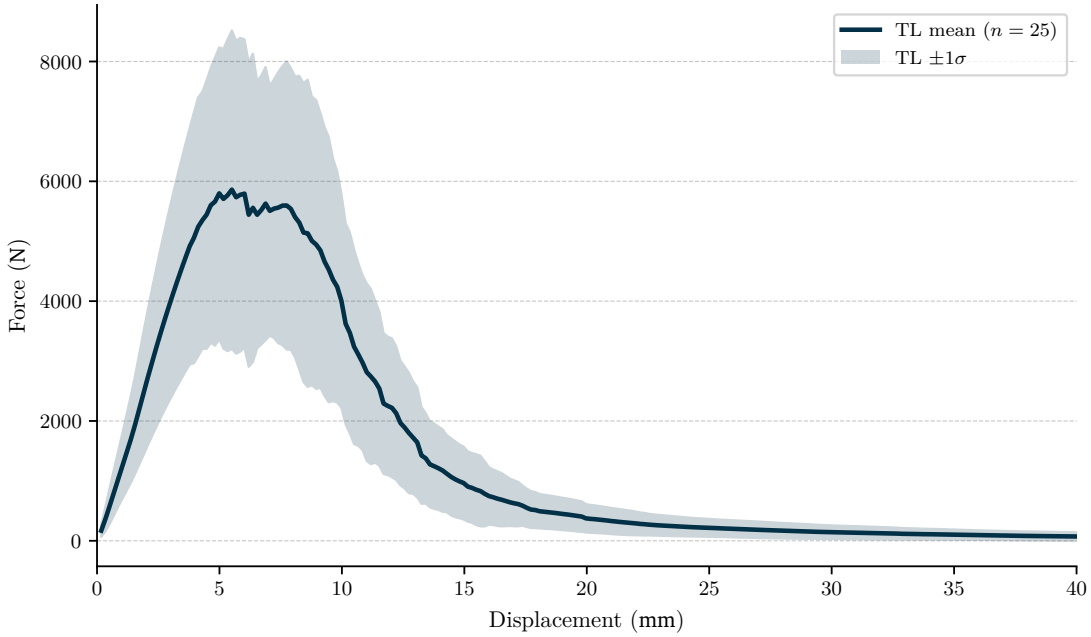

Figure A.33: ENF load-displacement curves, all batches, TL (cleaned), $n = 25$.

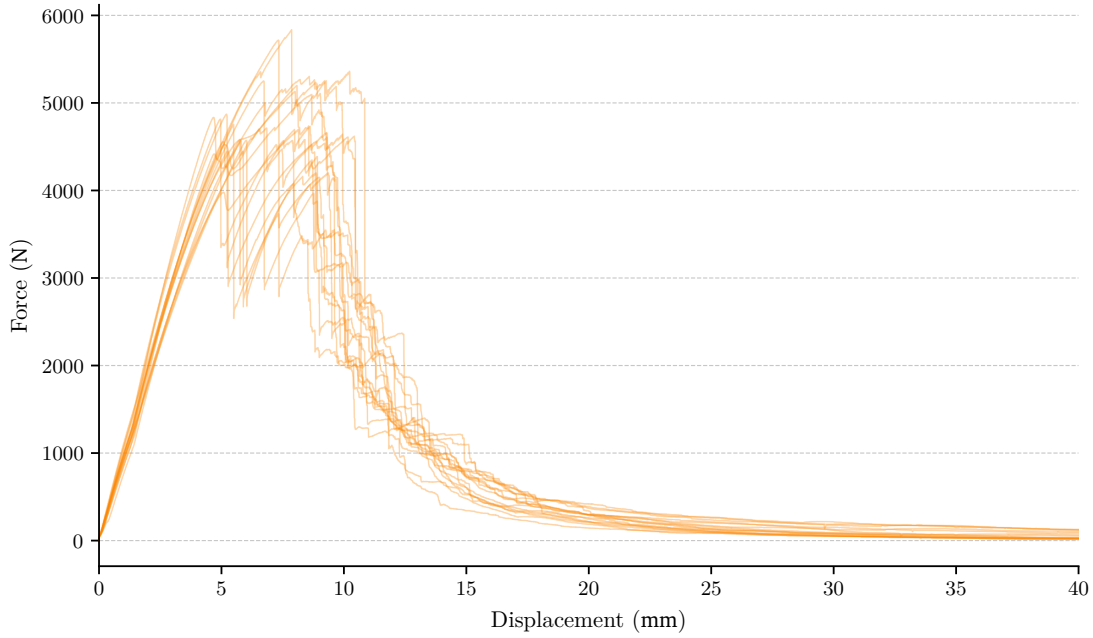

Figure A.34: ENF load-displacement curves, batch ENF-2-RL (cleaned), $n = 16$.

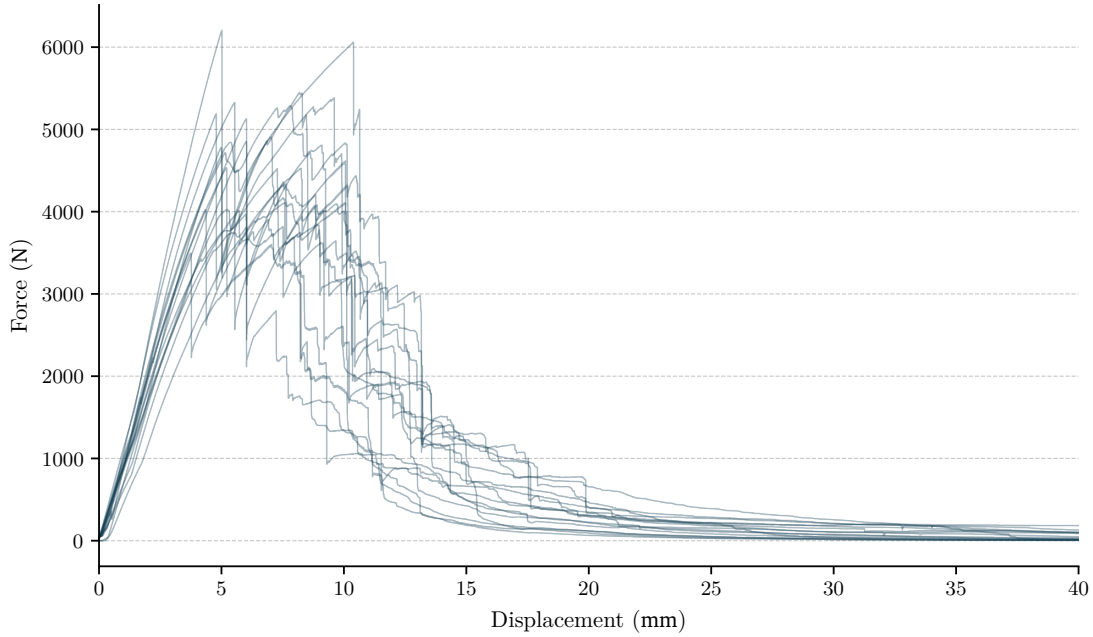

Figure A.35: ENF load-displacement curves, batch ENF-2-TL (cleaned), $n = 16$.

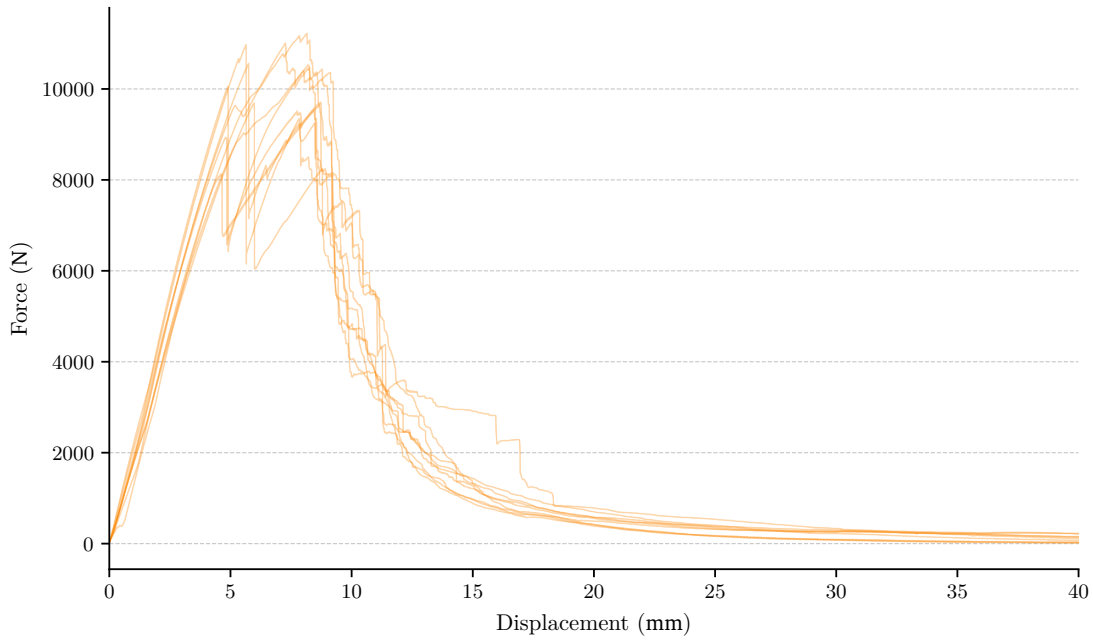

Figure A.36: ENF load-displacement curves, batch ENF-4-RL (cleaned), $n = 9$.

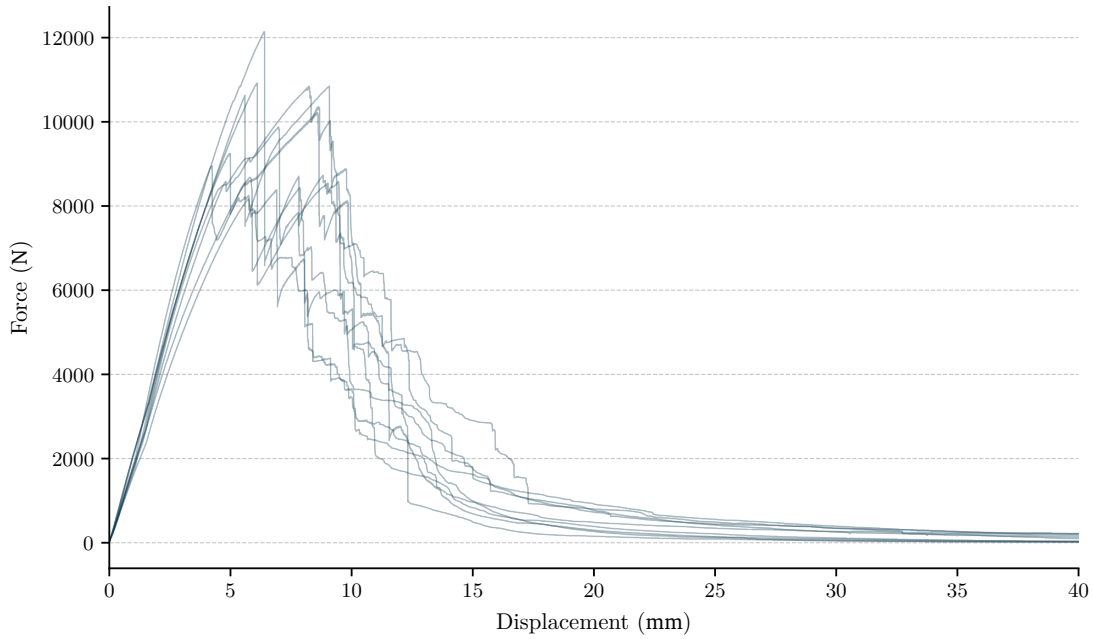

Figure A.37: ENF load-displacement curves, batch ENF-4-TL (cleaned), $n = 9$.

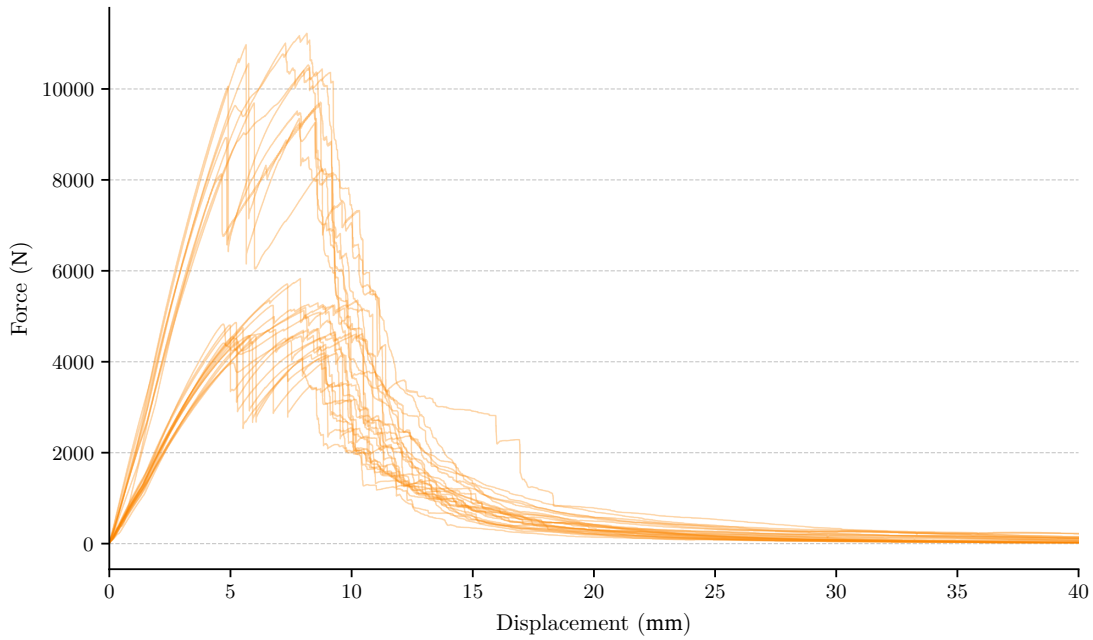

Figure A.38: ENF load-displacement curves, all batches, RL (cleaned), $n = 25$.

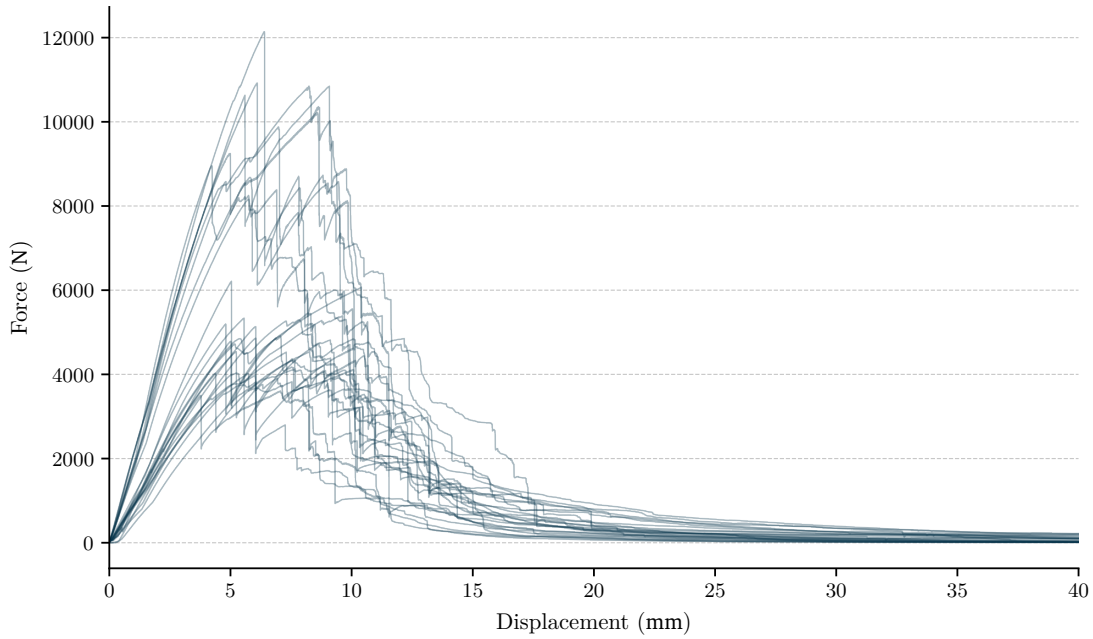

Figure A.39: ENF load-displacement curves, all batches, TL (cleaned), $n = 25$.

A.1.3 Splitting

Figure A.40: Fractured splitting specimen (LBL 960 × 161 × 51 mm TL) showing the dowel hole and the horizontal split running along the grain.

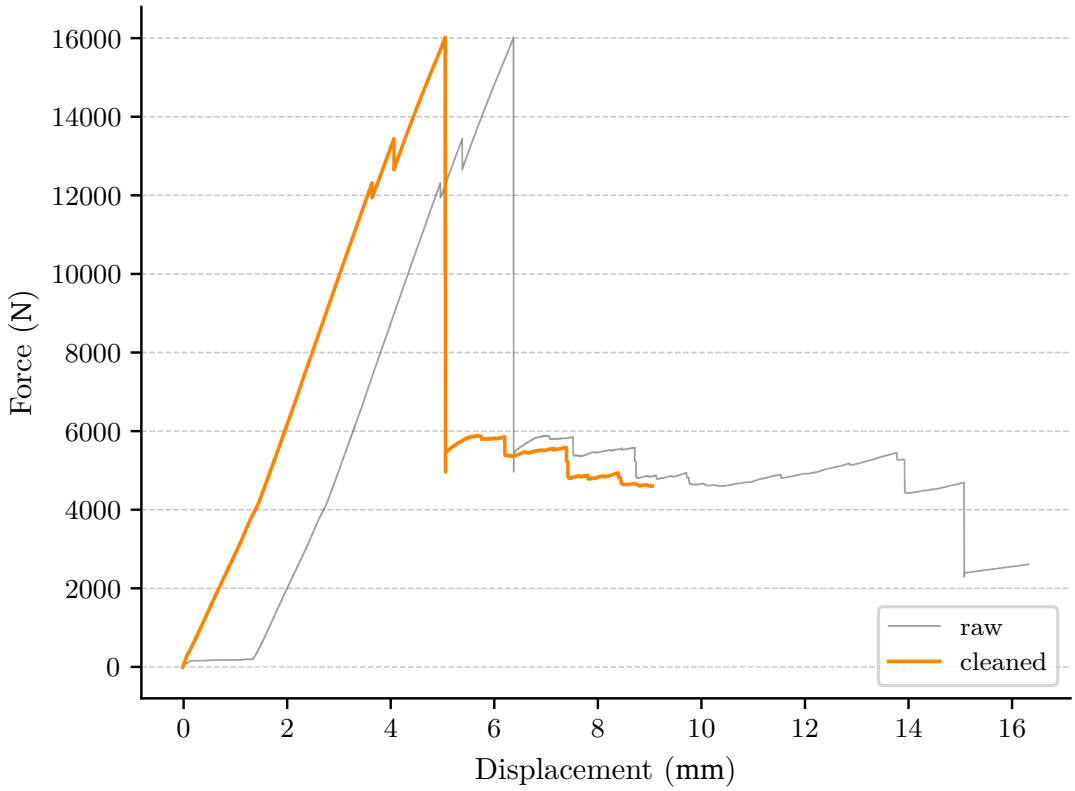

Figure A.41: Example raw vs. cleaned data for splitting specimen.

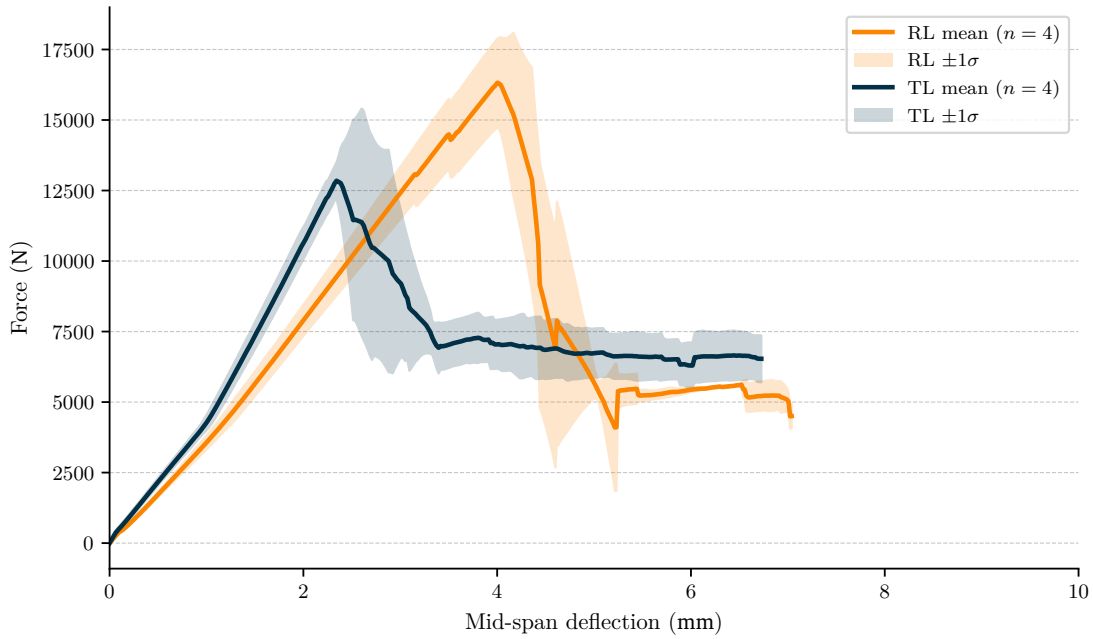

Figure A.42: splitting force vs. mid-span deflection, all batches (cleaned), $n = 8$.

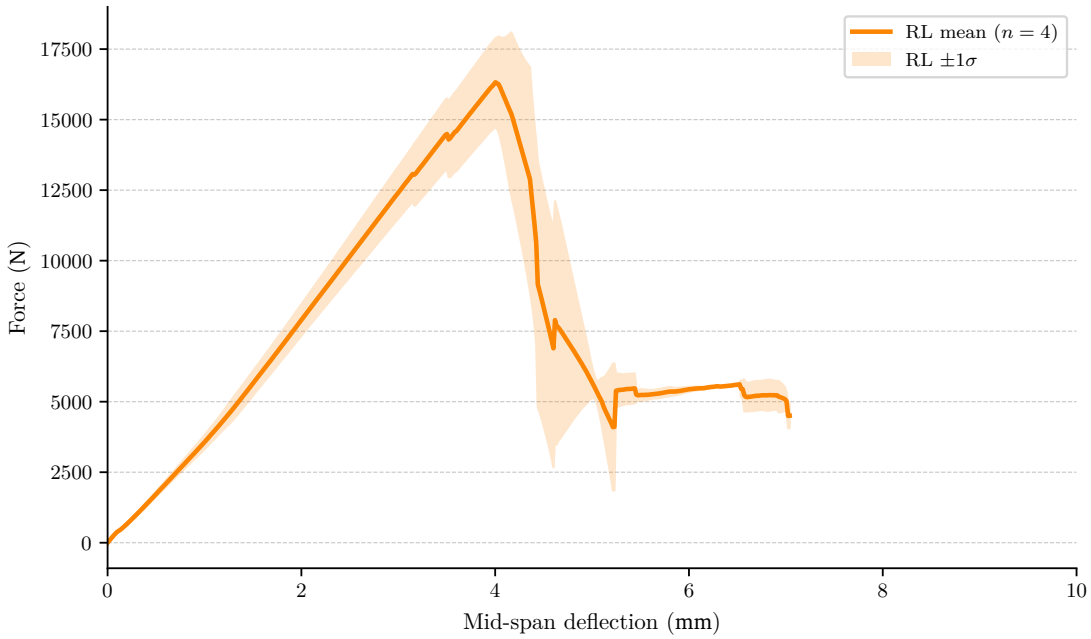

Figure A.43: splitting force vs. mid-span deflection, batch Splitting-1200x200x40-RL (cleaned), $n = 4$.

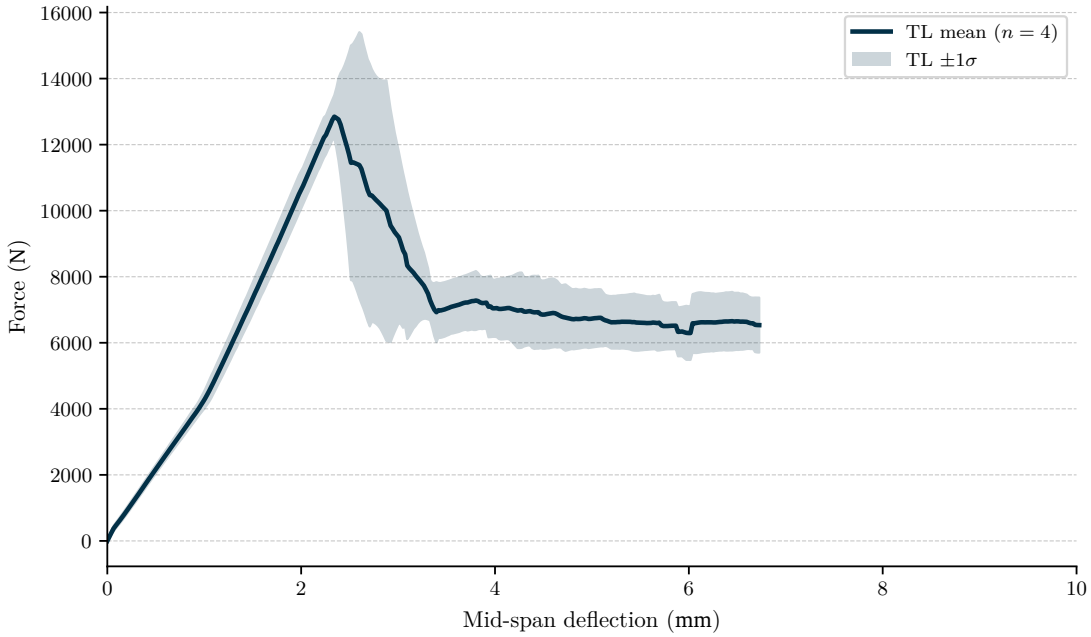

Figure A.44: splitting force vs. mid-span deflection, batch Splitting-960x161x51-TL (cleaned), $n = 4$.

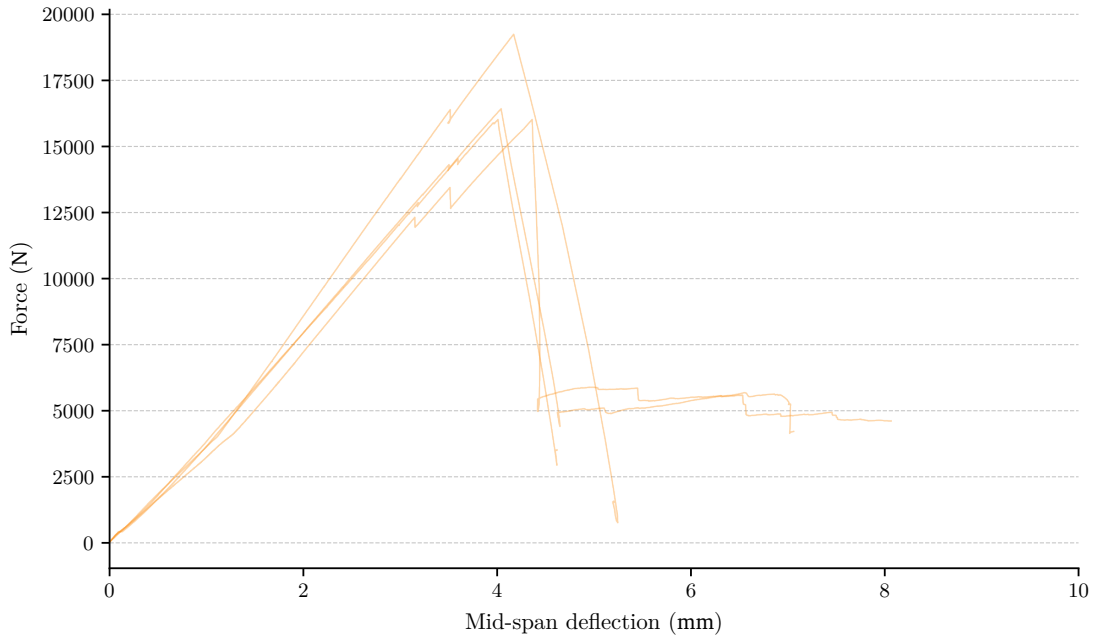

Figure A.45: splitting force vs. mid-span deflection, batch Splitting-1200x200x40-RL (cleaned), $n = 4$.

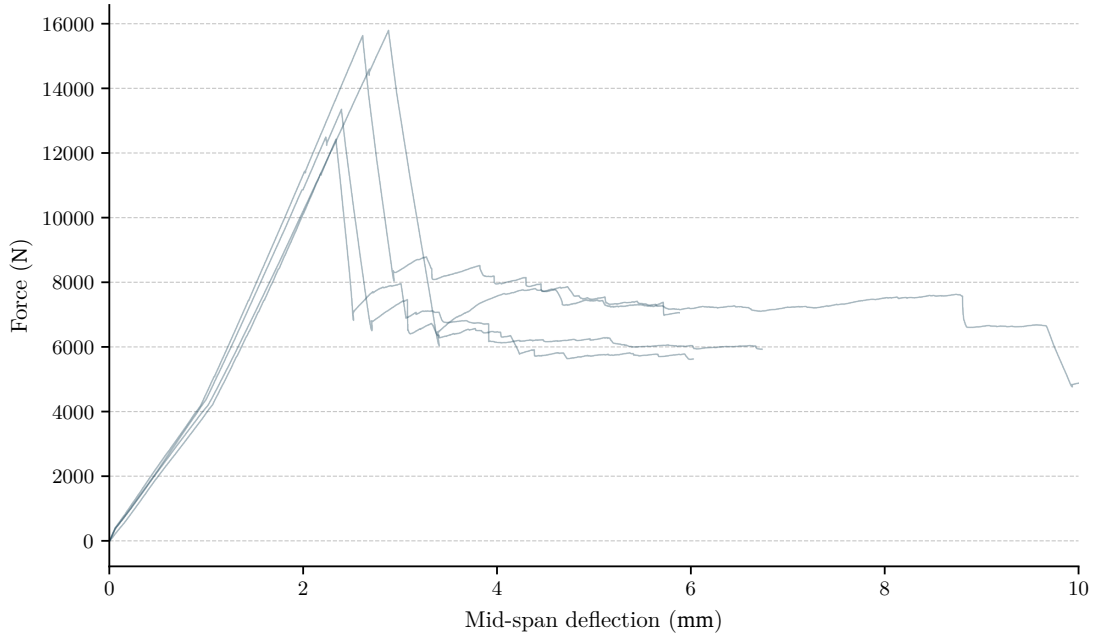

Figure A.46: splitting force vs. mid-span deflection, batch Splitting-960x161x51-TL (cleaned), $n = 4$.

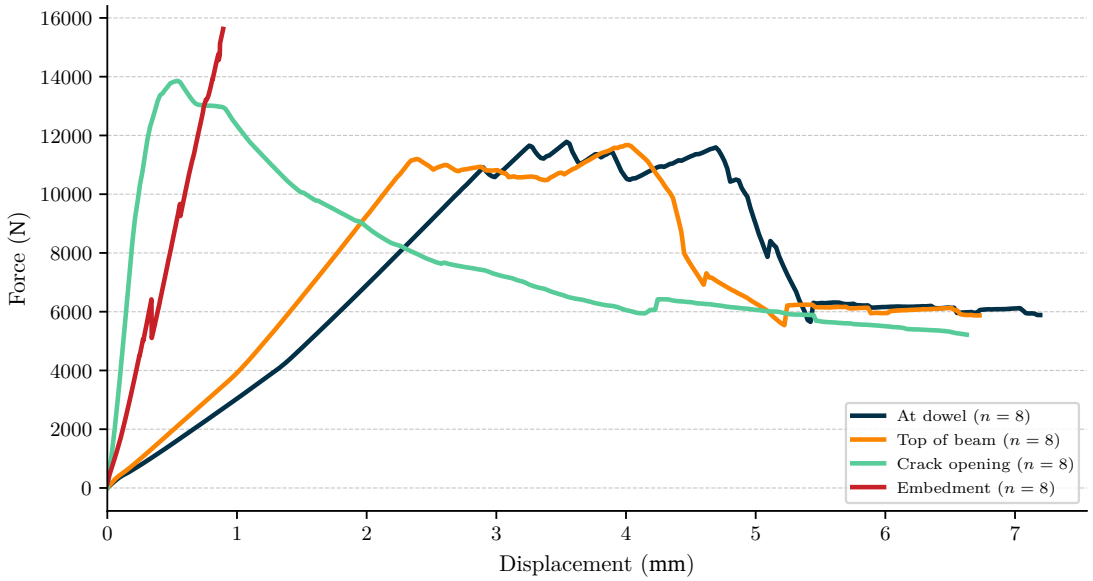

Figure A.47: Splitting displacement decomposition: channel-mean force vs. displacement for the four LVDT-derived channels (all batches (cleaned), $n = 8$).

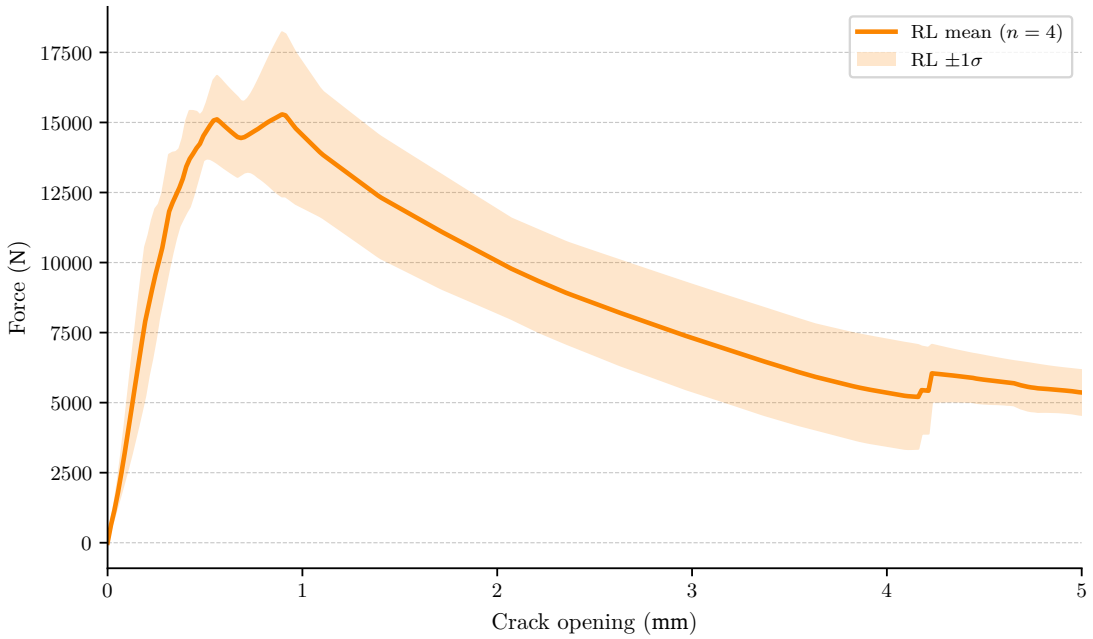

Figure A.48: splitting force vs. crack-opening displacement, batch Splitting-1200x200x40-RL (cleaned), $n = 4$.

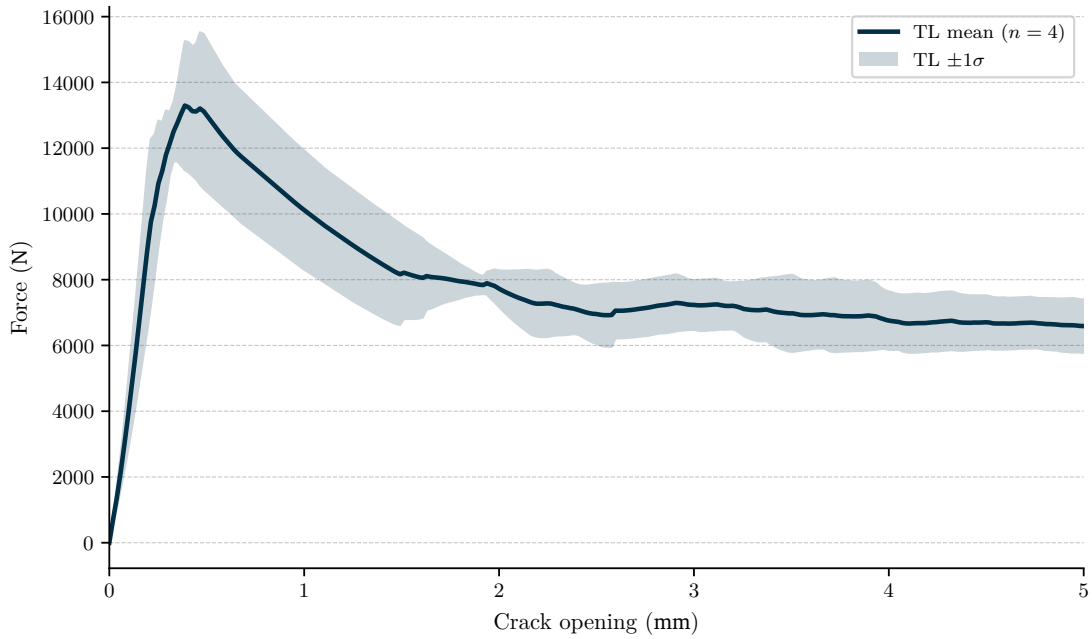

Figure A.49: splitting force vs. crack-opening displacement, batch Splitting-960x161x51-TL (cleaned), $n = 4$.

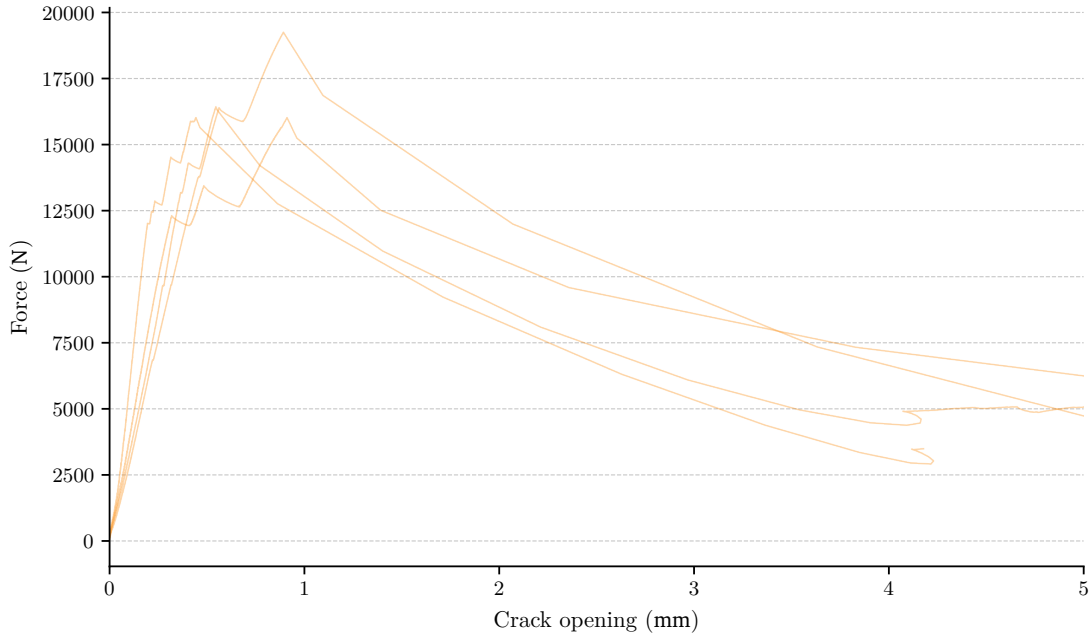

Figure A.50: splitting force vs. crack-opening displacement, batch Splitting-1200x200x40-RL (cleaned), $n = 4$.

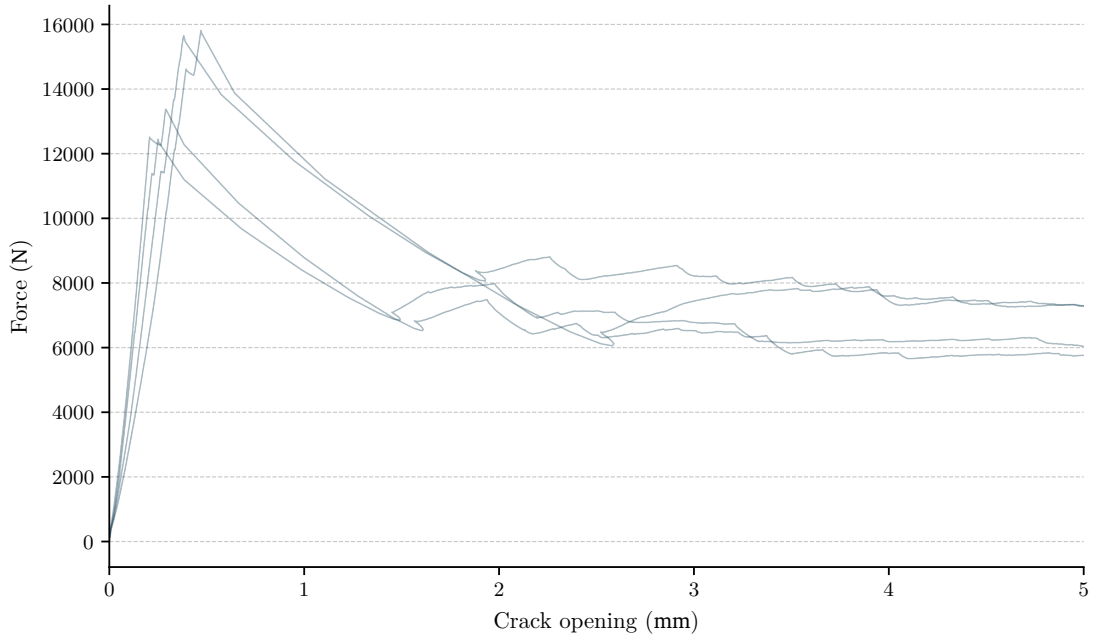

Figure A.51: splitting force vs. crack-opening displacement, batch Splitting-960x161x51-TL (cleaned), $n = 4$.

A.1.4 EC5 Calibration

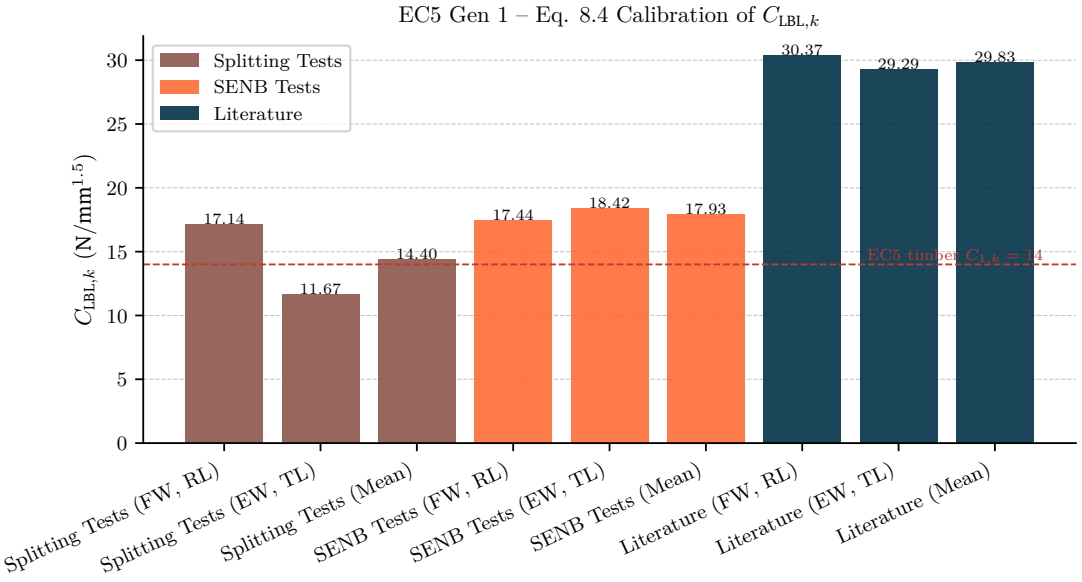

Figure A.52: Gen 1 EC5 eq. 8.4 characteristic $C_{\mathrm{LBL},k} = \sqrt{GG_c/0.6}$ by source and section ($n = 9$); dashed line is the timber benchmark $C_{1,k} = 14$.

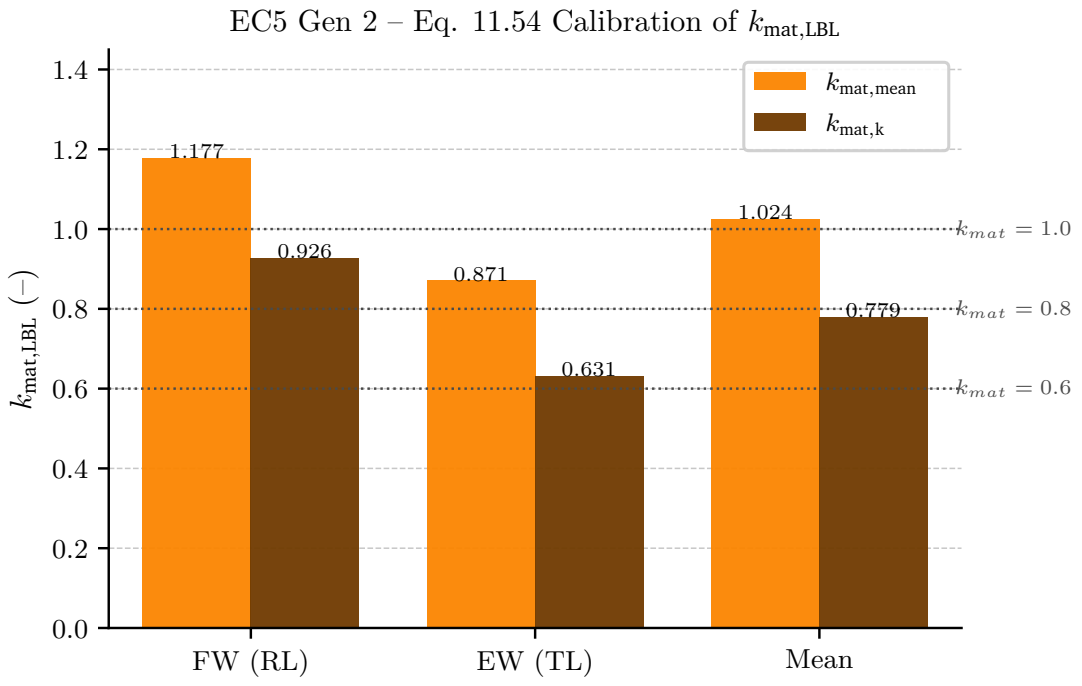

Figure A.53: Gen 2 EC5 $k_{\mathrm{mat,LBL}}$ (eq. 11.54) per section: $k_{\mathrm{mat,mean}}$ from mean splitting load and $k_{\mathrm{mat,k}}$ from the 5%-percentile.

A.1.5 FEM

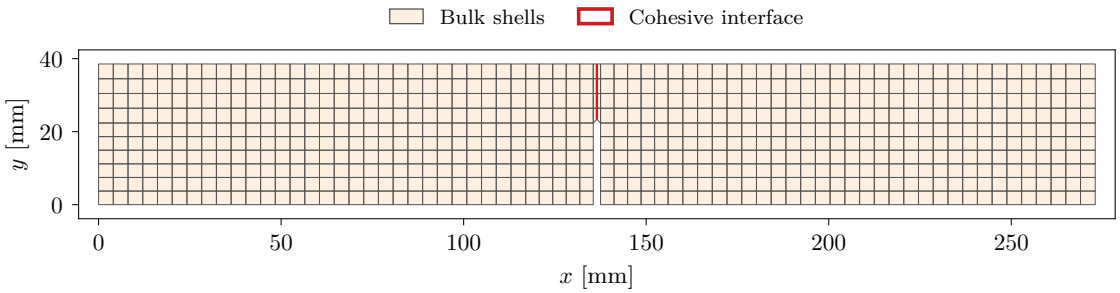

Figure A.54: SENB FEM mesh, structured quad shells with cohesive ligament (red) above the central notch. Shown at 4 mm element edge for legibility. Production runs used 0.5 mm. Depth-code 2 specimen geometry.

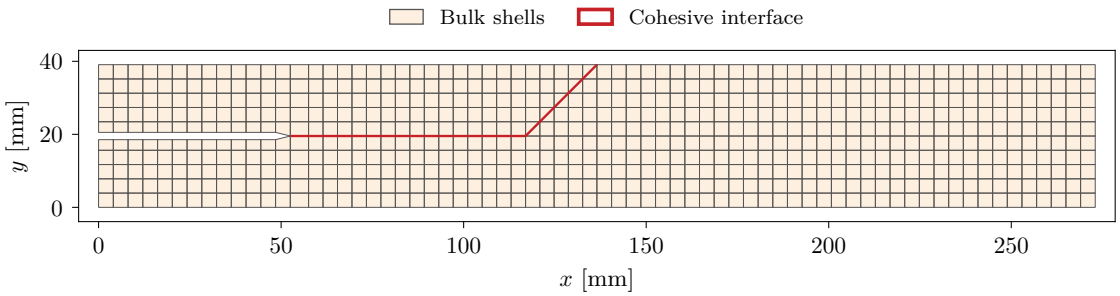

Figure A.55: ENF FEM mesh, structured quad shells with the L-shaped cohesive interface (red), a horizontal pre-crack plane and 45 degree wedge rising to the loading nose at midspan. Shown at 4 mm element edge for legibility. Production runs used 1 mm. Depth-code 2 specimen geometry.

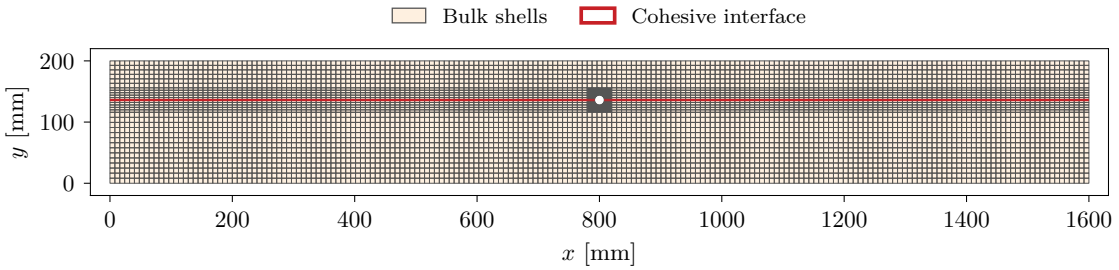

Figure A.56: Splitting FEM mesh for the 1200 × 200 × 40 mm RL geometry. Horizontal cohesive band (red) at edge-distance $h_e = 64$ mm with the unstructured ring transition around the 16 mm dowel hole at midspan. Shown at 8 mm element edge for legibility. Production runs used 5 mm.

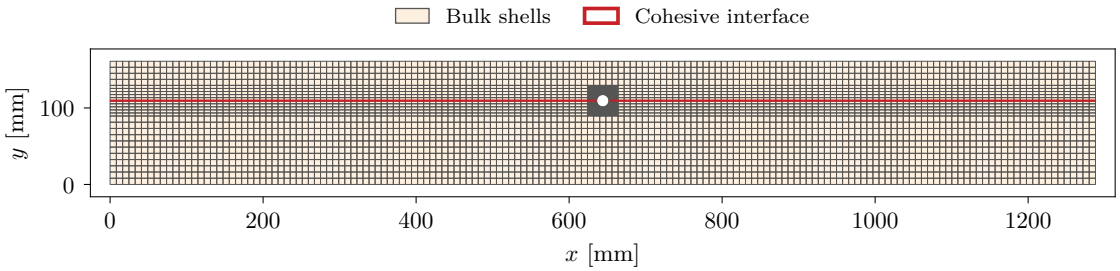

Figure A.57: Splitting FEM mesh for the 960 × 161 × 51 mm TL geometry. Horizontal cohesive band (red) at edge-distance $h_e = 51.5$ mm with the unstructured ring transition around the 16 mm dowel hole at midspan. Shown at 8 mm element edge for legibility. Production runs used 5 mm.

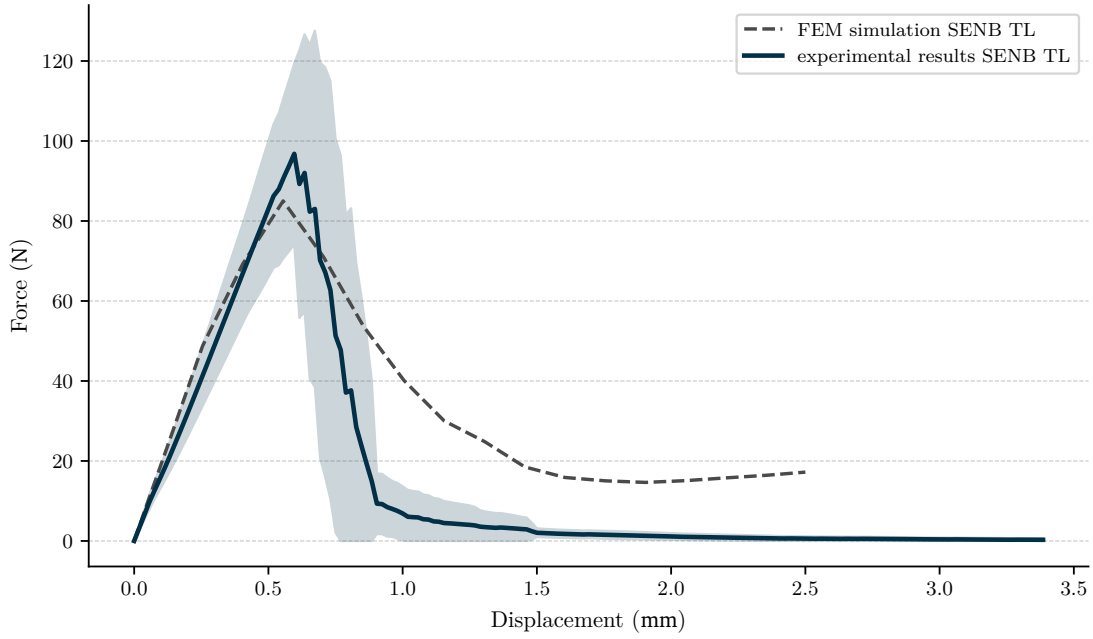

Figure A.58: FEM vs. experimental mean SENB TL.

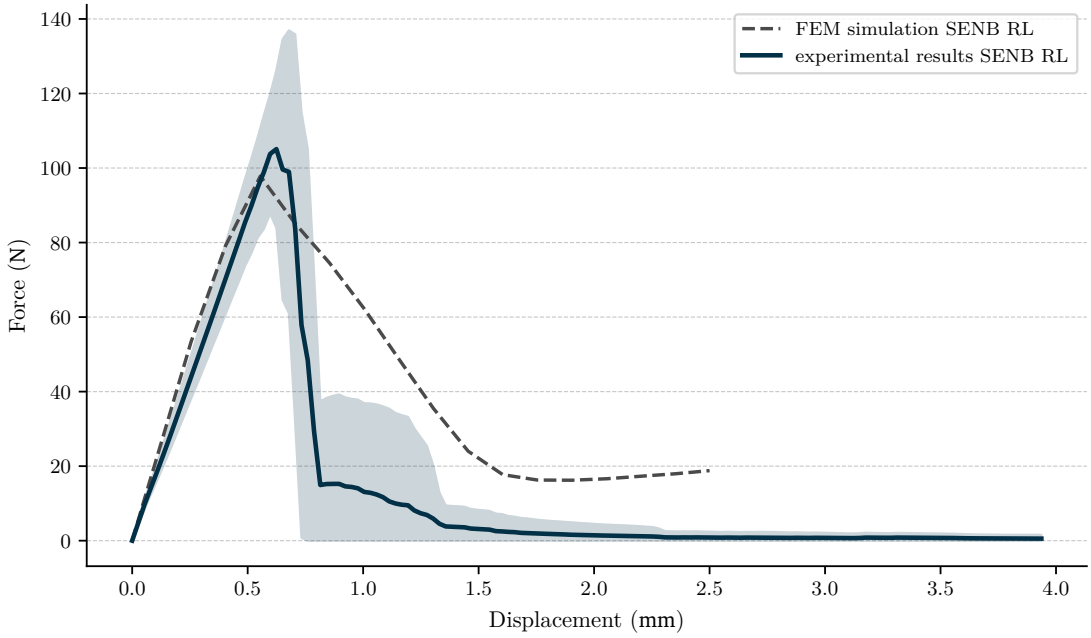

Figure A.59: FEM vs. experimental mean SENB RL.

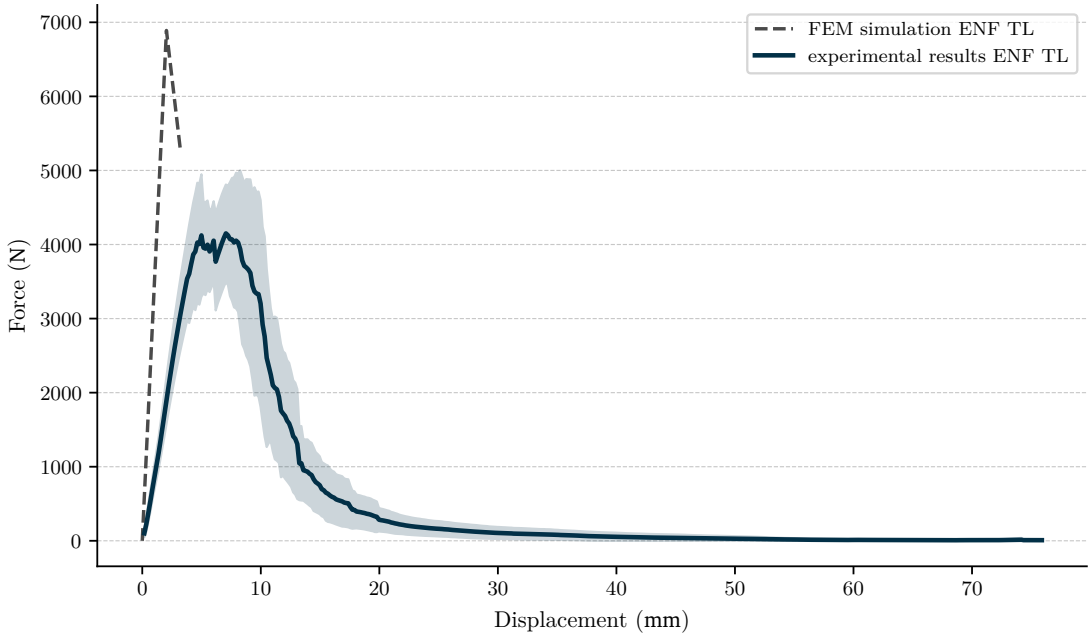

Figure A.60: FEM vs. experimental mean ENF TL.

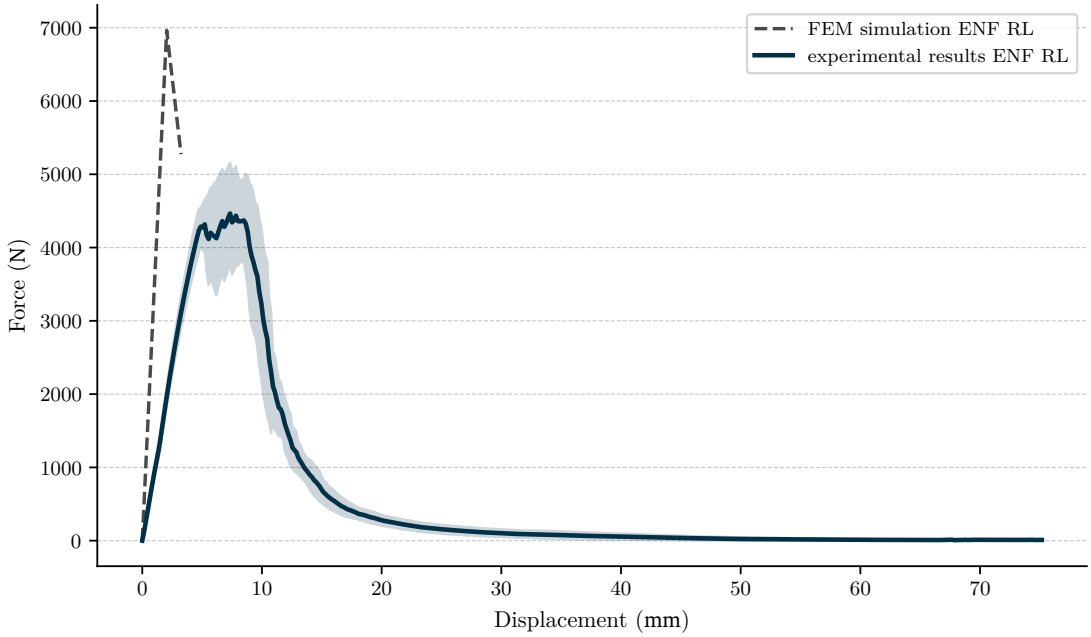

Figure A.61: FEM vs. experimental mean ENF RL.

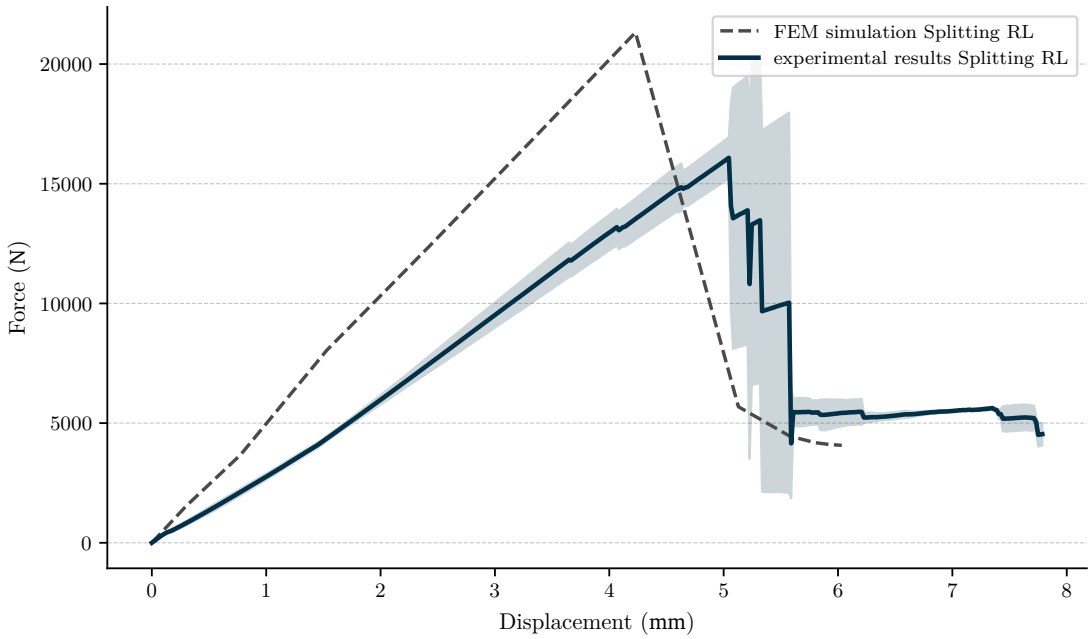

Figure A.62: FEM vs. experimental mean Splitting RL.

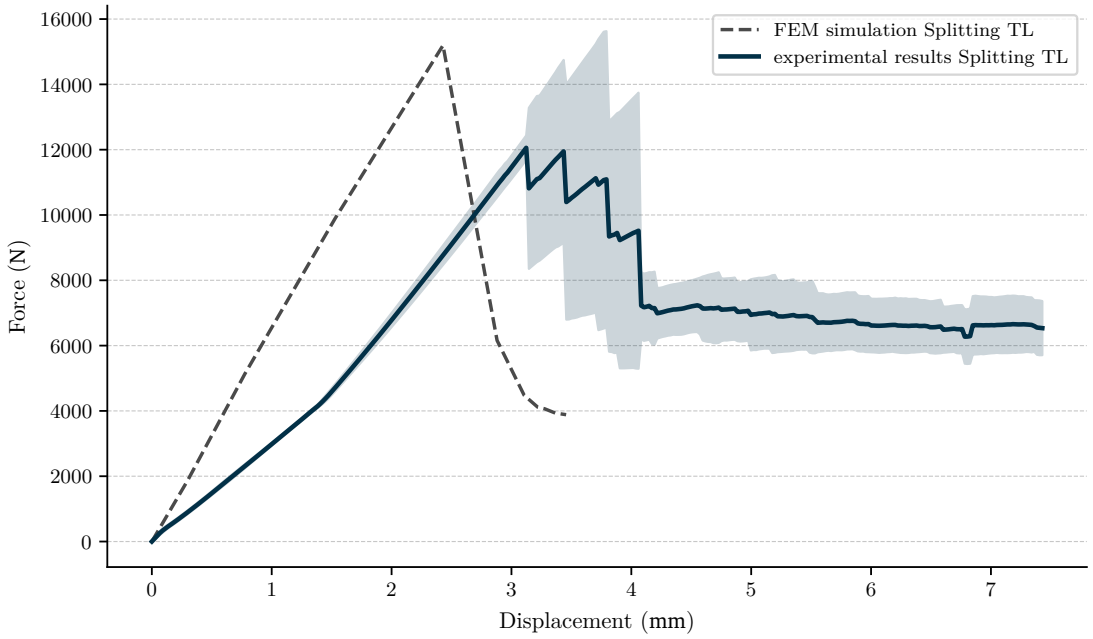

Figure A.63: FEM vs. experimental mean Splitting TL.

A.1.6 Tensile

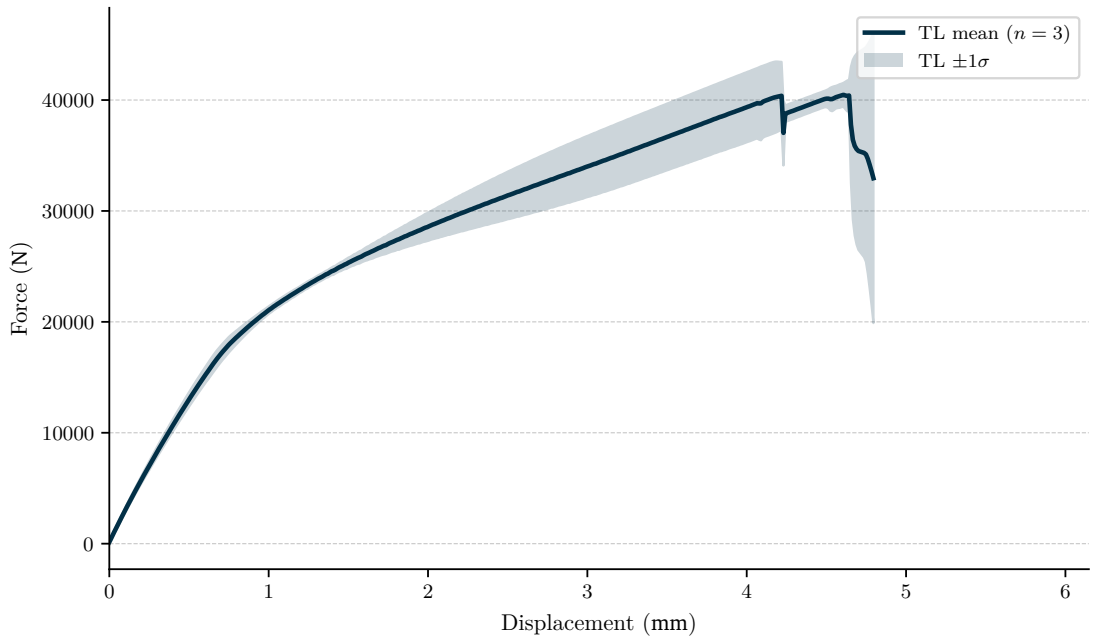

Figure A.64: tensile load-displacement curves, batch TT-L (cleaned), $n = 3$.

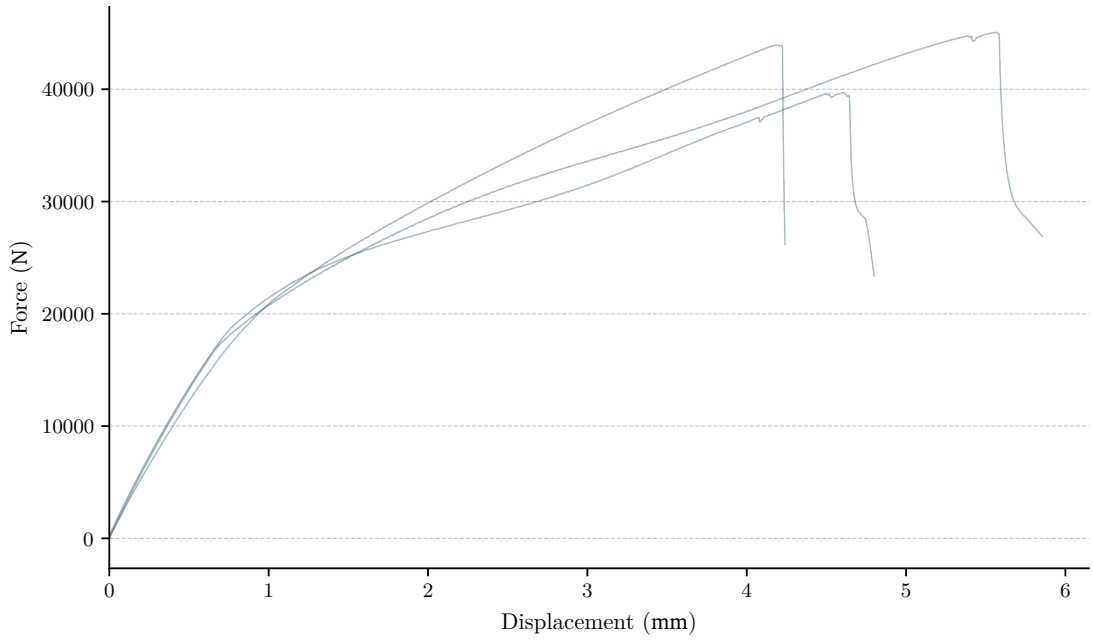

Figure A.65: tensile load-displacement curves, batch TT-L (cleaned), $n = 3$.

A.1.7 Density and Moisture Content

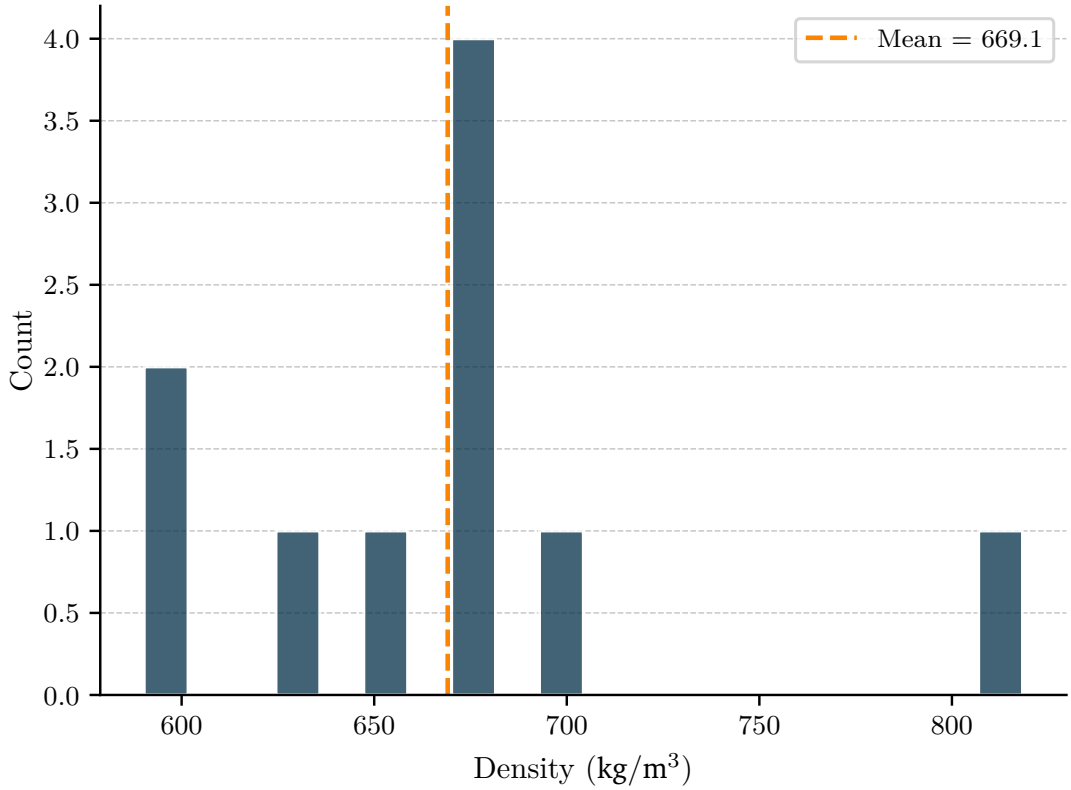

Figure A.66: Distribution of density ($n = 10$, mean = 669.1 kg/m^3, $\sigma = 64.0$ kg/m^3).

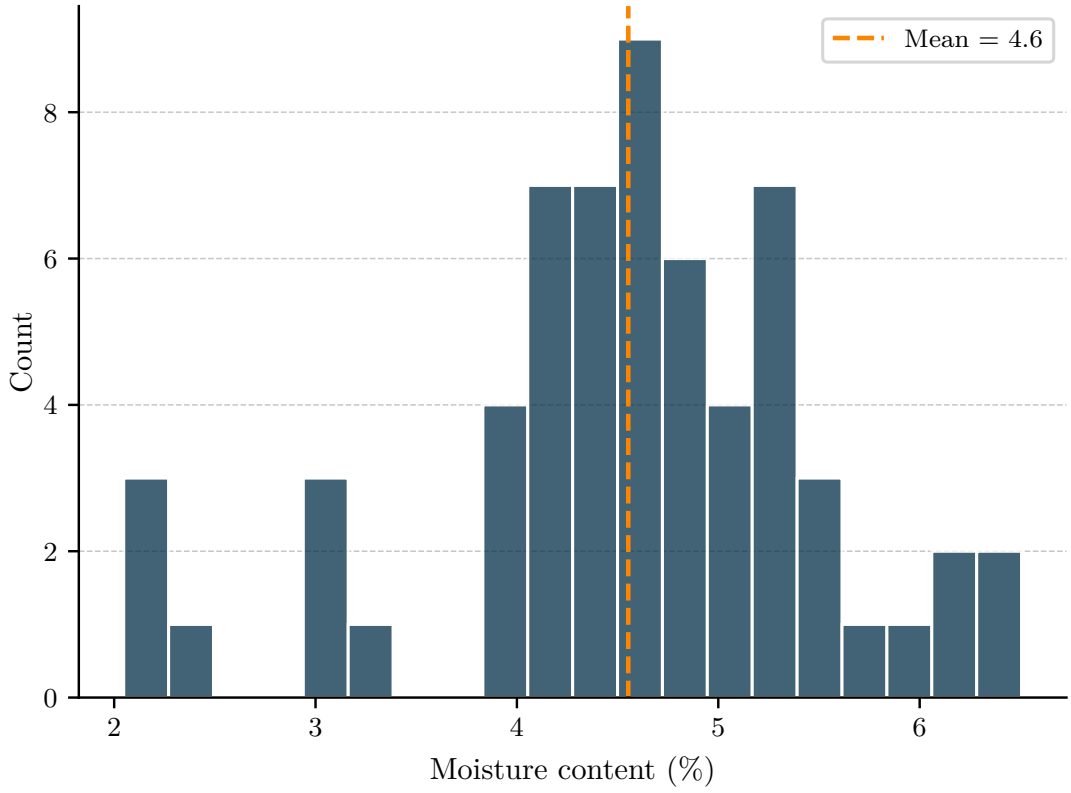

Figure A.67: Distribution of moisture content ($n = 61$, mean = 4.6 %, $\sigma = 1.0$ %).

A.2 Tables

A.2.1 SENB

Table A.1: Mode I calculations

Property	Method	Formula	Unit	Mean	Std Dev	n	W (neck of fracture) [0 mm]	u_0 (load displacement) [mm]	h_{-} (ligament height) [mm]	h (width) [mm]	m (specimen mass) [g]	R_{IC} (from LEFM) [MPa·m$^{0.5}$]	B' [0_5 or E_B] [MPa]	E_L (eng. modulus) [MPa]	E_T (trans. modulus) [MPa]	ν_{LT} (Poisson ratio)	G_{LT} (shear modulus) [MPa]	F_{max} (peak load) [N]	b (span) [mm]	B (width) [mm]	W (height) [mm]	a (crack length) [mm]	a/W	$f(a/W)$ geometry factor	G_{IC} ENF BESLD 4ΔG [J/m^2]
G_{IC} (J/m^2)	NT BESLD 4ΔG	$G_{IC} = -\frac{W}{m}\frac{dU}{da}\Big\vert_{u_0} \cdot \frac{h_{-}}{h_0}$	J/m^2	466.98	57.40	42	69.9 ± 31.7	4.51 ± 3.36	14.19 ± 0.24	25.48 ± 0.40	162.25 ± 44.96	-	-	-	-	-	-	-	-	-	-	-	-	-	-
G_{IC} (J/m^2)	LEFM SENB (simplified)	$G_{IC} = K_{IC}^2 \cdot \frac{1-\nu^2}{E}$ [plane]	J/m^2	376.10	116.61	42	-	-	-	-	-	0.7 ± 0.1	1401.3 ± 245.1	-	-	-	-	-	-	-	-	-	-	-	-
G_{IC} (J/m^2)	LEFM SENB (Mc-orthotropic)	$G_{IC} = K_{IC}^2 \cdot S_{comp}$ (orthotropic comp/linear fit)	J/m^2	239.23	94.65	42	-	-	-	-	-	0.7 ± 0.1	-	-	9769.5	17263	0.15 ± 0.00	19750.0	-	-	-	-	-	-	-	-
K_{IC} ($MPa·m^{0.5}$)	LEFM	$K_{IC} = \frac{P_{max}\,S}{B\,W^{1.5}} \cdot f(a/W)$	$MPa·m^{0.5}$	0.722	0.159	42	-	-	-	-	-	-	-	-	-	-	-	152.20 ± 40.99	250.80	23.10 ± 0.40	38.64 ± 0.54	22.44 ± 0.62	0.5806 ± 0.0093	3.51 ± 0.12	-	-
K_{IC} ($MPa·m^{0.5}$)	K_{IC} simplified (from G_{IC})	$K_{IC} = \sqrt{G_{IC} \cdot E'_L}$ / $\sqrt{MPa·m^{0.5}}$	$MPa·m^{0.5}$	0.540	0.075	42	-	-	-	-	-	-	1401.3 ± 245.1	-	-	-	-	-	-	-	-	-	-	-	-	266166 ± 57.49
K_{IC} ($MPa·m^{0.5}$)	K_{IC} orthotropic (from G_{IC})	$K_{IC} = \sqrt{G_{IC} \cdot S_{comp}}$ / $\sqrt{MPa·m^{0.5}}$	$MPa·m^{0.5}$	0.676	0.091	42	-	-	-	-	-	-	-	-	9769.5	17263	0.15 ± 0.00	19750.0	-	-	-	-	-	-	-	-	266166 ± 57.49

A.2.2 ENF

Table A.2: Mode II method comparison

Property	Method	Unit	n	Mean	Std	CoV	Min	Max	$f_{0.05}$
G_{IIC}	CBBM	J/m^2	50	8687.46	3507.49	40.4%	2254.54	16315.66	3779.24
G_{IIC}	SBT	J/m^2	50	1148.38	277.95	24.2%	565.76	2214.67	767.51
G_{IIC}	TBT	J/m^2	50	2110.35	526.08	24.9%	1115.55	3225.16	1346.92
G_{IIC}	CCM	J/m^2	50	9423.22	2433.33	25.8%	4966.35	14790.57	5940.48
K_{IIC}	Orthotropic	MPa·m$^{1/2}$	50	1.754	0.253	14.4%	1.393	2.368	1.387

Table A.3: Mode II by depth code and crack system

Group	n	G_{IIC} CBBM (J/m^2)	G_{IIC} SBT (J/m^2)	G_{IIC} TBT (J/m^2)	G_{IIC} CCM (J/m^2)	K_{IIC} ortho.
2_RL	16	9336.42 ± 3779.55	1154.66 ± 189.10	2132.49 ± 359.61	9462.41 ± 1595.14	1.629 ± 0.134
2_TL	16	8355.18 ± 3587.07	1078.44 ± 374.01	2022.18 ± 671.63	8997.60 ± 3003.09	1.850 ± 0.312
4_RL	9	8830.76 ± 3280.67	1256.87 ± 220.36	2261.23 ± 436.26	10193.31 ± 2212.16	1.676 ± 0.156
4_TL	9	7981.15 ± 3468.76	1153.05 ± 268.67	2076.83 ± 610.85	9340.15 ± 2941.41	1.882 ± 0.277
RL	25	9154.38 ± 3546.42	1191.46 ± 202.59	2178.84 ± 385.02	9725.53 ± 1830.23	1.646 ± 0.141
TL	25	8220.53 ± 3476.53	1105.30 ± 335.89	2041.86 ± 637.99	9120.92 ± 2923.82	1.862 ± 0.294
2	32	8845.80 ± 3658.77	1116.55 ± 294.09	2077.33 ± 532.90	9230.00 ± 2377.14	1.740 ± 0.262
4	18	8405.95 ± 3304.27	1204.96 ± 244.28	2169.03 ± 523.60	9766.73 ± 2562.63	1.779 ± 0.242

Table A.4: Mode II calculations

Property	Method	Formula	Unit	Mean	Std Dev	n	a₀ (pre-crack length) [mm]	L (half-span) [mm]	B (width) [mm]	2h (total height) [mm]	E_f (flexural modulus) [MPa]	a_eq (equiv. crack at peak) [mm]	F_peak (peak load) [N]	P_cr (peak load) [N]	B (width) [mm]	h (half-height) [mm]	E_L (longitudinal modulus) [MPa]	G_LT (in-plane shear modulus) [MPa]	shear correction factor	n specimens in batch	m (calibration slope) [mm^{-3}·N^{-1}]	R^2 of C vs a₀^3 fit	distinct a₀ values	G_IIC [J/m^2]	G_IIC method (TBT/CBBM)	E' (E_T or E_R) [MPa]
G_IIC (J/m^2)	CBBM	G_IIC = 9·f_peak^2·a_eq^2 / (16·E_f·B^2·h^3) × 1000	J/m^2	8687.46	3507.49	50	58.95 ± 5.50	234.00	25.70 ± 10.35	39.25 ± 0.61	16223.9 ± 2359.5	160.39 ± 34.95	6798.27 ± 2718.47	-	-	-	-	-	-	-	-	-	-	-	-	-
G_IIC (J/m^2)	SBT (Simple Beam Theory)	G_IIC = 9·P_cr^2·a₀^2 / (16·E_f·B^2·h^3) × 1000	J/m^2	1148.38	277.95	50	58.95 ± 5.50	-	-	-	16223.9 ± 2359.5	-	-	6798.27 ± 2718.47	25.70 ± 10.35	19.63 ± 0.30	-	-	-	-	-	-	-	-	-	-
G_IIC (J/m^2)	TBT (Timoshenko Beam Theory)	G_IIC = SBT × [1 + 0.2·(E_L/G₁₃)·(h/a₀)^2] × 1000	J/m^2	2110.35	526.08	50	58.95 ± 5.50	-	-	-	-	-	-	6798.27 ± 2718.47	25.70 ± 10.35	19.63 ± 0.30	9769.5	1970.0	1.1121 ± 0.0154	-	-	-	-	-	-	-
G_IIC (J/m^2)	CCM (Compliance Calibration)	G_IIC = 3·m·P_cr^2·a₀^2 / (2·B) × 1000 (m from C = C₁ + m·a₀^3)	J/m^2	9423.22	2433.33	50	-	-	-	-	-	-	-	-	-	-	-	-	-	-	0.00	0.4778	-	-	-	-
K_IIC (MPa·m$^{0.5}$)	K_IIC orthotropic (from G_IIC)	K_IIC = √(G_IIC · E') / 1000 (E' = E_T or E_R)	MPa·m$^{0.5}$	1.754	0.253	50	-	-	-	-	-	-	-	-	-	-	-	-	-	-	-	-	-	2110.35 ± 526.08	-	1495.3 ± 245.6

A.2.3 Splitting

Table A.5: Splitting per crack system. $f_{0.05}$ is the 5%-percentile.

	$F_{\max}$ (N)				Embedment (mm)				Stiffness (N/mm)				$\sqrt{GG_c}$ (N/mm$^{1.5}$)			
	n	Mean	Std	$f_{0.05}$	n	Mean	Std	$f_{0.05}$	n	Mean	Std	$f_{0.05}$	n	Mean	Std	$f_{0.05}$
RL	4	16902.10	1553.99	14859.44	4	0.77	0.29	0.35	4	4523.29	494.52	3874.18	4	16.87	1.55	14.83
TL	4	14298.45	1671.64	12018.38	4	0.85	0.20	0.57	4	5887.14	1372.59	3928.87	4	12.47	1.46	10.49

Table A.6: Splitting tests results per section build-up

Section	n	d (mm)	α	h_e (mm)	$F_{\max,\mathrm{mean}}$ (N)	$F_{\max,k}$ (N)	V_{mean} (N)	V_k (N)	$F/(b\alpha h)$ (MPa)	$\eta = S/h$	$\sqrt{GG_c}_{,\mathrm{mean}}$	$\sqrt{GG_c}_{,k}$
Flatwise (RL)	4	16	0.32	64.0	16902	13300	8451	6650	6.60	6.00	16.869	13.274
Edgewise (TL)	4	16	0.32	51.5	14298	10360	7149	5180	5.44	5.96	12.475	9.038

Table A.7: Splitting calculations

Property	Method	Formula	Unit	Mean	Std Dev	n	drop threshold [%]	F_max (running) [N]	F window lower [N]	F window upper [N]	R^2 of fit	points in window	t at F_max [s]	LVDT-07 [mm]	LVDT-09 [mm]	V_f (first-fracture force) [N]	b (beam width) [mm]	h (beam height) [mm]	h_e (loaded edge distance) [mm]	$\alpha = h_e/h$
F_fracture	First-fracture force	$F_{fracture} = F$ at first drop $\geq$ threshold $F_{running,max}$	N	3697.22	4777.93	120	5.00	3951.27 ± 4830.95	-	-	-	-	-	-	-	-	-	-	-	-
F_max	Peak force	$F_{max} = \max(F_{cleaned})$	N	3951.27	4830.95	120	-	-	-	-	-	-	-	-	-	-	-	-	-	-
stiffness	Initial stiffness (LVDT-09)	$k = \partial F/\partial(\text{LVDT-09})$ over best-R^2 force window	N/mm	5205.21	1201.54	8	-	-	6733.55 ± 2508.84	8293.58 ± 2653.73	1.0000 ± 0.0000	2965.50 ± 1460.87	-	-	-	-	-	-	-	-
embedment	Dowel embedment at F_max	embedment = LVDT-07 − LVDT-09 at $t(F_{max})$	mm	0.81	0.23	8	-	15690.27 ± 2041.91	-	-	-	-	408.50 ± 317.47	−4.16 ± 0.86	3.35 ± 0.87	-	-	-	-	-
sqrt_GG_c	$\sqrt{(GG\_c)}$	$\sqrt{(GG\_c)} = (V \cdot f(b, y/h)) / \sqrt{(\alpha/(0.6(1-\alpha)))}$	$\sqrt{(N/mm)}$	14.67	2.73	8	-	-	-	-	-	-	-	-	-	-	45.50 ± 5.88	180.50 ± 20.85	57.76 ± 6.67	0.32

A.2.4 EC5 Calibration

Table A.8: EC5 splitting capacity calibration proposals for LBL (Gen 1, eq. 8.4)

		$\sqrt{GG_c}$		C_{LBL}		V (N)		G_{IC} (J/m^2)		G_{shear} (MPa)		α	statistics		
Source	Section	mean	k	mean	k	mean	k	mean	k	mean	k	(–)	n	k_s	$\text{COV}_{\log}$
Splitting Tests	FW (RL)	16.869	13.274	21.778	17.137	8451	6650	—	—	—	—	0.320	4	2.68	0.009
Splitting Tests	EW (TL)	12.478	9.041	16.109	11.672	7149	5180	—	—	—	—	0.320	4	2.68	0.012
Splitting Tests	Mean	14.674	11.157	18.944	14.404	7800	5915	—	—	—	—	0.320	4	2.68	0.011
SENB Tests	FW (RL)	17.185	13.510	22.186	17.441	—	—	214.0	132.3	1380.0	1380.0	—	31	1.80	0.047
SENB Tests	EW (TL)	19.240	14.268	24.838	18.419	—	—	187.9	103.3	1970.0	1970.0	—	31	1.80	0.060
SENB Tests	Mean	18.212	13.889	23.512	17.930	—	—	200.9	117.8	1675.0	1675.0	—	31	1.80	0.053
Literature	FW (RL)	26.297	23.523	33.949	30.368	—	—	501.1	401.0	1380.0	1380.0	—	—	—	—
Literature	EW (TL)	28.243	22.684	36.461	29.286	—	—	404.9	261.2	1970.0	1970.0	—	—	—	—
Literature	Mean	27.270	23.104	35.205	29.827	—	—	453.0	331.1	1675.0	1675.0	—	—	—	—

Table A.9: EC5 Gen 2 ($k_{\text{mat,LBL}}$) calibration

		$k_{\text{mat,LBL}}$		F_{meas} (N)		ρ_k	k_G	k_{mod}	γ_M	b_{ef}	$k_{\text{con},0}$	$k_{\text{con},90}$	$k_{n,1}$	α	Statistics		
Source	Section	mean	k	mean	k	(kg/m^3)	(N/mm$^{1.5}$)	(–)	(–)	(mm)	(–)	(–)	(–)	(–)	n	k_s	$\text{COV}_{\log}$
Splitting Tests	FW (RL)	1.177	0.926	16902	13300	700	37.00	1.00	1.00	40.0	1.00	1.00	1.00	0.320	4	2.68	0.009
Splitting Tests	EW (TL)	0.871	0.631	14298	10360	700	37.00	1.00	1.00	51.0	1.00	1.00	1.00	0.320	4	2.68	0.012
Splitting Tests	Mean	1.024	0.779	15600	11830	700	37.00	1.00	1.00	—	1.00	1.00	1.00	0.320	4	2.68	0.011

A.2.5 Tensile

Table A.10: Tensile per crack system. $f_{0.05}$ is the 5%-percentile.

	E (MPa)				f_t (MPa)			
	n	Mean	Std	$f_{0.05}$	n	Mean	Std	$f_{0.05}$
Unknown	4	8236.81	4453.85	1970.49	4	49.41	31.82	3.04

A.2.6 Literature

Table A.11: Literature values, fracture properties

Author (Year)	Material	Product	Crack	Property	Symbol	Tensor	Loading	Value	SD	CoV (%)	n	Units	Method
Chen_2019	Culm (Moso)		RL	Mode I critical fracture energy release rate (RL crack)	G_IC_RL	G_IC_RL		536.67	—	—	5	J/m^2	DCB
Chen_2022	LBL (Moso)	LBL	RL	Mode I critical fracture energy release rate (RL crack)	G_IC_RL	G_IC_RL		501.08	—	—	5	J/m^2	
Chen_2022	LBL (Moso)	LBL	TL	Mode I critical fracture energy release rate (TL crack)	G_IC_TL	G_IC_TL		584.00	—	—	5	J/m^2	
Chen_2022	Culm (Moso)		TL	Mode I critical fracture energy release rate (TL crack)	G_IC_TL	G_IC_TL		358.00	—	—	5	J/m^2	
Ellison_2015	Culm (Moso)		TL	Mode II critical fracture energy release rate (TL crack)	G_IIC_TL	G_IIC_TL		630.00	155.00	24.6	43	J/m^2	ENF
Liu_2021	LBL (Moso)	LBL	RL	Mode I critical fracture energy release rate (RL crack)	G_IC_RL	G_IC_RL		501.08	—	—	6	J/m^2	DCB
Liu_2023	LBL (Moso)	LBL	TL	Mode I critical stress intensity factor (TL crack)	K_IC_TL	K_IC_TL		0.61	0.04	7.3	9	MPa.m$^{0.5}$	Arcan
Liu_2023	LBL (Moso)	LBL	TL	Mode II critical stress intensity factor (TL crack)	K_IIC_TL	K_IIC_TL		1.19	0.10	8.3	9	MPa.m$^{0.5}$	Arcan
Shao_2009	Culm (Moso)		TL	Mode I critical fracture energy release rate (TL crack)	G_IC_TL	G_IC_TL		358.00	61.18	16.9	17	J/m^2	DCB
Wang_2013	Culm (Moso)		TL	Mode II critical fracture energy release rate (TL crack)	G_IIC_TL	G_IIC_TL		1303.18	116.82	9.0	43	J/m^2	ENF
Wang_2014	Culm (Moso)		RL	Mode I critical fracture energy release rate (RL crack)	G_IC_RL	G_IC_RL		498.00	65.00	13.1	7	J/m^2	DCB
Wu_2022	LBL (Moso)	LBL	TL	Mode I critical fracture energy release rate (TL crack)	G_IC_TL	G_IC_TL		225.70	29.80	13.2	15	J/m^2	DCB

Table A.12: Literature values, mechanical properties

Author (Year)	Material	Product	Crack	Property	Symbol	Tensor	Loading	Value	SD	CoV (%)	n	Units	Method
Al-Rukaibawi_2024	LBL (Moso)	LBL		Elastic modulus (longitudinal), compression	E_L_C	E_11_C	Compression	8750.00	1550.00	0.2	5	MPa	Compression, Shear
Al-Rukaibawi_2024	LBL (Moso)	LBL		Elastic modulus (tangential), compression	E_T_C	E_22_C	Compression	2190.00	110.00	0.1	5	MPa	Compression, Shear
Al-Rukaibawi_2024	LBL (Moso)	LBL		Elastic modulus (radial), compression	E_R_C	E_33_C	Compression	1110.00	210.00	0.2	5	MPa	Compression, Shear
Al-Rukaibawi_2024	LBL (Moso)	LBL		Strength (longitudinal), compression	f_L_C	f_11_C	Compression	68.60	1.09	0.2	16	MPa	Compression, Shear
Al-Rukaibawi_2024	LBL (Moso)	LBL		Strength (tangential), compression	f_T_C	f_22_C	Compression	15.41	0.50	0.3	16	MPa	Compression, Shear
Al-Rukaibawi_2024	LBL (Moso)	LBL		Strength (radial), compression	f_R_C	f_33_C	Compression	13.16	4.43	0.3	16	MPa	Compression, Shear
Al-Rukaibawi_2024	LBL (Moso)	LBL		Poisson ratio (LT), compression	v_LT_C	v_12_C	Compression	0.23	0.07	0.3	5	-	Compression, Shear
Al-Rukaibawi_2024	LBL (Moso)	LBL		Poisson ratio (LR), compression	v_LR_C	v_13_C	Compression	0.32	0.07	0.2	5	-	Compression, Shear
Al-Rukaibawi_2024	LBL (Moso)	LBL		Poisson ratio (TR), compression	v_TR_C	v_23_C	Compression	0.53	0.25	0.5	5	-	Compression, Shear
Al-Rukaibawi_2024	LBL (Moso)	LBL		Shear modulus (LT)	G_LT	G_12		1970.00	—	—	5	MPa	Compression, Shear
Al-Rukaibawi_2024	LBL (Moso)	LBL		Shear modulus (LR)	G_LR	G_13		1380.00	—	—	5	MPa	Compression, Shear
Al-Rukaibawi_2024	LBL (Moso)	LBL		Shear modulus (TR)	G_TR	G_23		510.00	—	—	5	MPa	Compression, Shear
Chen_2019	LBL (Moso)	LBL		Elastic modulus (longitudinal), tension	E_L_T	E_11_T	Tension	11143.00	924.87	8.3	20	MPa	Compression, Tension, Flexure, Shear
Chen_2019	LBL (Moso)	LBL		Elastic modulus (longitudinal), bending	E_L_B	E_11_B	Bending	8870.00	887.00	10.0	20	MPa	Compression, Tension, Flexure, Shear
Chen_2019	LBL (Moso)	LBL		Strength (longitudinal), tension	f_L_T	f_11_T	Tension	107.70	11.52	10.7	20	MPa	Compression, Tension, Flexure, Shear
Chen_2019	LBL (Moso)	LBL		Strength (longitudinal), bending (MOR)	f_L_B	f_11_B	Bending	111.50	8.81	7.9	20	MPa	Compression, Tension, Flexure, Shear
Chen_2019	LBL (Moso)	LBL		Shear strength	f_v	f_12	Shear	17.50	1.23	7.0	20	MPa	Compression, Tension, Flexure, Shear
Li_2015	LBL (Moso)	LBL		Elastic modulus (longitudinal), bending	E_L_B	E_11_B	Bending	10912.00	739.00	6.8	20	MPa	Flexure
Li_2015	LBL (Moso)	LBL		Strength (longitudinal), bending (MOR)	f_L_B	f_11_B	Bending	63.95	7.18	11.2	20	MPa	Flexure
Sharma_2015	LBL (Moso)	LBL		Elastic modulus (longitudinal), bending	E_L_B	E_11_B	Bending	11000.00	605.00	5.5	10	MPa	Flexure, Tension
Sharma_2015	LBL (Moso)	LBL		Strength (longitudinal), tension	f_L_T	f_11_T	Tension	90.00	23.40	26.0	10	MPa	Flexure, Tension
Sharma_2015	LBL (Moso)	LBL		Strength (longitudinal), bending (MOR)	f_L_B	f_11_B	Bending	77.00	5.39	7.0	10	MPa	Flexure, Tension
Sharma_2015	LBL (Moso)	LBL		Strength (tangential), tension	f_T_T	f_22_T	Tension	2.00	0.26	13.0	10	MPa	Flexure, Tension
Sharma_2015	LBL (Moso)	LBL		Shear strength	f_v	f_12	Shear	16.00	0.80	5.0	10	MPa	Flexure, Tension
Sharma_2017	LBL (Moso)	LBL		Elastic modulus (longitudinal), tension	E_L_T	E_11_T	Tension	8387.50	629.06	7.5	40	MPa	Compression, Tension, Flexure, Shear
Sharma_2017	LBL (Moso)	LBL		Elastic modulus (longitudinal), bending	E_L_B	E_11_B	Bending	9323.75	536.12	5.8	40	MPa	Compression, Tension, Flexure, Shear
Sharma_2017	LBL (Moso)	LBL		Elastic modulus (tangential), tension	E_T_T	E_22_T	Tension	1287.00	199.49	15.5	40	MPa	Compression, Tension, Flexure, Shear
Sharma_2017	LBL (Moso)	LBL		Elastic modulus (radial), tension	E_R_T	E_33_T	Tension	1394.50	139.45	10.0	40	MPa	Compression, Tension, Flexure, Shear
Sharma_2017	LBL (Moso)	LBL		Strength (longitudinal), tension	f_L_T	f_11_T	Tension	44.55	5.12	11.5	40	MPa	Compression, Tension, Flexure, Shear
Sharma_2017	LBL (Moso)	LBL		Strength (longitudinal), bending (MOR)	f_L_B	f_11_B	Bending	60.90	3.65	6.0	40	MPa	Compression, Tension, Flexure, Shear
Sharma_2017	LBL (Moso)	LBL		Strength (tangential), tension	f_T_T	f_22_T	Tension	3.60	0.97	27.0	40	MPa	Compression, Tension, Flexure, Shear
Sharma_2017	LBL (Moso)	LBL		Strength (radial), tension	f_R_T	f_33_T	Tension	4.25	0.89	21.0	40	MPa	Compression, Tension, Flexure, Shear
Sharma_2017	LBL (Moso)	LBL		Shear strength	f_v	f_12	Shear	7.50	0.97	13.0	40	MPa	Compression, Tension, Flexure, Shear

Table A.13: Experimental vs literature comparison of LBL batch means with matching literature means

Property	Symbol	Tensor	Units	Lit mean	Lit SD	Lit CoV (%)	Exp mean	Exp SD	Exp CoV (%)	Exp n	Dev (%)
Mode I critical fracture energy release rate	G_IC	G_IC	J/m^2	397.89	49.80	12.5	200.98	57.49	28.6	62	-49.5
Mode I critical fracture energy release rate (RL crack)	G_IC_RL	G_IC_RL	J/m^2	507.88	65.00	12.8	214.03	70.31	32.9	31	-57.9
Mode I critical fracture energy release rate (TL crack)	G_IC_TL	G_IC_TL	J/m^2	337.65	46.47	13.8	187.92	37.76	20.1	31	-44.3
Mode I critical stress intensity factor	K_IC	K_IC	$MPa.m^{0.5}$	0.61	0.04	7.3	0.72	0.14	19.1	62	+19.0
Mode I critical stress intensity factor (RL crack)	K_IC_RL	K_IC_RL	—	—	—	—	0.76	0.11	14.3	31	—
Mode I critical stress intensity factor (TL crack)	K_IC_TL	K_IC_TL	$MPa.m^{0.5}$	0.61	0.04	7.3	0.69	0.16	22.8	31	+13.3
Mode II critical fracture energy release rate	G_IIC	G_IIC	J/m^2	966.59	135.91	14.1	2110.35	526.08	24.9	50	+118.3
Mode II critical fracture energy release rate (RL crack)	G_IIC_RL	G_IIC_RL	—	—	—	—	2178.84	385.02	17.7	25	—
Mode II critical fracture energy release rate (TL crack)	G_IIC_TL	G_IIC_TL	J/m^2	966.59	135.91	14.1	2041.86	637.99	31.2	25	+111.2
Mode II critical stress intensity factor	K_IIC	K_IIC	$MPa.m^{0.5}$	1.19	0.10	8.3	1.75	0.25	14.4	50	+47.4
Mode II critical stress intensity factor (RL crack)	K_IIC_RL	K_IIC_RL	—	—	—	—	1.65	0.14	8.6	25	—
Mode II critical stress intensity factor (TL crack)	K_IIC_TL	K_IIC_TL	$MPa.m^{0.5}$	1.19	0.10	8.3	1.86	0.29	15.8	25	+56.5
Elastic modulus (longitudinal), tension	E_L_T	E_11_T	MPa	9306.00	727.66	7.8	10356.31	1673.77	16.2	3	+11.3
Elastic modulus (radial), tension	E_R_T	E_33_T	MPa	1394.50	139.45	10.0	1878.32	0.00	0.0	1	+34.7
Strength (longitudinal), tension	f_L_T	f_11_T	MPa	69.09	9.56	13.8	64.98	8.06	12.4	3	-5.9
Strength (radial), tension	f_R_T	f_33_T	MPa	4.25	0.89	21.0	2.71	0.00	0.0	1	-36.3

Appendix B

Fracture Mechanics Calculation Methods

B.0.1 B.1 Mode I - SENB Methods Used

I-1 - NT BUILD 422 (work-of-fracture, primary).

$$G_{IC} = \frac{W_f + m\,g\,u_0}{h_c\,b}, \qquad W_f = \int_0^{u_0} F(u)\,\mathrm{d}u, \qquad m = \tfrac{5}{6}\,m_{\text{tot}}$$

I-2a - Peak-load LEFM (simplified E').

$$K_{IC} = \frac{F_{\max}\,S}{B\,W^{3/2}}\,f(a/W), \qquad G_{IC} = \frac{K_{IC}^2}{E'}$$

$$f(x) = \frac{3\sqrt{x}\,\big[\,1.99 - x\,(1-x)\,(2.15 - 3.93\,x + 2.7\,x^2)\big]}{2\,(1+2x)\,(1-x)^{3/2}}, \qquad x = a/W$$

with $E' = E_T$ for TL and $E' = E_R$ for RL. The argument is written x rather than the conventional α to avoid collision with the EC5 splitting ratio $\alpha = h_e/h$ used in §4.

I-2b - Peak-load LEFM (full orthotropic, Sih et al. 1965 [40]).

$$G_{IC} = K_{IC}^2\,\sqrt{\frac{a_{11}\,a_{22}}{2}}\,\left[\sqrt{\frac{a_{22}}{a_{11}}} + \frac{2\,a_{12} + a_{66}}{2\,a_{11}}\right]^{1/2}$$

with reduced compliance entries $a_{11} = 1/E_L$ in both crack systems, and the crack-normal entries dispatched per system: TL gives $a_{22} = 1/E_T$, $a_{12} = -\nu_{LT}/E_L$, $a_{66} = 1/G_{LT}$. RL gives $a_{22} = 1/E_R$, $a_{12} = -\nu_{LR}/E_L$, $a_{66} = 1/G_{LR}$.

I-3 - E_f cross-check (QC).

$$E_f = \frac{S^3}{48\,C_0\,I_{\text{eff}}}, \qquad I_{\text{eff}} = \frac{B\,h_c^3}{12}$$

Setup-quality gate, not a G.

B.0.2 B.2 Mode II - ENF Methods Used

II-1 - SBT (simple beam theory).

$$G_{IIC} = \frac{9\,P_{\text{cr}}^2\,a_0^2}{16\,E_f\,B^2\,h^3}$$

II-2 - TBT (Timoshenko, shear-corrected).

$$G_{IIC} = \frac{9\,P_{\text{cr}}^2\,a_0^2}{16\,E_L\,B^2\,h^3}\left[1 + 0.2\,\frac{E_L}{G_{13}}\left(\frac{h}{a_0}\right)^2\right]$$

with $G_{13} = G_{LT}$ for TL and G_{LR} for RL.

II-3 - CBBM (compliance-based, primary, R-curve).

$$a_{\text{eq}} = \left[\frac{C_{\text{corr}}}{C_{0,\text{corr}}}\,a_0^3 + \tfrac{2}{3}\left(\frac{C_{\text{corr}}}{C_{0,\text{corr}}} - 1\right)L^3\right]^{1/3}, \qquad G_{IIC} = \frac{9\,P^2\,a_{\text{eq}}^2}{16\,E_f\,B^2\,h^3}$$

with shear-corrected compliances $C_{0,\text{corr}} = C_0 - 3L/(10\,G_{13}\,B\,h)$ and $C_{\text{corr}} = C - 3L/(10\,G_{13}\,B\,h)$ (G_{13} as in II-2), and corrected flexural modulus

$$E_f = \frac{2\,L^3 + 3\,a_0^3}{12\,C_{0,\text{corr}}\,B\,h^3}.$$

This E_f is the value reused as input to II-1 and II-2.

II-4 - CCM (compliance calibration, multi-specimen).

$$C = C_1 + m\,a_0^3, \qquad G_{IIC} = \frac{3\,m\,P_{\text{cr}}^2\,a_0^2}{2\,B}$$

with m fitted across ≥ 3 specimens of different a_0.

II-5 - CCM-NPC/PC (multi-position).

$$G_{IIC} = \frac{3\,m\,F_{\max}^2\,a_0^2}{2\,B}$$

with m from compliance at three crack positions on the same specimen.

B.0.3 B.3 Derived Quantities

D-1 - K_{IC} (simplified). $K_{IC} = \sqrt{G_{IC}\,E'}$, with E' as in I-2a.

D-2 - K_{IC} (orthotropic). Inverse of the I-2b expression: $K_{IC}^2 = G_{IC}/S_{\text{ortho}}$, where S_{ortho} is the bracket factor of I-2b. Tensor entries follow the same TL / RL dispatch as I-2b.

D-3 - K_{IIC} (orthotropic). Same form as D-2 with $G_{IC} \to G_{IIC}$ from II-3.

D-4 - EC5 splitting parameter $\sqrt{GG_c}$ [33]. Two routes are evaluated. Route A calculates from the splitting tests of §3.1.5,

$$\frac{V_f}{b\sqrt{h}} = \sqrt{GG_c}\,\sqrt{\frac{\alpha}{0.6\,(1-\alpha)}}, \qquad \alpha = h_e/h,$$

with V_f the support-shear at failure (one side of the joint, $V_f = F/2$ for a single mid-span dowel), b the beam thickness, h the beam height, and h_e the loaded-edge distance. Route B calculates from fracture properties,

$$\sqrt{GG_c} = \sqrt{G_{\text{shear}}\,G_{IC}}, \qquad G_{\text{shear}} = \begin{cases} G_{LT} & \text{(TL, edgewise)} \\ G_{LR} & \text{(RL, flatwise)} \end{cases}$$

with G_{IC} from I-1 (taken in N/mm, with the J/m^2 value divided by 1000). The G in $\sqrt{GG_c}$ is the in-plane shear modulus, *not* a perpendicular Young's modulus, Mode II has no role here, splitting being Mode-I dominant.

Appendix C

MOSO N-finity Indoor Beams Datasheet

Property	Side-pressed (edgewise, SP/EW)	Plain-pressed (flatwise, PP/FW)
Density [kg/m^3]	≈ 700	≈ 700
Moisture content @ 20 °C / 65 % RH [%]	10	10
Moisture content @ 20 °C / 50 % RH [%]	8	8
Shrink / swell per 1 % MC change [%]	0.14	0.14
Modulus of Elasticity (EN 408) [N/mm^2]	≈ 9 721	≈ 8 866
Bending strength (EN 408) [N/mm^2]	≈ 56.7	≈ 50.8
Brinell hardness (EN 1534) [kg/mm^2]	≈ 4	≈ 4
Reaction to fire (EN 13501-1)	D-s2-d0	D-s2-d0
DIBt approval	Z-9.1-895	Z-9.1-895
Glue	D4 water-resistant	D4 water-resistant

Table C.1 - MOSO N-finity Indoor Beams datasheet [28].